WANL-PR-(DD)-014
November 1, 1966

Westinghouse Astronuclear Laboratory

ANALYTICAL INVESTIGATION OF TURBINE EROSION PHENOMENA

Interim Technical Report Number I, Volume II

Contract NAS7-390

WANL-PR-(DD)-014
November 1, 1966

Westinghouse Astronuclear Laboratory

ANALYTICAL INVESTIGATION OF TURBINE EROSION PHENOMENA

Interim Technical Report Number I, Volume II

Contract NAS7-390

INFORMATION CATEGORY

Unclassified

D. M. Dingley 10/28/66

AUTHORIZED CLASSIFIER DATE

Astronuclear Laboratory

VOLUME II

FLUID, DYNAMIC AND THERMODYNAMIC PROCESSES INVOLVED IN TURBINE BLADE EROSION

Authors:

R. E. Kothman, W. K. Fentress, W. D. Pouchot, J. D. Milton

PREFACE

This report presents analytical models of the various fluid dynamic and thermodynamic processes involved in turbine blade erosion. The general categories of processes examined are: (1) condensation, (2) bulk and boundary layer flows and deposition of condensate and (3) atomization and subsequent trajectories of damaging liquid.

By use of the analytical models selected, two wet vapor turbines are examined, and the results of the calculations are reported. The turbines investigated are analytical simulations of: (1) the low pressure steam turbine of the Yankee Atomic Power Plant and (2) the General Electric two-stage potassium test turbine of Contract NAS 5-1143. The estimated results are in qualitative agreement with experimental observations. Available quantitative experimental data is too sparse to allow definite conclusions to be drawn. The process models selected appear to be adequate for at least order of magnitude turbine erosion estimation usage and provide a basis for further refinement.

TABLE OF CONTENTS

LIST OF ILLUSTRATIONS

LIST OF TABLES

PART A

INTRODUCTION

Volume I contains a listing of the various processes involved in erosion on the leading edge and nose of rotor blades of wet vapor turbines when they are operated for protracted periods at design conditions. In broad terms, the overall model consists of: (1) Condensation in the bulk vapor by spontaneous nucleation followed by near equilibrium accretion of moisture on the nuclei. (The ultimate size of the condensate particles is less than 1 micron in diameter.) (2) Deposition of a small percentage of the condensate flowing past on blade surfaces (which is the moisture causing erosion damage). (3) Detachment and atomization of the collected condensate from the stator vanes in the form of drops which are large by condensate standards (20 - 400 microns diameter). (4) Acceleration of these drops to velocities substantially below the bulk stream vapor velocity in the spacing available between stator and rotor. (5) Impingement of the drops on the rotor blade surfaces at the nose and convex leading edge with substantial components of velocity normal to the blade surfaces. (6) Material removal after repeated impacts.

Models of the detail fluid dynamic and thermodynamic processes involved in an overall synthesis of an analytical model of turbine blade erosion are presented in this volume. These detail processes have been investigated numerically for turbines simulating the low pressure steam turbine of the Yankee Atomic Power Plant and the General Electric two-stage potassium test turbine of Contract NAS 5-1143. The various processes involved are discussed and the results presented in the approximate chronological order in which they occur in a turbine. The processes covered are: (1) condensation by spontaneous nucleation, (2) condensation by accretion on nuclei, (3) row by row one-dimensional and axisymmetric bulk flow, (4) two-dimensional aspects of vapor boundary layers and blade wakes, (5) collection of condensate moisture on blade surfaces, (6) movement of collected moisture over the blade surfaces, (7) detachment, primary and secondary atomization and acceleration of detached liquid and (8) impingement velocities on rotor blades.

Comparison of the calculational results with the generally sparse experimental data available indicate qualitative agreement with the models selected. However, in most instances, the data is not sufficient to allow definite quantitative comparisons to be drawn and many of the detail process models are controversial. In some instances, from the point of view of the overall erosion model, these controversies can be regarded as arguments between specialists, but not, unfortunately, in all cases.

In the area of condensation theory there is disagreement as to the changes required in applying steam condensation theory to associating vapors such as potassium. In the use here only those changes resulting from the gross thermodynamics of the association were factored into the theory, and further investigation of the model is necessary. The treatment of the condensed moisture carried over from upstream equipment as it enters the turbine is another area of uncertainty. It has been treated as a supersaturation of the entering vapor. This is probably a reasonable assumption for the nine-stage steam turbine since the effect "washes" out in a few rows. It is not such a good assumption in the two-stage potassium turbine.

The bulk vapor flow in the example turbines is partially described by conventional one-dimensional state condition calculations assuming thermodynamic equilibrium condensation of moisture. This is a good approximation in the nine-stage steam turbine as near equilibrium is achieved in the first few stages. It is a poorer approximation for the two-stage potassium turbine as the moisture content in the two-stage turbine is probably not that of equilibrium. It is, however, probably adequate for the inputs required here for boundary layer wake flows and two-dimensional potential flow calculations.

The variation of the bulk flow from one-dimensional conditions in the radial direction and in the blade boundary layers [1] is treated in terms of 2 D calculational methods of many years standing. The standard procedures do not take into account the 3 D effects of

secondary flows at turbine hub and tip. The errors involved are not great at blade midspan, certainly, but may have a substantial influence on the local flows near the extremities of the blades.

The treatment of the stator blade wakes is based on viscous dissipation assuming near zero trailing edge thickness plus an ad hoc correction for finite thicknesses of trailing edge. Drop trajectory calculations using wakes so described agree reasonably well with available experimental observations in a steam cascade.

The movement of moisture on blade surfaces is given a simple but adequate viscous flow treatment, since the results do not enter directly, in a numerical sense, into the erosion calculations.

The relative importance of the various mechanisms of collection of the condensate particles on turbine surfaces is a technical area of substantial dispute. Gyarmathy, [2] believes that a direct inspection mechanism such as that associated with raindrops on aircraft accounts for most of the deposition. Whereas, Gardner [3] concludes that the condensate particles are too small for this mechanism to function effectively and that the predominant causes of condensate particle deposition are Brownian Motion and eddy diffusion in the boundary layers. The direct impaction model has been used here. Even so, the impaction calculations of Gyarmathy cannot be reconciled with those of Brun et al [4]. While further analytical work is indicated, it is probable that the differences can only be resolved fully by well planned and conducted experiments. With condensate particles of .2 → .4μ the various calculational methods give orders of magnitude differences in numerical results.

On atomization of damaging liquids from stator vanes the experimental observations have, to date, been confined to interesting details of the processes rather than to an overall summation of the results of the processes in terms of drop distributions. Because of this, the proposed model of atomization can only be said to be in qualitative agreement with experimental observations.

B. CONDENSATION

R. E. Kothmann

1.0 SUMMARY AND CONCLUSIONS

The process of vapor condensation in turbines has been described by an analytical model. This model has been used to obtain the flow performance and droplet size distributions in the Yankee Atomic Plant steam turbine and in the General Electric two-stage potassium test turbine of Contract NAS 5-1143.

The present analysis follows the same general method of solution which was first described by Oswatitish[1]. The basic method is to describe the condensing flow by the one-dimensional energy, momentum, and continuity equations including the effects of condensation. The flow was assumed to be one-dimensional and to be uniform over the flow area. Thus the calculations give only mean diameter results.

Since the exact form of the moisture at the inlet to the turbines was unknown, it was assumed that the vapor was in a supersaturated state for both the steam and potassium turbines.

For the steam turbine, the steam remained supersaturated throughout the first stator. The Wilson point or the start of rapid condensation was reached in the first rotor at 2.18% theoretical moisture. This point was reached in a region of low expansion rate $\dot{P}$ of approximately 345/sec which accounts for the relatively large diameter of the resulting droplets. Even with the slow expansion rate, the droplet size distribution was practically uniform. The mean droplet diameter at the exit from the eighth rotor was 0.71 microns.

For the potassium turbine the vapor also remained supersaturated throughout the first stator. The Wilson point was reached in the first rotor at 3.72% theoretical moisture. The expansion rate $\dot{P}$ at the Wilson point was 3000/sec and thus relatively small drops were produced. At the entrance to the second stator the mean drop diameter was 0.24 microns. The flow velocities and pressure ratios obtained with the condensation program did not agree well with equilibrium calculations due to the different expansion characteristics of a supersaturated vapor. The condensation results for both steam and potassium agree reasonably well with other

authors' theoretical calculations.[2] Up to the present time, no condensation droplet size measurements have been made in turbines. Nozzle condensation experiments with steam have been well correlated by Oswatitish's method. However, nozzle experiments for potassium have not yet been reported in which the condensation point was definitely determined. Predictions are that condensation would occur in the convergent section for initially saturated vapor. In this case, no condensation shock would be present and detection of the condensation point would be difficult.

The condensation results depend strongly on the value of surface tension. For the potassium turbine a 20% decrease in surface tension shifted the Wilson point from 3.72% to 2.5% theoretical moisture. An increase in surface tension would tend to delay condensation. Further uncertainties regarding surface tension are its radial dependence and the effect of this radial dependence on the nucleation rate. It is not clear whether the concept of surface tension remains valid when applied to clusters of 10 to 100 molecules.

It is believed that the association of liquid metal vapors plays an important role in the nucleation process. Conflicting theoretical predictions exist in the literature concerning its effect on the nucleation rate. The present calculations neglected any effects of association.

The following conclusions have been reached concerning the condensation process in turbines.

The degree of supersaturation at which condensation occurs and the resultant size of droplets are strongly dependent upon the expansion rate at which condensation occurs. When the Wilson point occurs in a region of low expansion rate, condensation occurs at smaller supersaturations and larger drops are produced. It is believed by Gyarmathy[2] that it may be possible to control condensation and to a large extent erosion by shifting the operating conditions such that condensation occurs at high expansion rates so that smaller droplets are produced.

The droplet size is very nearly uniform for both steam and potassium. Less than 1/2% of all droplets formed by nucleation have diameters which exceed the mean diameter by more than 35%.

For the Yankee turbine the carryover moisture* is likely to have a significant effect on the nucleation process. If the mean diameter of the carryover moisture is less than 2 microns, adequate surface area would be available for all additional condensation. Larger sizes would have insufficient area so that additional nucleation would occur. Since the carryover size is probably larger than 2μ, additional nucleation would occur but at a later stage than for the case of supersaturated inlet steam.

There is a definite need for complete nozzle condensation experiments with liquid metals so that results of theoretical calculations can be compared. Further theoretical work should be continued in an effort to quantitatively determine the effects of association using the theory of Katz, Saltsburg and Reiss[3].

2.0 NOMENCLATURE

Symbol	Definition	Units
A	Cross sectional area normal to flow	ft^2
A_a	Cross sectional area normal to turbine axis	ft^2
$\hat{A}$	Parameter, see equation 34	ft
a'	Empirical constant	-
B	Parameter, see equation 41	ft^2
c	Jet velocity relative to blade	ft/sec
C	Parameter, see equation 42	ft^{-1}
C_{p_v}	Specific heat of vapor at constant pressure	Btu/lb°R
C_{p_L}	Specific heat of condensate at constant pressure	Btu/lb°R
D_1, D_{1i}, D_{1o}	Inner diameter of turbine blade passage, inner diameter at blade row inlet, at blade row exit	ft
D_2, D_{2i}, D_{2o}	Outer diameter of turbine blade passage, outer diameter at blade row inlet, at blade row exit	ft

*Carryover moisture from the moisture separator between high and low pressure stages.

Symbol	Definition	Units
F	Friction force per unit volume	lb/ft^3
$\hat{F}$	Function, see equation 43	ft^2
g	Gravitational constant	$32.2\ ft/sec^2$
h_c	Heat transfer coefficient	$Btu/sec\ ft^2\ ^oR$
h_{fg}	Latent heat of vaporization	Btu/lb
h_L	Specific enthalpy of condensate	Btu/lb
h_v	Specific enthalpy of vapor	Btu/lb
i	Subscript denoting group of drops	-
J	Heat equivalent	778 ft-lb/Btu
$\dot{J}$	Nucleation rate	$nuclei/sec\ ft^3$
k_v	Thermal conductivity of vapor	$Btu/sec\ ft\ ^oR$
L	Axial length of blade row	ft
N_o	Molecules per pound	lb^{-1}
N_i	Number of drops per pound in group i	lb^{-1}
p	Static pressure	lb/ft^2
p_s	Saturation pressure at actual vapor temperature	lb/ft^2
$\dot{P}$	Expansion rate, see equation 32	sec^{-1}
R	Specific gas constant	$ft\text{-}lb/lb^oR$
r	Drop radius	ft
r_i	Radius of condensate drop of group i	ft
r_{crit}	Critical droplet radius	ft
t_b	Blade thickness in peripheral direction	ft
t_{bo}	Minimum blade thickness	ft
t_{bm}	Maximum blade thickness	ft
t_{bs}	Blade spacing in peripheral direction	ft

Symbol	Definition	Units
T_L	Condensate temperature	^oR
T_{LC}	Critical point temperature	^oR
T_v	Vapor temperature	^oR
T_s	Saturation temperature at the actual vapor pressure	^oR
ΔT	Supercooling	^oR
U_a, u_a	Axial velocity component	ft/sec
v_m	Specific volume of mixture	ft^3/lb
v_v	Specific volume of vapor	ft^3/lb
w_r	Weight of critical size drop	lb
x	Vapor quality	-
y	Total moisture fraction	-
y_e	Equilibrium moisture fraction	-
y_i	Moisture fraction of condensate belonging to group i	-
y_w	Moisture fraction associated with formation of critical size drops	-
Δy	Moisture deficiency	-
z	Axial coordinate, along turbine axis	ft
β	Blade angle	radians
β_i	Blade angle at inlet to row	radians
η_p	Polytropic efficiency	-
γ	Ratio of specific heat, at constant pressure to that of constant volume	-
β_o	Blade angle at exit from row	radians
$\wedge$	Logarithmic supersaturation	-
ν_v	Kinematic viscosity	ft^2/sec
ρ_L	Density of condensate	lb/ft^3
σ_L	Surface tension of condensate	lb/ft
σ_∞	Surface tension of flat film of condensate	lb/ft

3.0 INTRODUCTION

The form of moisture present in a turbine is more important to the erosion process than the overall quantity of moisture. In particular, moisture present in the form of tiny droplets entrained in the flow is far less damaging than the same quantity of water in the form of large drops. In order to describe the condensate behavior it is necessary to consider the details of the condensation process in which the moisture is formed. The goal of the condensation study is to determine the size and number distribution of condensate droplets formed in a turbine as a function of axial position. This information is required as a starting point for predicting the distribution of moisture in its various forms in the turbine.

A large number of experimental and theoretical condensation studies have been reported and excellent reviews are given by Stever[4] and by Courtney[5]. Condensation theory has been applied to condensing flow in nozzles by Oswatitish[1], Glassman[6] and others [7] [2]. The present analysis follows the same general method of solution which was first described by Oswatitish[1] but using improvements introduced by Gyarmathy[2] and others. The basic method is to describe the condensing flow by the one dimensional energy, momentum and continuity equations including the effects of condensation. The condensation process is described by the rate of formation of droplets and their rate of growth. The rate of formation of condensation nuclei in a supersaturated vapor is predicted by nucleation theory. Thermodynamic and heat transfer principles are then applied to predict rate of growth.

From a fundamental viewpoint condensation processes can be divided into nucleation, growth, and agglomeration. Nucleation is defined as the formation of the smallest molecular clusters or droplets of the new phase which are stable. Growth is the atom by atom addition of new material onto the droplets, and agglomeration includes coalescence of two or more particles and the collection on solid surfaces. The present section considers only the nucleation and growth processes.

4.0 NUCLEATION AND GROWTH THEORY

The concept of a critical drop size which is in thermodynamic equilibrium with a supersaturated vapor is fundamental to all nucleation theory. This critical radius is given by the Helmholtz equation (eq. 1):

$$r_{crit} = \frac{2\ \sigma_L}{\rho_L\ R\ T_v\ \wedge} \tag{1}$$

$$\text{where } \wedge = f(n\ (p/p_s)). \tag{2}$$

The equilibrium defined by this relation is metastable; smaller drops tend to evaporate, larger ones tend to grow by condensation. Where a vapor becomes supersaturated, to obtain the lowest energy state the vapor should condense, but condensation must start with the formation of small drops which are unstable. As supersaturation is increased, the critical size decreases and the likelihood of survival increases until at a certain supersaturation, appreciable condensation into a fog of droplets occurs.

Nucleation theory is concerned with predicting the net rate at which nuclei reach critical size. According to the classical theory attributed to Frenkel[8], the steady state rate of formation of condensation nuclei per unit volume within the bulk of a pure supersaturated vapor is given by the following equation:

$$\dot{j} = \frac{N_o\ p^2}{\rho_L\ (R\ T_v)^2} \sqrt{\frac{2g\ \sigma_L\ N_o}{\pi}}\ \exp\left\{ \frac{-16\pi\ \sigma_L^3\ N_o}{3\ \rho_L^2\ (R\ T_v)^3\ \wedge^2} \right\} \tag{3}$$

Although many modifications of the classical theory have been derived to account more precisely for additional effects such as variation of surface tension with radius, the above equation is usually chosen to describe the nucleation rate. A time delay may be involved before the nucleation reaches its steady rate[9]. If the time constant were as large as 10μ sec, the location of the condensation point in the turbine would only be shifted several hundredths of an inch downstream Thus it is reasonable to neglect the transient nucleation effects. One of the most questioned limitations of nucleation theory involves surface tension. The accuracy of surface tension measurements for the liquid metals is uncertain due to the scatter in reported data. The second limitation concerns the application of the surface tension concept to small

clusters of molecules. In some instances the critical nuclei contain only a few tens of molecules and it is difficult to visualize such a cluster as being a spherical droplet having surface tension corresponding to that of a flat surface. Head[10] and Tolman[11] developed a correction for surface tension of a curved surface of the form:

$$\sigma_L = \frac{\sigma_\infty}{1 + \delta/r_L} \quad , \tag{4}$$

where δ is a length lying between 0.25 and 0.6 of the molecular radius in the liquid state. There is still disagreement as to the radial dependence of surface tension and its effect on nucleation rate[4]. The present calculations have included the variation of surface tension with temperature only.

Until the nuclei reach the critical size, they are considered to belong to the vapor phase. The rate of increase in the number of drops per pound of mixture is $\dot{J} v_m$, and the rate of formation per pound per unit length in the axial direction is given by $\dot{J} v_m / u_a$. Each drop has a weight given by:

$$w_r = \frac{4}{3} \pi \rho_L r^3_{crit} \tag{5}$$

The change of moisture fraction with respect to axial length due to the formation of new nuclei is then given by:

$$\frac{dy_N}{dz} = \frac{w_r \dot{J} v_m}{u_a} \quad . \tag{6}$$

Once the nuclei are formed, their growth rate is primarily governed by the rate at which the latent heat can be transferred from the drops to the surrounding vapor. The mode of heat transfer from the drop to the vapor may differ depending on existing conditions. The mean free path in the vapor is considerably larger than the critical sized nuclei so that during the early growth of drops heat transfer is by free molecular processes. As size increases, the process

passes through the transition region and at large sizes normal gaseous conduction or convection occurs. Gyarmathy[2] used the following expression for the heat transfer coefficient which is approximately valid for free molecular, transition, and continuum flow conditions:

$$h_c = \frac{k_v}{r_L + \frac{2.38\,\nu_v}{\sqrt{g R T_v}}} \tag{7}$$

It is assumed that the droplets are not in motion relative to the flowing vapor.

An energy balance between heat transferred and heat released by condensation gives the change of radius as:

$$\frac{dr_L}{dt} = \frac{h_c\,(T_r - T_v)}{\rho_L\, h_{fg}} \quad . \tag{8}$$

The rate of change with axial position is obtained by dividing by the axial velocity, thus:

$$\frac{dr_L}{dz} = \frac{h_c\,(T_r - T_v)}{\rho_L\, h_{fg}\, u_a} \quad . \tag{9}$$

At the critical size the droplet temperature is equal to the vapor temperature. As the droplet grows, its temperature T_r must remain somewhat lower than the saturation temperature corresponding to the local pressure due to the effect of surface tension.

The subcooling due to the surface tension effect is termed "capillary supercooling" by Gyarmathy and is equal to the product of the supercooling and the ratio of the critical radius to the droplet radius. Thus, the maximum temperature difference between the drop and the vapor is a function of radius, namely:

$$T_r - T_v = (T_s - T_r)\left(1 - \frac{r_{crit}}{r}\right) \quad . \tag{10}$$

The assumption is made that droplet growth is controlled solely by heat transfer limitations, and that there is an adequate number of molecular collisions with the drop to supply growth. This would not be the case, for example, if water condensation in air were being considered. In that case, diffusion of water molecules through air to the droplet surface would be a definite factor limiting growth rate. With heat transfer controlling the growth rate, it is assumed that the drop always has its maximum permissible temperature which is given by equation 10. Then, equations 9, 7 and 10 define the rate of change of drop radius with axial position.

If the number of drops formed during the increment ΔL_i is N_i and their radius is r_i, then the rate of increase of moisture fraction due to growth of this group of drops is:

$$\frac{dy_i}{dz} = \rho_L \, 4\pi \, r_i^2 \, N_i \, \frac{dr_i}{dz} \cdot \tag{11}$$

Then the total rate of increase of moisture fraction due to formation of new nuclei and growth of existing nuclei is given by:

$$\frac{dy}{dz} = \frac{dy_N}{dz} + \sum_{\substack{\text{all} \\ \text{groups}}} \frac{dy_i}{dz} \cdot \tag{12}$$

5.0 FLUID FLOW AND STATE EQUATIONS

It is assumed that the flow of vapor through turbine nozzles and blades can be adequately described by applying the one-dimensional form of the energy, momentum and continuity equations. It is assumed that the flow is adiabatic and radial variations are neglected. The calculations thus apply to the mean stream tube. Following Gyarmathy[2], it is assumed that friction loss is proportional to the isentropic static enthalpy drop. The momentum equation for a stream tube can be written as:

$$\frac{1}{g} \, c \, \frac{dc}{dz} = - v_m \, \frac{dp}{dz} - v_m \, F, \tag{13}$$

where c is the jet velocity and F is the friction force per unit volume of the flowing mixture. The work per pound against friction is v_m Fdz, which is taken to be $\left[- (1 - \eta_p)\ dh_s \right]$, where dh_s is the isentropic enthalpy change. Using $dh_s = v_m\ dp$, the momentum equation becomes:

$$\frac{c}{g} \frac{dc}{dz} = - \eta_p v_m \frac{dp}{dz} \quad . \tag{14}$$

The total energy equation relative to a coordinate system fixed on the blade is:

$$\frac{d}{dz} \left(\frac{c^2}{2g\ J} + x\ h_v + y\ h_L \right) = 0 \, . \tag{15}$$

The continuity equation is expressed by:

$$\frac{1}{c} \frac{dc}{dz} + \frac{1}{A} \frac{dA}{dz} - \frac{1}{v_m} \frac{d\ v_m}{dz} = 0. \tag{16}$$

The ideal gas law is used for the equation of state for the vapor,

$$p\ v_v = R\ T_v, \tag{17}$$

and the specific volume of the mixture is

$$v_m = x\ v_v + y\ v_L \cong x\ v_v, \tag{18}$$

where the volume occupied by the liquid is assumed to be negligible. The enthalpy change of the liquid and vapor is described by:

$$\frac{d\ h_v}{dz} = C_{p_v} \frac{d\ T_v}{dz} \tag{19}$$

$$\frac{d h_L}{dz} = C_{p_L} \frac{d T_v}{dz} \quad (20)$$

The variation of surface tension with temperature is accounted for with the empirical relation

$$\sigma_L = \text{const} \left[1 - \left(\frac{T_L}{T_{Lc}} \right)^{1.4} \right] . \quad (21)$$

The Clasius-Clapeyron relation is used to describe the variation of saturation pressure as a function of temperature in the form:

$$\ell n\, p_s = a' - \frac{J h_{fg}}{R T_v} ,$$

where a' is an empirical constant for a particular substance. The Clasius-Clapeyron relation also permits the supercooling ΔT to be expressed in terms of the supersaturation:

$$\Delta T = T_s - T_v = \frac{\wedge T_v}{\frac{J h_{fg}}{R T_v} - \wedge} .$$

6.0 DESCRIPTION OF TURBINE GEOMETRY

The blade passages are curved so that the flow continually changes direction as it proceeds through the turbine. The axial component of the velocity u_a is related to the jet velocity c by:

$$u_a = c \sin \beta , \quad (22)$$

where β is the local blading angle measured as shown below. The jet velocity is taken as the velocity relative to the blade and the equations hold for both stator and rotor when radial flow and Coriolis forces are neglected.

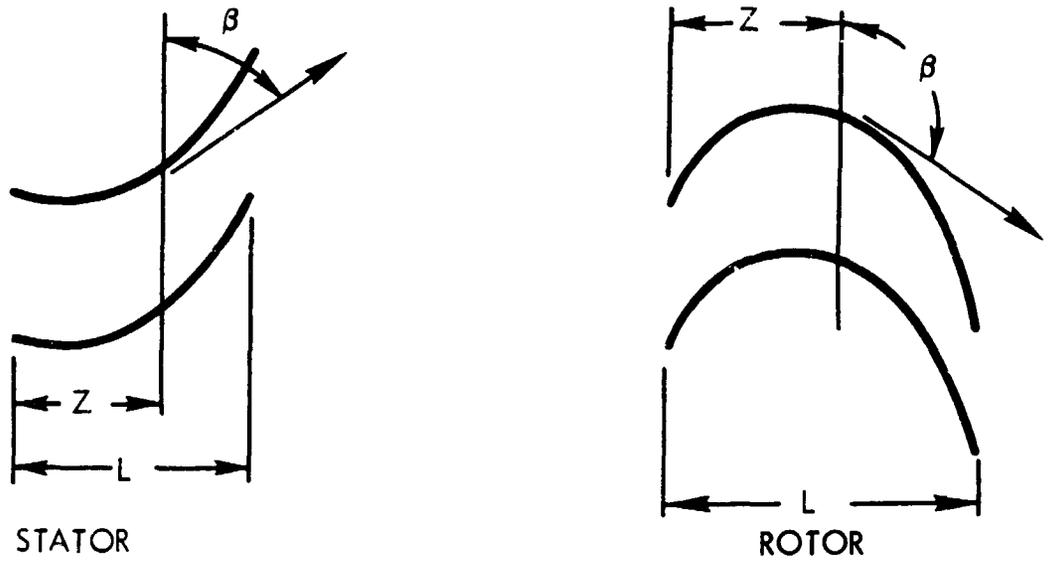

611131-50B

The blade shape is assumed to be parabolic which gives the variation in blade angle with axial position as:

$$\cot \beta = \cot \beta_i + (\cot \beta_o - \cot \beta_i) \frac{z}{L} \tag{23}$$

and

$$\frac{d\beta}{dz} = \frac{\sin^2 \beta}{L} (\cot \beta_o - \cot \beta_i). \tag{24}$$

The cross sectional flow area normal to the axis is described by:

$$A_a = \frac{\pi}{4} (D_2^2 - D_1^2) \left(1 - \frac{t_b}{t_{bs}}\right), \tag{25}$$

which is the area of an annulus having inner and outer diameters D_1 and D_2 and the fraction t_b/t_{bs} being taken up by the blade. The diameters D_1 and D_2 are taken to vary linearly with axial position and the blade thickness is assumed to vary as a parabola.

$$D_1 = D_{1i} + (D_{1o} - D_{1i}) \frac{z}{L} \tag{26}$$

$$D_2 = D_{2i} + (D_{2o} - D_{2i}) \frac{z}{L} \tag{27}$$

$$t_b = t_{bo} + \left(\frac{2z}{L} - 1\right)^2 (t_{bm} - t_{bo}) \cdot \tag{28}$$

In this case, z is the axial coordinate measured from the leading edge of the blade and L is the axial dimension of the blade.

Using the relation $A = A_a \sin \beta$, the continuity, energy, momentum and state equations can be in the following form for stepwise integration:

$$\frac{1}{p} \frac{dp}{dz} = \frac{\left(\frac{h_{fg}}{C_{p_v} T_v} - \frac{1}{x}\right) \frac{dy}{dz} - \frac{1}{A_a} \frac{dA_a}{dz} - \cot \beta \frac{d\beta}{dz}}{\left[1 - \eta_p \frac{x(\gamma - 1)}{\gamma} + \frac{g v_m p}{c^2}\right]} \tag{29}$$

$$\frac{1}{u_a} \frac{du_a}{dz} = \cot \beta \frac{d\beta}{dz} - \frac{g v_m \eta_p}{c^2} \frac{dp}{dz} \tag{30}$$

$$\frac{1}{T_v} \frac{dT_v}{dz} = \left[\frac{1}{x} \frac{dy}{dz} + \frac{1}{p} \frac{dp}{dz} + \frac{1}{A_a} \frac{dA_a}{dz} + \frac{1}{u_a} \frac{du_a}{dz}\right]. \tag{31}$$

Thus, at any axial position nucleation and growth theory permit one to calculate $\frac{dy}{dz}$ using equation 12. The turbine geometry description gives $\frac{1}{A_a}\frac{dA_a}{dz}$ (eq. 25) and $\frac{d\beta}{dz}$ (eq. 24). Then, equations 29, 30, 9 and 12 are solved numerically by a stepwise integration process to give pressure, velocity, temperature, droplet radii and moisture fraction. (See Appendix 4 for a computer program.)

7.0 RESULTS FOR CONVERGENT-DIVERGENT NOZZLE

The results of a calculation in which superheated steam is expanded in a convergent-divergent nozzle are shown in figures B-1 to B-4. The condensation does not occur until the divergent section is reached, so only the divergent portion is shown. The nozzle had a conical shape with a length of 0.205 ft and an area ratio of 1.5. Superheated steam with stagnation temperature 280°F and stagnation pressure of 22 psia was assumed at the entrance to the convergent section of the nozzle. The area ratio, temperature and pressure variations with length are shown in figure B-1. The variation of nucleation rate is shown in figure B-2. The maximum value of the nucleation rate was 1.8×10^{21} nuclei/ft^3 sec. The range of experimental values compared by Glassman[6] varied from 10^{18} to 10^{24}. The Wilson point corresponds to the peak of the nucleation rate curve. The equilibrium moisture and calculated moisture fraction are shown in figure B-3. It can be seen that the Wilson point occurs at 2.8% theoretical moisture. The expansion rate for the nozzle which Gyarmathy describes by:

$$\dot{P} = -\frac{1}{p}\frac{dp}{dt} \; ; \quad \text{or approximately } 10^4/\text{sec} \tag{32}$$

The Wilson point occurs at about 3% moisture for $\dot{P} = 10^4$. Thus, the results are in good quantitative agreement with other authors' calculations. The total number of droplets per pound of mixture formed during the condensation process was 1.89×10^{17} drops. At the end of the nozzle the mean diameter of these drops was 0.067 microns. The size variation of the eight groups of drops is shown in figure B-4. The number of drops in each group is shown in table B-1 along with the radius and moisture fraction at the nozzle exit.

TABLE B-1

The Distribution of Number and Size of Drops at the Exit of the Divergent Portion of the Nozzle and the Moisture Fraction Associated with Each Size

Group	Diameter (microns)	Number/lb	Moisture Fraction
1	0.116	1.02×10^{12}	0.000002
2	0.105	1.44×10^{13}	0.00002
3	0.101	1.3×10^{14}	0.00015
4	0.094	8.36×10^{14}	0.00077
5	0.085	4.11×10^{15}	0.00289
6	0.076	1.62×10^{16}	0.00822
7	0.067	5.15×10^{16}	0.01750
8	0.057	1.16×10^{17}	0.02421

8.0 CONDENSATION RESULTS FOR YANKEE TURBINE

The computer program input data to describe the Yankee turbine consisted of steam properties, turbine tip diameter, hub diameter, mean blade angles, blade spacing and blade thickness. The inlet steam was assumed to be supersaturated at 57.5 psia with 1% moisture equivalent. First, an adiabatic frictionless process was assumed which corresponds to a polytropic efficiency $\eta_p = 1.0$.

The pressure, temperature, axial velocity, and moisture at the exit of the blade rows are presented in table B-2. This table also shows mean diameter calculations which are based on the equilibrium expansion mode. These calculations were performed at the Westinghouse Steam Division. The results are not directly comparable due to the small difference in inlet pressure. The results of the two methods compare very well, except in the first stator, where the assumed inlet supersaturation affects the temperature. The calculations were terminated at the end of the third stage. At this point the flow very

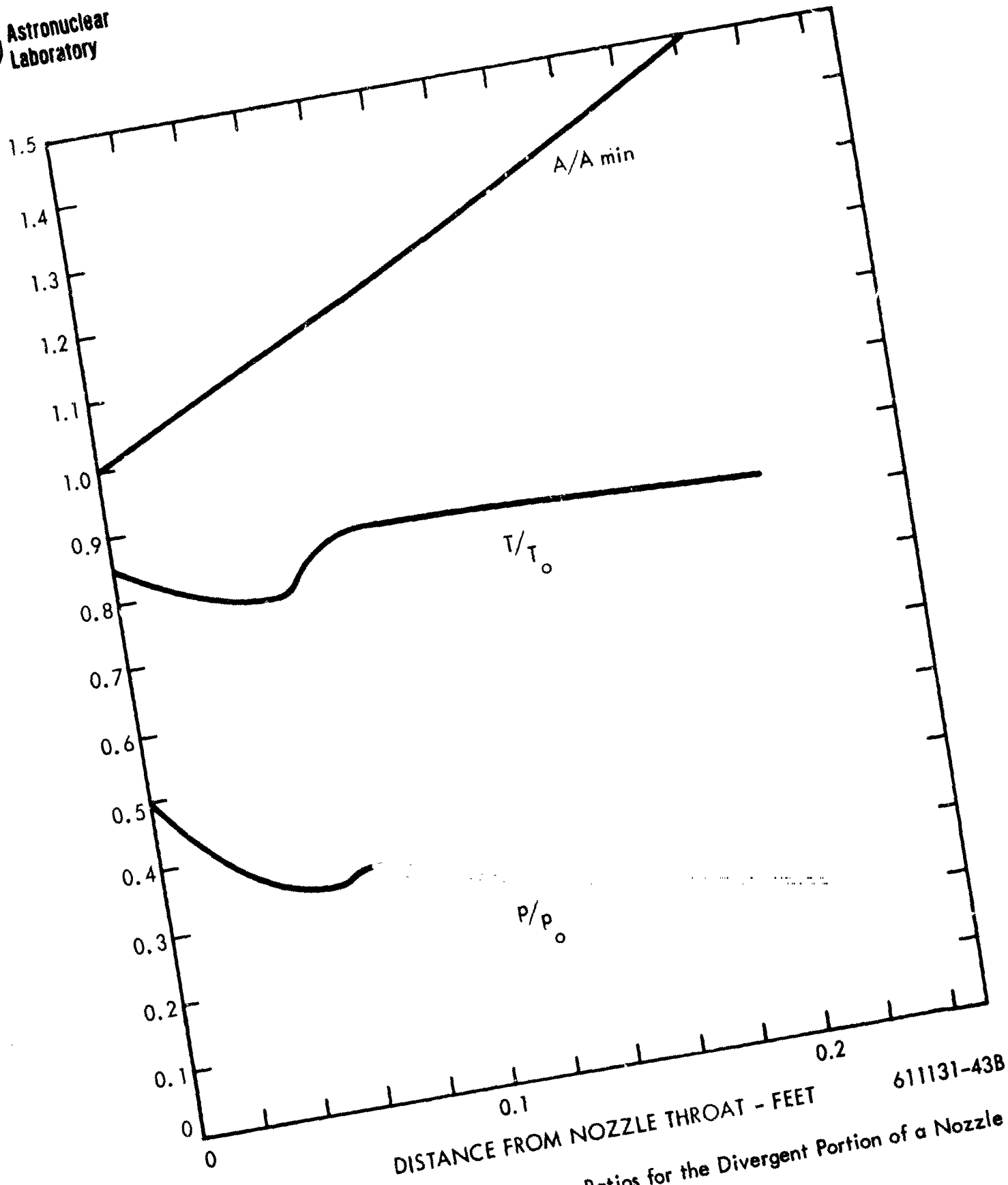

Figure B-1. Area, Temperature and Pressure Ratios for the Divergent Portion of a Nozzle with Condensing Flow

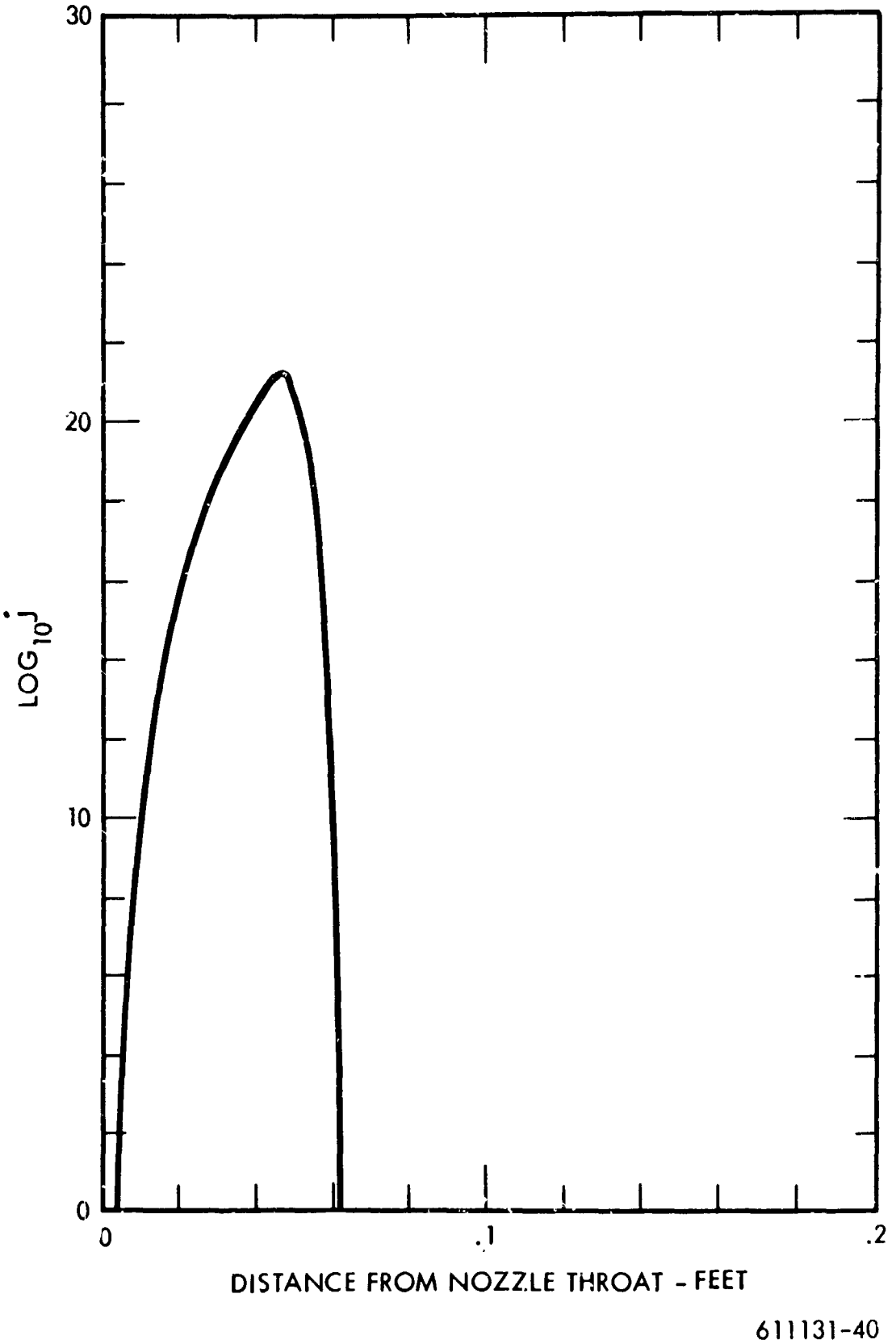

Figure B-2. Nucleation Rate in Divergent Portion of Nozzle

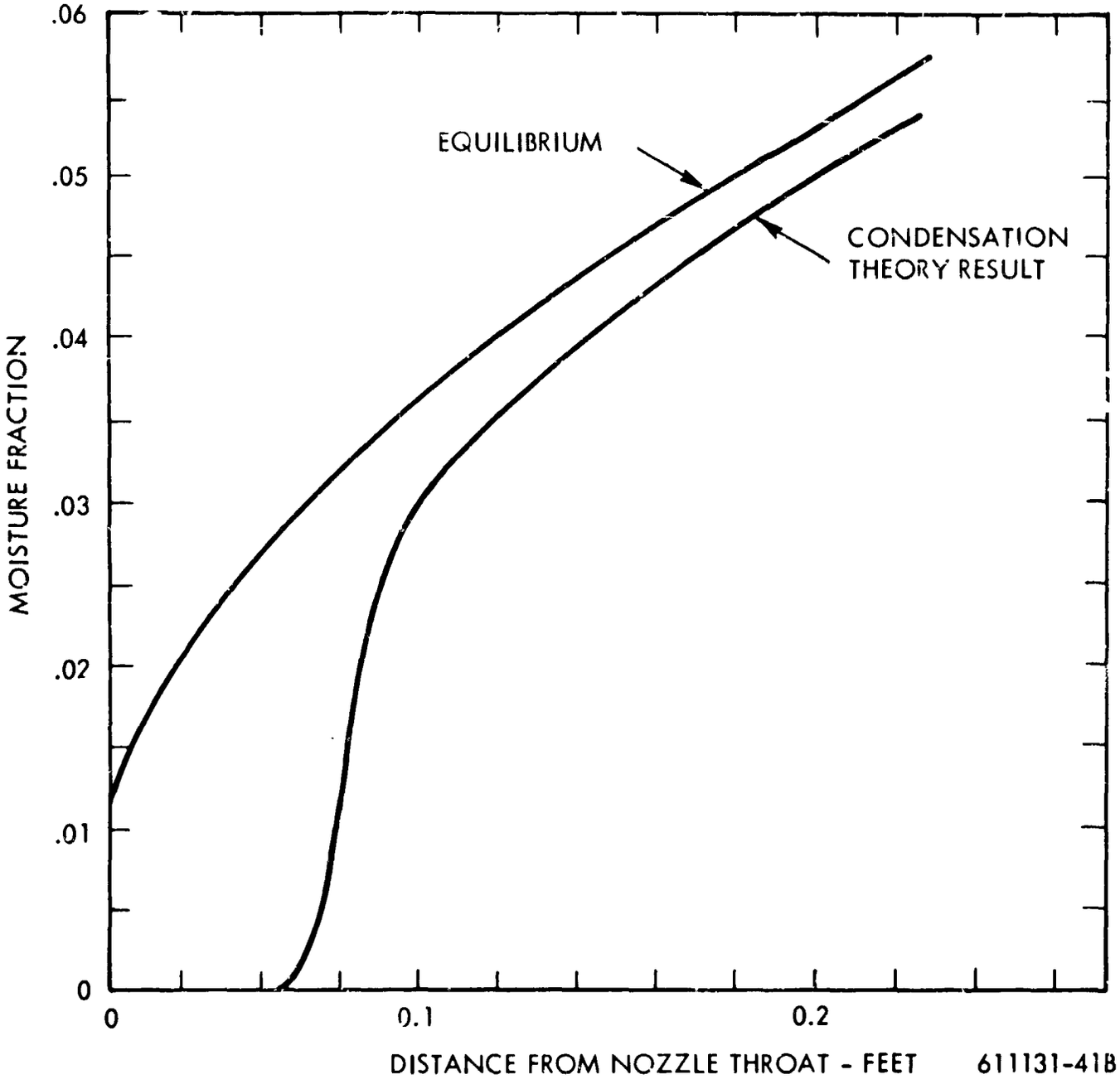

Figure B-3. Moisture Fraction in Divergent Portion of Nozzle

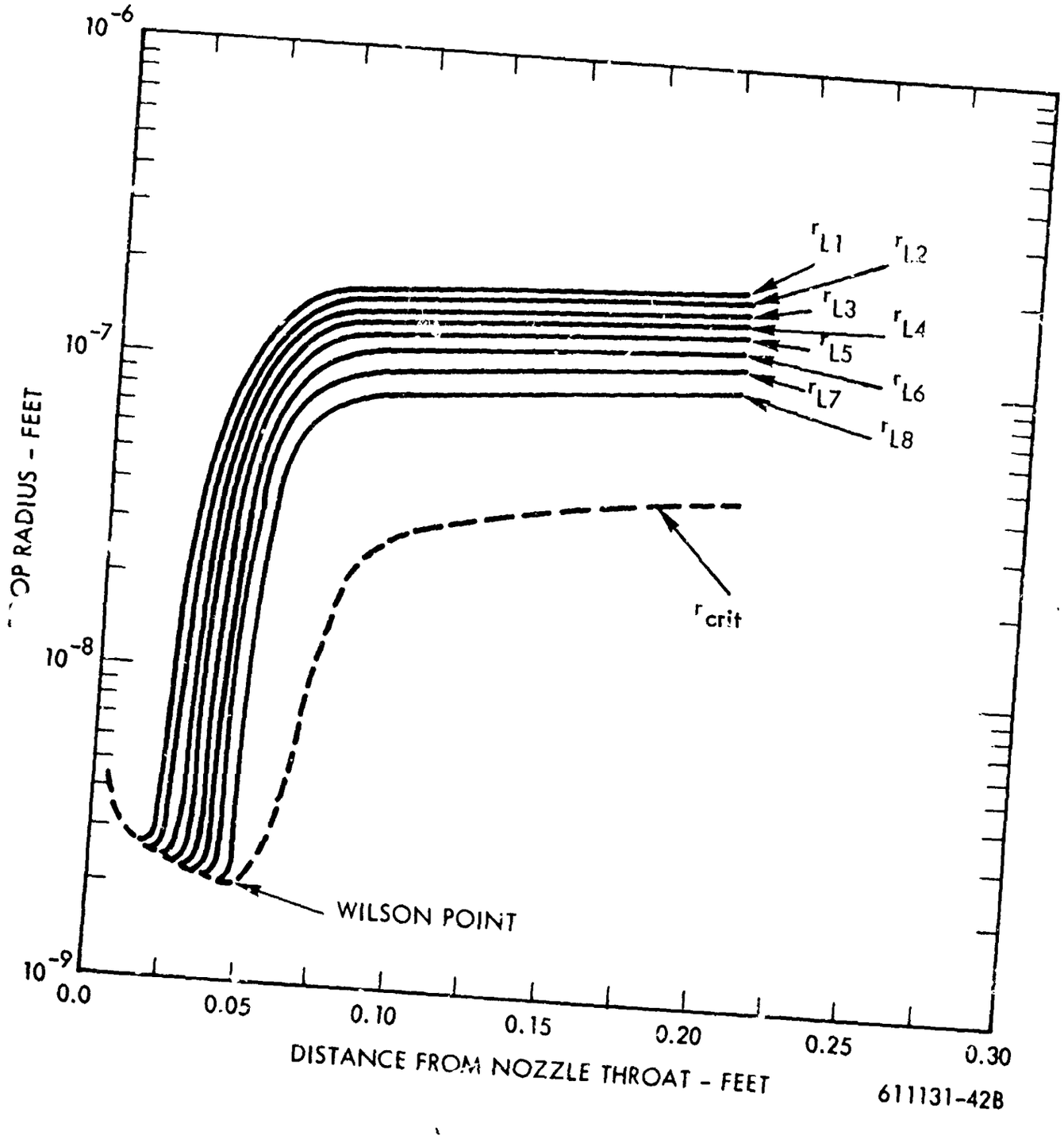

Figure B-4. Droplet Growth : the Divergent Portion of a Nozzle

TABLE B-2

Comparison of Condensation-Performance Program Results with Equilibrium Expansion at Mean Diameter for the Yankee Turbine

	Condensation-Performance Program Polytropic Efficiency $\eta_p = 1.0$				W Steam Division Program Equilibrium Moisture			
	Pressure (psia)	Axial Velocity (fps)	Temperature (°F)	Moisture	Pressure (psia)	Axial Velocity (fps)	Temperature (°F)	Moisture
Inlet	57.5	119.7	269	0	59.2	---	292	0.010
Stator No. 1	50.7	165.8	247	0	51.9	165	283	0.017
Rotor No. 1	44.4	183.3	258	0.0165	45.3	180	274.9	0.0240
Stator No. 2	39.0	196.1	264	0.0303	39.7	192	267	0.0310
Rotor No. 2	34.3	199.8	257	0.0374	34.9	198	259	0.0380
Stator No. 3	30.6	192	250.5	0.0438	30.5	196	251.3	0.0440
Rotor No. 3	27.0	195	243	0.04997	26.5	202	243.2	0.0500

nearly approached equilibrium with a supercooling of only 0.6°F. A hand calculation indicated that sufficient droplet surface area was available for subsequent condensation to proceed with negligible supercooling.

During the expansion, the steam remained supersaturated throughout the first stator. Condensation began in the first rotor. The Wilson point was reached at 70% of the axial distance through the rotor and corresponded to 2.18% theoretical moisture. The total number of drops formed per pound of mixture was found to be 3.19×10^{14}. The number of these drops in each size group is given in table B-3 and the droplet radii of each group are presented in table B-4 at the exit of the blade rows. All droplets formed by the homogeneous nucleation are within a small size range by the time the third stage is reached, as can be seen from table B-4. As the flow proceeds through the turbine, the spread between maximum and minimum sized droplets decreases. This is explained by noting that they all have approximately the same lifetime and that smaller droplets tend to grow slightly faster than larger ones.

TABLE B-3

Distribution of Droplets Among the Various Groups in the Yankee Turbine, Each Group of Uniform Size. Results Obtained for Polytropic Efficiency $\eta_p = 1.0$.

Group	Number (drops/lb)	Percent of Total
1	7.20×10^{10}	0.023
2	3.15×10^{11}	0.099
3	1.10×10^{12}	0.348
4	4.20×10^{12}	1.32
5	1.54×10^{13}	4.84
6	9.16×10^{13}	28.8
7	2.06×10^{14}	64.5

TABLE B-4

Droplet Diameters in Microns in Each Size Group at the Exit of the Blade Rows in the First Three Stages of the Yankee Turbine. (Results are for $\eta_p = 1.0$)

Group	1st Stator	1st Rotor	2nd Stator	2nd Rotor	3rd Stator	3rd Rotor
1	-	0.58	0.64	0.67	0.69	0.71
2	-	0.54	0.61	0.63	0.65	0.68
3	-	0.51	0.58	0.61	0.63	0.65
4	-	0.47	0.55	0.58	0.60	0.61
5	-	0.44	0.51	0.54	0.57	0.59
6	-	0.38	0.46	0.49	0.52	0.54
7	-	0.33	0.41	0.45	0.47	0.49

Calculations based on equilibrium moisture were carried out for the remaining six stages in the turbine. These mean droplet sizes are presented in table B-5.

In addition to the adiabatic frictionless case, calculations were carried out for the first stage with an assumed polytropic efficiency $\eta_p = 0.85$. This resulted in a slight delay of the Wilson point and a reduction of the expansion rate at which the Wilson point occurred. The distribution among the relative sizes was very much like that for the case $\eta_p = 1.0$, and, likewise, the size range is expected to be quite small. The total number of droplets generated was 1.98×10^{14} droplets per pound. The mean droplet size based on equilibrium moisture are also given in table B-4 for the case $\eta_p = 0.85$.

The results of the present calculation can be compared with the theoretical results presented by Gyarmathy and Meyer[12]. For the two cases described by $\eta_p = 1.0$ and $\eta_p = 0.85$, the expansion rate at the Wilson point was $\dot{P} = 345$/sec and 290 /sec respectively. At a pressure of approximately 3 atmospheres and the foregoing expansion rates, Gyarmathy and Meyers'[12] results give 6.1 and 10^{13} and 4.5×10^{13} droplets/lb. Thus, the

TABLE B-5

Mean Droplet Diameter Based on Equilibrium Moisture and Number of Drops Obtained from Condensation Performance Program for Yankee Turbine

	$\eta_p = 1.0$	$\eta_p = 0.85$
	Mean Diameter (microns)	Mean Diameter (microns)
1st Stator	-	-
1st Rotor	-	-
2nd Stator	-	-
2nd Rotor	0.470	0.568
3rd Stator	0.495	0.595
3rd Rotor	0.52	0.62
4th Stator	0.54	0.648
4th Rotor	0.56	0.67
5th Stator	0.58	0.695
5th Rotor	0.60	0.72
6th Stator	0.62	0.738
6th Rotor	0.635	0.757
7th Stator	0.65	0.785
7th Rotor	0.67	0.806
8th Stator	0.695	0.834
8th Rotor	0.71	0.853
9th Stator	0.73	0.877
9th Rotor	0.755	0.908

number of droplets per pound obtained by the present calculations is greater by factors of 5.2 and 4.4 respectively as compared to Gyarmathy. The mean radii would then be smaller by factors of 1.73 and 1.64 respectively for the two cases.

Part of the disagreement is due to the present method of solution in which drops are not permitted to grow immediately upon being formed. This lag tends to overestimate the number of drops formed. Additional factors causing disagreement may be differences in property values such as surface tension which have a strong effect on the nucleation rate.

9.0 EFFECT OF MOISTURE AT TURBINE INLET

The complete Yankee Atomic turbine system consists of high pressure turbines and low pressure turbines in series. The exhaust of the high pressure turbines contains 11% to 12% or more moisture and is fed to a moisture separator in the line between the high and low pressure turbines. By measurement, the moisture fraction of the steam leaving the separator is about 1%. This moisture fraction is then carried over into the inlet of the low pressure turbines. The low pressure turbine condensation calculations assumed that this moisture was present in the supersaturated state at the entrance to the turbine.

A simple model is proposed to obtain the probable effect on the condensation calculations of assuming that the 1% carryover is in the form of drops of 2 micron and 0.8 micron average diameter. If the carryover is in the form of 0.8 micron average diameter drops, these drops would provide adequate surface area for all subsequent condensation without additional nucleation. If the carryover drops are as large as 2 microns in diameter, additional nucleation would occur before the turbine exit.

To our knowledge, no accurate measurements of these carryover drop sizes have been made. Based on the incomplete measurements reported by Campbell-Murray in commenting on a paper by Gardner[13], it seems likely that on a weight percentage basis, these drops are from 5 to 10 microns in diameter, rather than from 1 to 2 microns. If this is the case, then ignoring the carryover, except for its heat balance effect, is a reasonable procedure.

The following model can be used to estimate the growth of carryover droplets and the extent of supercooling as the steam flows through the turbine. Assume that the overall equilibrium expansion process is known and that the effects of supersaturation do not substantially

effect the steam velocity or work done by the steam. Thus, we know the equilibrium moisture at inlet and exit from each blade row and the axial velocity. The droplet growth equation used by Gyarmathy[12] is:

$$(r + \hat{A}) \frac{dr}{dz} = \frac{k_v (T_s - T_v) (1 - r/r_{crit})}{\rho_L U_a h_{fg}} , \tag{33}$$

where:

$$\hat{A} = 2.38 U_v / \sqrt{R_g T_v \sigma} . \tag{34}$$

Using a constant enthalpy process between supersaturated and equilibrium states as a means of relating supercooling to moisture deficiency (the equilibrium moisture minus the actual moisture), one obtains:

$$\Delta T = T_s - T_v = \frac{h_{fg}}{C_{p_v}} (\Delta y) = \frac{h_{fg}}{C_{p_v}} (y_e - y). \tag{35}$$

Also, if it is assumed that the mixture is near equilibrium (low supercooling), the critical radius will be large compared to the actual drop radius. The growth equation then becomes:

$$(r + \hat{A}) \frac{dr}{dz} = \frac{k_v \Delta y}{\rho_L U_a C_{p_v}} \tag{36}$$

Within any given row, T_v remains approximately constant as does the axial velocity. Then, if one assumes Δy to vary linearly from inlet to exit with U_a and T_v assumed constant, the equation can be integrated to give:

$$\left(\frac{r^2}{2} + \hat{A}r \right) - \left(\frac{r_i^2}{2} + \hat{A}r_i \right) = \frac{k L}{\rho_L U_a C_{p_v}} \frac{\Delta y + \Delta y_i}{2} , \tag{37}$$

where L is the axial length of the blade row. Since the number of drops at entrance is known and their size may be assumed to be uniform, the moisture fraction can be expressed in terms of the droplet size:

$$y = 4\pi \rho_L N r^3/3, \tag{38}$$

where N is the number of droplets per pound of mixture. Then the definition of y is used to obtain the average moisture deficiency.

$$\Delta y + \Delta y_i = (y - y_e) + (y_i - y_{ei}) \tag{39}$$

Substituting from equations 38 and 39 into equation 37 gives.

$$\left(\frac{r^2}{2} + Ar + Cr^3\right) - \left(\frac{r_i^2}{2} + Ar_i + Cr_i^3\right) = B\,(y_e + y_{ei} - 2\,y_i)\,, \tag{40}$$

where

$$B = \frac{k_v\, L}{2\,\rho_L\, U_a\, C_{p_v}} \tag{41}$$

and

$$C = \left(\frac{4\pi\,\rho_L\, N}{3}\right) B \tag{42}$$

Let $$\hat{F}(r) = \hat{A}r + \frac{1}{2}\,r^2 + Cr^3\,, \tag{43}$$

then the droplet growth equation becomes:

$$\hat{F}(r) = \hat{F}(r_i) + B\,(y_e - 2\,y_i + y_{ei}). \tag{44}$$

Hence, if y_i is known at the entrance, and the entrance and exit equilibrium moisture fractions are known, equation 44 can be solved graphically to obtain the new drop radius. Then, equation 38 gives the new moisture fractions and equation 35 gives the supercooling. The solution of equation 44 is greatly simplified if $\hat{A}$, B, and C are constant throughout the turbine. This can be satisfied if L/U_a is constant and if T_v does not vary appreciably. For the Yankee turbine, the values of L/U_a for the 18 blade rows ranged from 1.4×10^{-3} sec to 2.72×10^{-3} sec with the average value being 1.93×10^{-3} sec. The temperature at inlet is 752°R and at exit 557.5°R. If $T_v = 650°R$ is used, the largest error in the value of $\hat{A}$ due to this assumption is 8%. Table B-6 compares the moisture distributions obtained using this analysis for equilibrium inlet moisture with diameters of 0.8 micron and 2 microns with the equilibrium theory and with the result of condensation theory. The table also gives supercooling at exit from each stage. The number of drops per pound in the three modes compared in table B-6 was 3.19×10^{14} from nucleation theory, 1.1×10^{12} for 2 micron initial diameter and 1.74×10^{13} for 0.8 micron initial diameter.

TABLE B-6

Comparison of Moisture and Subcooling for Various Inlet Steam Conditions Assumed for Yankee Turbine

	Equilibrium Moisture	Condensation Performance Program, $\eta_p = 1.0$		Initial 2μ Droplets Diameter		Initial 0.8μ Droplets Diameter	
	y_e	y	ΔT, °F	y	ΔT, °F	y	ΔT, °F
Inlet	0.010	0	23	0.010	0	0.010	0
1st rotor	0.024	0.0165	15.8	0.0132	22	0.0185	11
2nd rotor	0.038	0.0374	0.7	0.024	28	0.036	4
3rd rotor	0.050	0.04997	0.6	0.037	26	0.048	4
4th rotor	0.063	-	-	0.055	16	0.061	4
5th rotor	0.077	-	-	0.066	22	0.075	4
6th rotor	0.091	-	-	0.080	22	0.090	2
7th rotor	0.108	-	-	0.100	16	0.104	8
8th rotor	0.130	-	-	0.118	24	0.130	1
9th rotor	0.152	-	-	0.136	32	0.142	20

10.0 CONDENSATION RESULTS FOR POTASSIUM TURBINE

The same set of equations and computer program used to describe the steam condensation was also used to predict condensation in the potassium turbine. In the present analysis as well as those of Glassman [6] and Hill [7], it has been assumed that condensation of liquid metal vapors is determined by the same mechanisms as water vapor. One important influence which is believed to affect the nucleation process and the location of the Wilson point is the association of liquid metal vapors. Frisch and Willis [14] neglect the thermodynamic influence of association and theoretically predict increased nucleation rates. Katz, Saltsburg, and Reiss [3] predict a decrease in nucleation rate by including the thermodynamic effect. Their modified theory would delay the Wilson point relative to the present analysis.

The inlet potassium vapor was also assumed to be supersaturated with one percent equivalent moisture. The results of the condensation performance program are compared with the equilibrium calculations in table B-7. There is considerable disagreement between the two sets of calculations. This disagreement is for the most part due to the assumption of supersaturation. Supersaturated flow has greater density than the equilibrium flow and is assumed to have a specific heat ratio (γ) of 1.6. Since the equilibrium flow has an effective specific heat ratio near 1.2[15], there are appreciable differences in expansion characteristics. Additional differences are due to slight disagreement in area ratios.

TABLE B-7

Comparison of Condensation and Equilibrium Performance Calculations for Potassium Turbine.

	Condensation Performance Program				Equilibrium Calculations			
	Static Pressure (lb/in^2)	Axial Velocity (ft/sec)	Static Temperature (^oR)	Moisture Fraction (lb/lb)	Static Pressure (lb/in^2)	Axial Velocity (ft/sec)	Temperature (^oR)	Moisture Fraction (lb/lb)
Inlet	38.2	360	1996	0	38.2	-	2060	0.01
Stator 1	31.3	296	1882	0	28.1	346	1987	0.035
Rotor 1	26.5	372	1966	0.04	22.6	408	1940	0.048
Stator 2	24.2	269	1954	0.047	15.9	398	1869	0.069
Rotor 2	-	-	-	-	11.9	543	1811	0.085

The condensation is predicted to occur in the first rotor passage with the Wilson point being reached at 68% of the axial distance through the rotor. The theoretical moisture was 3.72% at the Wilson point and $\dot{P}$ was 3000/sec which is a rapid expansion rate. The drop size distribution at the end of the first rotor is given in table B-8.

TABLE B-8

Moisture and Drop Size Distribution at Exit from First Stage Rotor of Potassium Turbine

Group	Number of Drops	Droplet Diameter (microns)	Moisture Fraction
1	7.3×10^{11}	0.384	0.00003
2	2.8×10^{12}	0.362	0.00011
3	1.3×10^{13}	0.339	0.0004
4	4.3×10^{13}	0.321	0.0012
5	1.5×10^{14}	0.295	0.0032
6	6.2×10^{14}	0.268	0.0097
7	2.8×10^{15}	0.223	0.0252

The total number of drops per pound was 3.6×10^{15}, and the average diameter was 0.238 microns at the exit from the first rotor.

The calculations were performed for a second case with all properties and turbine dimensions as before, except that surface tension was reduced by 20%. In this case, condensation occurred at about two-thirds of the way through the first stator. The Wilson point occurred at 2.5% theoretical moisture and the expansion rate was $\dot{P}$ = 1700/sec. The total number of drops formed was 6.68×10^{15} per pound. Thus, a lower surface tension has the effect of shifting the Wilson point toward saturation, and also of increasing the number of drops formed. There were almost twice as many drops formed for the case of reduced surface tension even though the expansion rate was much lower. The pressure drop and axial velocity at exit from the first rotor were in better agreement with equilibrium calculations for this case since the condensation occurred in the first stator.

C. BULK AND BOUNDARY LAYER FLOWS AND DEPOSITION OF CONDENSATE

W. K. Fentress

1.0 INTRODUCTION

This section deals with the vapor and liquid flow in turbines after the condensate particles have grown to substantial size (for condensate particles). The presentation is in terms of an examination of a large central station type steam turbine and of a very small two-stage potassium turbine. The steam turbine is the lo-pressure turbine of the Yankee Atomic Plant. The two-stage potassium turbine is a simulation* for erosion discussion purposes of the General Electric two-stage potassium test turbine of NASA Contract NAS 5-1143.

In Section 2, the parameters of the two example turbines are repeated from Volume I to provide a reference for the reader.

Section 3 describes numerically the bulk flow as a function of radial position at inlet and exit of the four rows of the potassium turbine and the last four rows of the steam turbine. The local wake and boundary layer flow aft of the last stator row is described, numerically, for a position 3/4 of the way towards the tip of the blade from the hub. In the steam turbine, in a technical sense, the wake of the last stator is of large size and persists to the plane of the rotor. However, the wake velocity deficit is small beyond 1 inch downstream of the stator in the direction of flow. In the potassium turbine because of the smaller spacing between rows, a substantial velocity deficit persists to the plane of the rotor. While the depth of wake velocity decrement predicted for the Yankee turbine, taken in conjunction with maximum drop size stability criteria, give reasonable agreement (see Section D) with observations on the maximum size of drops striking the rotor of an English turbine, the maximum size predicted is only on the order of 75% of the observed maximum size. Additional analytic effort in the area of stator vane wakes is in order since the calculations use an arbitrary correction to allow for finite trailing edge thickness.

---

* The two-stage potassium turbine design presented here was constructed on the basis of the readily available data on the G.E. two-stage potassium test turbine from References 1, 2, and 3. These references do not contain information on the stationary blading sections, or the turbine seal arrangement and appear to be inconsistent with respect to stationary row gauging. Therefore, the design as presented has Westinghouse stationary rows. It is not believed that this makes any important difference with respect to the erosion model discussion.

In connection with the bulk flow through the turbine, it may be observed that the condensate particles would have a tendency to drift outward with respect to the vapor flow. This is because of their large inertia compared to gas molecules in a centrifugal field. However, in the Yankee turbine (certainly also in the potassium turbine) this radial drift velocity is in the order of an inch or so per second in a stream of hundreds of feet per second axial velocity. The significant observation is that the fog particles are "locked" to the flow in a radial as well as axial direction for most practical purposes.

Section 4.0 discusses the collection of the condensate fog particles on the nose section of blade surfaces from the standpoint of an impingement collection analysis as by Brun, Lewis, Perkins, and Serafini [4] for "continuum flow" and as by Gyarmathy [5] for "slip flow". Collection on the concave surface of the blades is examined by the method of Gyarmathy [5]. The basic treatment of collection by both methods is the same except for evaluating the drag coefficient of the particle. The work of Brun et al varies the drag coefficient as a function of Reynolds Number and neglects the effect of Knudsen Number as a measure of the continuum nature of the flow. The work of Gyarmathy uses a "Stokes Law" drag coefficient with an empirical Knudsen Number correction to allow for the "slip flow" which exists because of the small size of the fog particles.

Numerical differences for collection between the two impingement methods vary by factors of 2 to infinity at the particle sizes of interest in turbines.* It is probable that in the regime of interest in turbines both the Reynolds Number correction and Knudsen Number corrections to drag coefficient should be applied. The Reynolds Number correction is the least important in the range of interest. In any case, the numerical discrepancies between Gyarmathy's calculations and those presented by Brun et al are not fully explained by reconciling the Knudsen and Reynolds Numbers corrections. In addition as observed by Gardner [6] other mechanisms besides direct impingement may play an important role in the collection of sub-micron particles. Since calculable differences are substantial, it is recommended that tests on collection of sub-micron particles under turbine like conditions be conducted.

---

*Both references present results in terms of dimensionless plots which were applied to the particular physical situation of the two turbines examined.

Section 5.0 uses the viscous terms of the Navier-Stokes equation to calculate rotor and stator blade liquid film thicknesses and velocities as a function of assumed uniformly distributed liquid flow rate. In the case of the stators it is assumed that the sole force moving the liquid along the blade surface is the shear force exerted by the bulk flow. In the case of rotors, the centrifugal force is added to that of the bulk flow shear force. There is an additional force present because of the increase in vapor static pressure from hub to tip to establish bulk flow radial equilibrium. However, this force is much smaller than the axial shear force which in turn is much smaller than the centrifugal force. The bulk radial pressure field has a negligible tendency to move liquid from tip to hub.

2.0 EXAMPLE TURBINES

2.1 Steam Turbine

The steam turbine for the example calculations is the low-pressure turbine of a tandem compound steam turbine. This turbine is used in the Yankee atomic power plant.

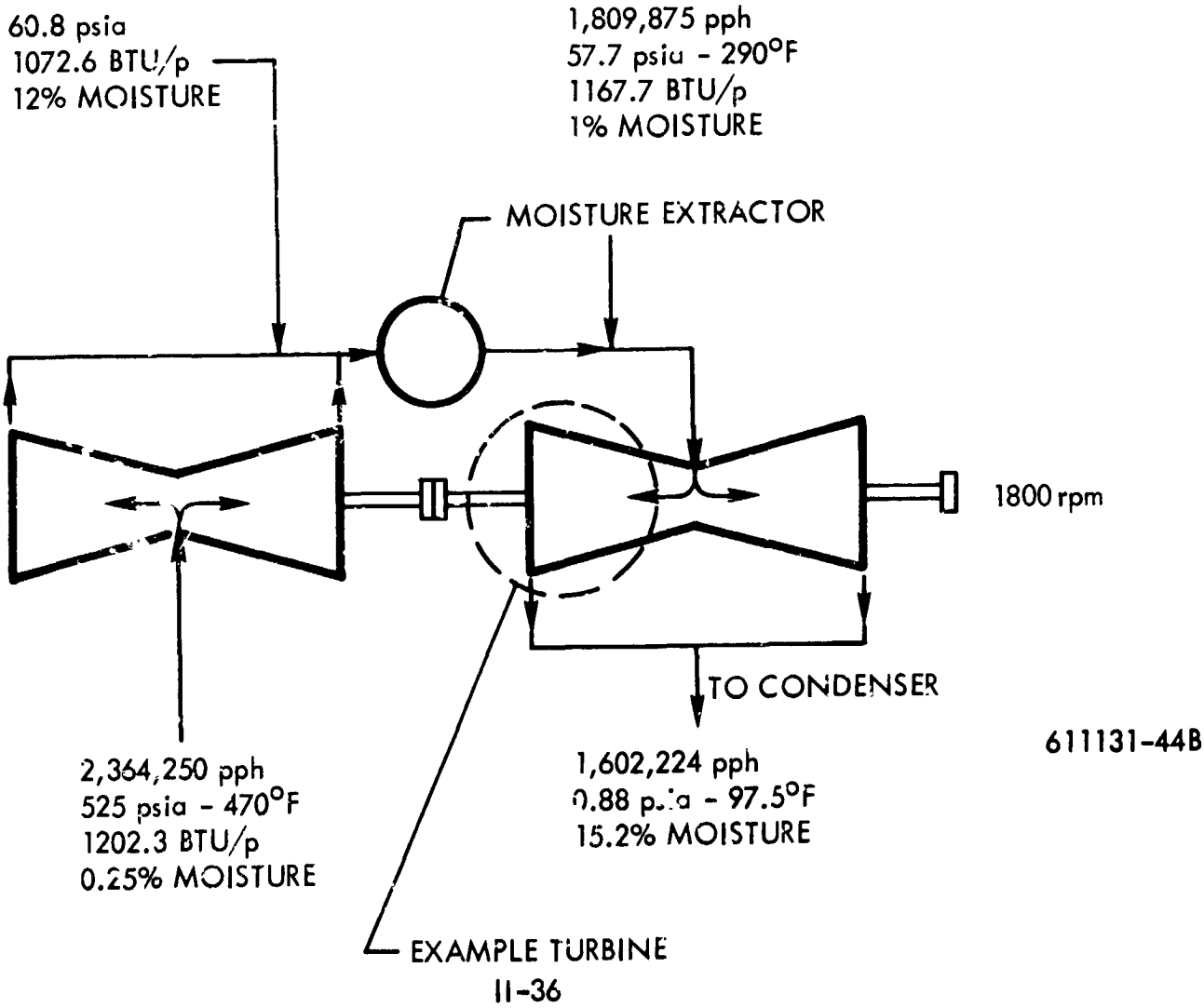

The reasons for selecting this particular turbine are threefold: the blade erosion has been observed for an approximate period of five years, the exhaust moisture content is high, and the expansion is entirely below the saturation line. The latter feature is similar to that postulated for alkali metal space power systems.

Geometric and fluid dynamic data for design operation are given in table C-1. As shown, the moisture content of the vapor varies from 1% at turbine inlet to about 15% at exit, the static pressure varies from 59.2 to 0.88 psia, the vapor specific volume from 8.08 to 318.9 ft^3/lb, the maximum tip speed is 1238 fps, the axial spacing varies from 0.5 in. at inlet to 1.9 in. at exit, the trailing edge thickness of the blades is in the order of 0.055 to 0.075 in. at the exhaust end and the last stage rotor blade has an effective mean diameter of 117.5 in. with an effective height of 40 in.

2.2 Two-Stage Potassium Turbine

The two-stage potassium test turbine of Contract NAS 5-1143 is, to our knowledge, the only multi-stage alkali metal vapor turbine of a space type which has been operated for a substantial length of time (some 2,000 hours). As such, it is an obvious choice as an example turbine in connection with the analytical investigation of turbine blade erosion. While the two-stage potassium test turbine was designed as the third and fourth stages of a five-stage turbine for a space Rankine power plant[2], the actual operation has been as though it was the first two stages of a turbine insofar as the inlet vapor quality is concerned.

For reasons which have been explained previously, the two-stage potassium turbine design given here approximates the test turbine design, but is not identical. The design condition of operation was taken from Reference 1 and is:*

Speed - 19,100 rpm	Flow - 2.64 pps
Inlet temperature - 1600°F	Inlet pressure - 38.2 psia
Inlet moisture content - 1%	Total to total pressure ratio - 2.95

*The actual test operating conditions used by G. E.[14] during the endurance test of their two-stage turbine were more nearly: inlet temperature-1475-1510°F, inlet pressure-25.-26. psia., and inlet moisture content-<1%.

Other fluid dynamic and geometric data are given in table C-2, assuming complete thermodynamic equilibrium at all times in the turbine. As shown, the moisture content of the vapor varies from 1% at turbine inlet to 8-1/2% at exit, the static pressure varies from 38.2 to 11.9 psia, the vapor specific volume from 13.2 to 36.8 ft^3/lb, the maximum tip speed is 805 ft/sec, the trailing edge thickness of the blades is 0.015 in., the axial spacing between rows is 0.2 in. and the effective mean diameter of the last stage rotor blade (bucket) has an effective mean diameter of 8.71 in. with an effective height of 0.937 in.

TAB

Yankee Ste

Row No.	9th Rotor	9th Stator	8th Roror	8th Stator	7th Rotor	7th Stator	6th Rotor	6th Stator
Effective Blade Height, in.	40.00	37.44	27.23	24.46	21.01	19.47	15.07	14.04
Effective Mean Diameter, in.	117.50	118.40	110.64	109.41	106.01	104.78	100.13	98.54
Average Guaging	0.600	0.421	0.433	0.341	0.341	0.279	0.330	0.291
Exit Flow Angle, deg	37.0	25.0	25.6	20.0	20.0	16.2	19.2	16.9
Static Pressure, psia	0.88	1.515	2.313	3.411	5.072	6.573	8.745	10.695
Moisture Content	0.152	0.140	0.130	0.120	0.108	0.100	0.0911	0.0846
Temperature, °F	97.5	115.9	131.5	146.5	162.8	174.1	187.0	196.4
Specific Volume, cfpp	318.9	194.5	131.9	92.6	64.7	51.19	39.59	33.03
Jet Velocity, fps	1133.	1057.	1016.	1026.	857.0	903.7	779.8	811.5
Mean Wheel Speed, fps**	922.8	929.9	869.0	859.3	832.6	823.0	786.4	773.7
Tip Wheel Speed, fps**	1237.0	1224.0	1082.8	1051.4	997.6	975.9	904.8	884.2
Inlet Flow Angle to Next Row, deg	90.0	86.27	83.92	73.32	65.34	79.52	97.74	89.62
Inlet Velocity to Next Row, deg	690.	456.	453.	378.	297.	266.	265.	242.
Blade Reynolds No. x 10^{-5} ***	1.5	5.9	2.2	7.9	3.4	8.2	5.7	6.1
Steam Flow, pph x 10^{-3}	801.1	801.1	801.1	801.1	801.1	801.1	801.1	801.1
Centrifugal Force, G's								
Mean Diameter	5400.							
Tip Diameter	7220.							
Axial Space Stator Exit to Rotor Inlet, in.	1.9		1.7		1.1		0.6	
Trailing Edge Thickness, in.	0.066	0.077	0.065	0.063	0.060	0.055	0.045	0.015
Blading Material	12% Chromium Steel							
Stellite Shields	yes		yes		yes		yes	

*Generally, values are for exit of blade row.

**Stator blade "wheel speed" is that speed equivalent to a rotor of the same diameter.

***Reynolds Number based on the blade chord and exit velocity.

C-1

n Turbine

5th Rotor	5th Stator	4th Rotor	4th Stator	3rd Rotor	3rd Stator	2nd Rotor	2nd Stator	1st Rotor	1st Stator	Inlet
12.77	11.81	10.57	9.98	9.15	8.47	7.42	6.84	6.49	6.30	7.55
96.77	95.25	93.50	92.51	91.35	90.27	89.28	88.64	88.35	88.10	89.35
0.270	0.266	0.300	0.286	0.278	0.274	0.277	0.268	0.248	0.231	--
15.7	15.4	17.5	16.6	16.1	15.9	16.1	15.5	14.4	13.4	--
13.331	16.367	19.386	22.748	26.473	30.521	34.852	39.679	45.345	51.931	59.2
0.0768	0.0693	0.0630	0.0560	0.0500	0.0440	0.0380	0.0310	0.0240	0.0170	0.010
207.1	217.5	226.3	234.9	243.2	251.3	259.0	266.8	274.9	283.4	292.0
27.11	22.56	19.39	16.81	14.68	12.93	11.50	10.25	9.11	8.08	--
800.0	744.2	727.3	709.7	700.6	686.5	692.7	699.0	705.4	689.1	--
760.0	748.1	734.4	726.6	717.5	709.0	701.2	696.2	693.9	692.0	--
860.3	840.8	817.9	805.0	789.3	775.5	759.5	749.9	744.9	741.4	--
87.36	98.72	100.5	103.1	103.1	104.8	100.94	97.2	93.7	97.8	90.0
222.	203.	224.	210.	202.	196.	198.	192.	180.	165.	--
7.6	6.4	5.3	6.3	5.2	11.6	8.4	8.2	9.5	14.7	--
801.1	801.1	904.9	904.9	904.9	904.9	904.9	904.9	904.9	904.9	904.9

	0.5		0.5		0.5		0.5	4050.	0.5	
0.045	0.015	0.038	0.0125	0.037	0.010	0.038	0.010	0.033	0.010	
yes		yes		no		no		no		no

11-38 (2)

TABLE C-2

Potassium Turbine, Row by Row Mean Diameter Data*

	Inlet	1st Stator	1st Rotor	2nd Stator	2nd Rotor
Effective blade height, in.	0.595	0.745	0.761	0.992	0.937
Effective mean diameter, in.	7.575	8.078	8.120	8.677	8.713
Average guaging	-	0.322	0.435	0.360	0.520
Exit flow angle, deg.	-	18.75	25.8	21.1	31.45
Static pressure, psia	38.2	28.03	22.6	15.92	11.9
Moisture content	0.01	0.035	0.048	0.069	0.085
Temperature, ^{o}R	2060.	1987.	1940.	1859.	1811.
Specific volume, cfpp	13.2	17.2	20.8	28.3	36.8
Jet velocity, fps	-	1075.	939.	1105.	1041.
Mean wheel speed, fps**	-	673.	681.	724.	726.
Tip wheel speed, fps**	-	-	737.	-	805.
Incident flow angle to next row row, deg.		45.0	68.4	52.4	73.4
Incident velocity to next row, fps	344	490	438	503	566.
Blade Reynolds No. x 10^{-5}***		3.66	1.81	2.78	1.38
Mass flow, pps	2.64	2.64	2.64	2.64	2.64
Centrifugal force (G's),					
mean diameter	-	-	42100	-	45200
tip diameter	-	-	45900	-	50000
Axial space, stator exit to rotor inlet, in.			0.2		0.2

*Values are for exit of blade row unless otherwise indicated.

**Stator blade "wheel speed" is the equivalent speed for a rotor of the same diameter.

***Reynolds No. based on the blade chord and exit velocity.

3.0 VAPOR FLOW PATHS

The flow in the example turbines are described from the standpoint of the axisymmetric bulk flow downstream of the blade rows, the boundary layer on the surface of the blades, and the wakes downstream of the blade rows.

3.1 Axisymmetric Bulk Flow Downstream of the Blade Rows

The row by row fluid properties are calculated by a computer program that has been used for a number of years by the Westinghouse Steam Division. Inputs to this code are turbine geometry (diameter, blade heights, and blade angles) and turbine duty (flow, rpm, inlet pressure and temperature, and outlet pressure). Calculations are made by using continuity, energy, momentum, and thermodynamic relations. Simple radial equilibrium and constant specific heat ratio (γ) gas properties are assumed. Actually, the program provides for full equilibrium (effect of the meridional stream tube curvature) using steam properties, but, by the option of simple radial equilibrium and constant gas properties, the program is applicable to other working fluids such as liquid metals with a higher degree of flexibility. It can be shown that these assumptions have little effect on the accuracy of the results.

Outputs from the program are row by row fluid conditions (pressure, temperature, velocity) with respect to blade height. Row by row properties for the mean diameter section have already been given in tables C-1 and C-2. Row by row data with respect to blade height are shown by table C-3 for the eighth and ninth stage blade rows of the Yankee steam turbine. Similar information on the two-stage potassium turbine is shown in table C-4.

3.2 Boundary Layer on the Surface of the Blades

Boundary layer calculations were performed by a Westinghouse Steam Division computer code based on the method of Truckenbrodt[7]. This program is briefly described in the following outline:

Input to code:

1) Blade surface velocity distribution - by other computer program
2) Blade Reynolds Number (Re_1) based on exit fluid properties and chord length

TABLE

Fluid Properties Along the Height
Yankee Ste

Row	8th Rotor Exit					8th Rotor Inlet		
Approximate section	Hub	1/4	Mean Dia.	3/4	Tip	Hub	1/4	Mean Dia.
Diameter, inches	80.27	96.21	112.15	128.09	144.03	82.51	96.51	110.5
Gauging, inches	0.538	0.489	0.449	0.416	0.385			
Exit flow angle, degrees	32.5	29.2	26.6	24.6	22.6	19.0	18.7	18.9
Static pressure, psia			2.263			2.612	3.025	3.3
Temperature, °F			130.4					145.7
Specific volume, cfpp			134.0			118.8	103.9	94.8
Jet velocity, fps	848.9	932.5	1015.1	1095.9	1184.7	1282.2	1138.8	1028.4
Axial velocity, fps	456.7	456.0	455.8	455.9	456.1	417.8	365.4	333.6
Wheel speed, fps	630.4	755.6	880.8	1006.0	1131.2	648.0	758.0	867.9
Inlet flow angle to next row, degrees	79.15	82.6	86.95	91.1	95.2	36.52	48.74	72.55
Inlet velocity to next row, fps	465.0	459.8	456.4	456.0	459.8	702.0	486.0	349.7

Row	9th Rotor Exit					9th Rotor Inlet		
Approximate section	Hub	1/4	Mean Dia.	3/4	Tip	Hub	1/4	Mean Dia.
Diameter, inches	76.84	97.27	117.7	138.2	158.6	78.63	98.63	118.63
Gauging, inches	0.733	0.674	0.618	0.560	0.499			
Exit flow angle, degrees	47.1	42.3	38.3	34.8	31.8	26.3	24.4	24.2
Static pressure, psia			0.88			1.011	1.285	1.4
Temperature, °F			97.5					115.6
Specific volume, cfpp			318.0			282.0	226.0	197.5
Jet velocity, fps	949.0	1030.0	1117.0	1211.0	1315.0	1390.1	1192.5	1051.2
Axial velocity, fps	695.0	693.0	693.0	694.0	695.0	615.4	494.1	432.2
Wheel speed, fps	603.5	764.0	924.4	1085.4	1245.3	682.6	774.6	931.7
Inlet flow angle to next row, degrees	86.5	90.0	93.9	97.3	100.5	44.4	57.3	86.5
Inlet velocity to next row, fps	696.0	693.0	695.0	699.0	706.0	880.0	583.6	433.0

11-41

C-3

· the Blade; Eighth and Ninth Stages
m Turbine

8th Stator Exit					8th Stator Inlet					
3/4	Tip	Hub	1/4	Mean Dia.	3/4	Tip	Hub	1/4	Mean Dia.	3/4	T
124.51	138.51	83.41	97.41	109.41	123.41	137.41					
		0.343	0.346	0.350	0.358	0 3695					
19.4	20.0	20.4	20.2	20.5	21.0	21.7					
3.592	3.789	583	3.078	3.348	3.590	3.785			.991		
				145.7					162.2		
88.9	84.4	115.9	102.1	94.7	88.9	84.5			65.7		
940.2	868.4	1257.5	1120.6	1028.4	941.1	870.0					
312.5	297.6	440.0	388.2	360.0	337.4	321.5					
977.9	1087.8	655.1	765.1	859.3	969.3	1079.2					
106.26	132.43	40.98	53.60	73.87	105.05	130.10					
325.5	403.2	683.4	482.2	374.0	349.4	420.3					

9th Stator Exit					9th Stator Inlet					
3/4	Tip	Hub	1/4	Mean Dia.	3/4	Tip	Hub	1/4	Mean Dia.	3/4	T
138.63	158.63	78.4	98.4	118.4	138.4	158.4					
		0.428	0.428	0.432	0.440	0.453					
24.7	25.6	27.6	25.8	25.6	26.1	26.9					
1.637	1.751	1.021	1.289	1.487	1.635	1.746			2.263		
				115.6					130.4		
181.0	170.2	280.0	226.0	197.5	181.0	170.5			134.0		
945.0	862.9	1383.0	1190.0	1051.0	947.0	866.0					
395.7	372.1	641.0	518.0	454.0	417.0	392.0					
1088.8	1245.9	615.8	772.8	929.9	1067.0	1244.1					
120.2	141.5	46.5	60.1	87.7	119.6	140.3					
458.0	597.4	884.6	597.6	454.7	479.1	613.3					

(2)

Row	1st Stator Inlet					1st Stator Exit		
Appropriate section	Hub	1/4	Mean Dia.	3/4	Tip	Hub	1/4	Mean Dia.
Diameter, inches	6.98		7.575		8.17	7.28	7.68	8.08
Gauging, inches						0.3114	0.3160	0.3208
Exit flow angle, degrees						18.15	18.40	18.75
Static pressure, psia			37.86			26.59	27.36	28.03
Temperature, °R			2053.1			1980.6	1985.9	1990.9
Specific volume, cfpp			13.55			18.30	17.90	17.48
Jet velocity, fps						1158.8	1113.0	1072.2
Axial velocity, fps						360.9	351.7	344.0
Wheel speed, fps						606.6	639.9	673.2
Inlet flow angle to next row, degrees						36.1	40.2	45.1
Inlet velocity to next row, fps						612.3	544.8	485.3

Row	2nd Stator Inlet					2nd Stator Exit		
Appropriate section	Hub	1/4	Mean Dia.	3/4	Tip	Hub	1/4	Mean Dia.
Diameter, inches	7.385	7.815	8.246	8.677	9.107	7.677	8.177	8.677
Gauging, inches						0.3487	0.3509	0.3540
Exit flow angle, degrees						20.4	20.6	20.75
Static pressure, psia			23.2			14.83	15.42	15.95
Temperature, °R			1945.2			1865.0	1867.0	1869.0
Specific volume, cfpp			21.25			30.81	29.65	28.75
Jet velocity, fps						1226.6	1175.7	1130.0
Axial velocity, fps	391.2	391.2	391.1	391.1	391.1	427.7	412.6	400.0
Wheel speed, fps	615.9	651.8	687.8	723.7	759.6	639.8	681.5	723.1
Inlet flow angle to next row, degrees	63.4	64.4	65.6	66.7	67.9	40.0	44.5	50.16
Inlet velocity to next row, fps	437.4	433.7	429.6	425.8	422.0	665.4	588.4	520.9

LE C-4

es Along the Height of the Blades

1st Rotor Inlet							1st Rotor Exit				
3/4	Tip	Hub	1/4	Mean Dia.	3/4	Tip	Hub	1/4	Mean Dia.	3/4	Tip
8.48	8.88	7.287	7.687	8.087	8.487	8.887	7.36	7.74	8.12	8.50	8.88
0.326	0.3317						0.4842	0.4735	0.4638	0.4544	0.44
9.0	19.35						28.9	28.2	27.6	27.0	26.45
8.65	29.21	26.60	27.36	28.03	28.64	29.20			22.60		
5.3	1999.1	1980.6	1985.9	1990.9	1995.3	1999.1			1940.0		
7.15	16.85	18.30	17.88	17.48	17.15	16.87			20.8		
4.2	999.3	1158.2	1112.7	1072.2	1034.4	999.8	924.0	944.7	964.4	984.4	1004.0
7.3	331.5	370.3	361.0	353.2	346.3	340.4	447.4	447.3	447.3	447.3	447.2
5.6	739.9	607.3	640.6	674.0	707.3	740.6	613.9	645.6	677.2	708.9	740.6
1.2	58.5	37.08	41.23	46.22	52.32	59.62	66.4	67.3	68.3	69.4	70.5
2.7	388.6	614.2	547.7	489.1	437.6	394.5	488.3	485.0	481.3	477.9	474.5

2nd Rotor Inlet							2nd Rotor Exit				
3/4	Tip	Hub	1/4	Mean Dia.	3/4	Tip	Hub	1/4	Mean Dia.	3/4	Tip
9.177	9.677	7.675	8.175	8.675	9.175	9.675	7.752	8.2325	8.713	9.1935	9.67
0.3577	0.3620						0.5473	0.5340	0.5220	0.5107	0.4
0.95	21.20						33.1	32.2	31.5	30.7	30.0
6.42	16.85	14.84	15.42	15.95	16.42	16.84			11.88		
1.0	1873.0	1864.6	1866.7	1868.7	1870.7	1872.7			1811.0		
7.95	27.35	30.75	29.65	28.75	28.0	27.40			36.6		
8.5	1050.7	1225.8	1175.3	1130.0	1088.9	1051.4	1024.9	1049.8	1073.5	1096.9	1120.3
3.4	380.3	440.4	424.9	412.1	401.3	392.0	560.9	560.6	560.4	560.2	560.0
4.8	806.5	639.6	681.3	723.0	764.6	806.3	646.6	686.6	726.7	766.8	806.9
7.1	65.54	41.13	45.74	51.38	58.35	66.65	69.3	70.2	71.3	72.5	73.7
3.8	417.8	669.5	593.7	527.5	471.7	426.9	599.6	595.7	591.5	587.4	583.5

Calculational method:

1) Method of Truckenbrodt. The main equation:

$$(\theta/\ell)_{x/\ell = 1} = \left[\left(\frac{C_f}{2}\right)^{(n+1)/n} \int_0^{\ell} \left(\frac{V}{V_{exit}}\right)^{3+2/n} d\,(x/\ell)\right]^{n/(1.0+n)}$$

where θ/ℓ is the momentum thickness per unit chord length, $n = 6$, x/ℓ is the referred distance from the inlet edge of the blade, and

$$C_f = 0.074\, Re_{\ell}^{-1/5}$$

2) Additional equations for calculation of boundary layer shape factor (H) and momentum mixing loss downstream of blade row.

3) Assumption: turbulent boundary layer on entire chord length of blade.

Output of program:

1) θ/ℓ at blade exit - pressure and suction surface.

2) H at blade exit - both sides of blade.

3) Blade energy coefficient - including downstream momentum mixing loss.

The main equation, as shown, is adapted from the original Truckenbrodt equation for the case of turbulent flow along the entire length of the blade. Due to this assumption, the laminar flow term does not appear in the equation. Though it is disputable to ignore the laminar flow at the leading edge of the blade, this does not appear to have an appreciable effect on the calculation. Further, it is implied that laminar flow does not occur in the actual turbine due to the turbulence and unsteady flow at the inlet of the blade row, contrary to the situation in a turbine cascade where there is undisturbed flow to the blades[8].

Calculated values for the Yankee steam turbine are shown in table C-5 for the boundary layer thickness and form factor at the trailing edge of the eighth rotor and ninth stator blade rows at the 3/4 blade height position. The boundary layer thickness is found to be roughly 40% higher in the case of the rotor blade due in large part to the lower blade Reynolds Number

TABLE C-5

Calculated Boundary Layer Properties *

Yankee Steam Turbine

		θ/ℓ	H	δ^*/ℓ	δ/ℓ	δ-in.	n	Re_θ	C_f	τ-ppsf
Eighth Rotor Blade at 3/4 Blade Ht. Position	Pressure Side	0.001180	1.41	0.001664	0.00978	0.0308	4.88	294.	0.00606	0.677
where D = 125.3", ℓ = 3.15" and $RE_\ell = 2.49 \times 10^5$	Suction Side	0.003831	1.55	0.005938	0.02747	0.0865	3.64	955	0.00348	0.390
	Total	0.005011		0.007602	0.03725	0.1173				
Ninth Stator Blade at 3/4 Blade Ht. Position	Pressure Side	0.000829	1.41	0.001168	0.00686	0.0761	4.88	532.	0.00504	0.392
where D = 137.0", ℓ = 11.1" and $Re_\ell = 6.1 \times 10^5$	Suction Side	0.002705	1.51	0.004085	0.02013	0.2234	3.92	1740.	0.00317	0.246
	Total	0.003534		0.005253	0.02699	0.2995				

where:

$$Re_\ell = V\rho\ell/\mu;\ n = 2/(H-1);\ Re_\theta = V\rho\theta/\mu,\ C_f = \frac{\tau}{\frac{1}{2}\rho V^2} = 2. \times .123 \times 10^{-.678H} \times Re_\theta^{-.268}$$

θ, δ^*, and δ are the momentum thickness, displacement thickness, and full (actual) thickness of the boundary layer at the trailing edge of the blade.

*All values are point values for the trailing edge position; e.g., C_f is the local skin friction coefficient at the trailing edge position.

(249,000 versus 610,000). Values also are shown for the Reynolds Number based on momentum thickness, the skin friction coefficient, and the shearing stress. These quantities are local blade surface values for the trailing edge position and are based on conventional turbulent boundary layer relations.

Table C-6 lists boundary layer properties for the second stator blade row of the two-stage potassium test turbine. Since the actual blade sections of the GE two-stage potassium test turbine stators were not readily available, the calculations were carried out using a Westinghouse blade. As the inlet and exit angles, chord length, and Reynolds Number are similar to those of the actual blade, there is probably no appreciable difference in properties.

Comparing the tabulated quantities for the potassium turbine with those for the Yankee steam turbine blade, the actual boundary layer thickness and vapor film Reynolds Number are less, due in large part to the smaller chord length of the potassium turbine blade. The shearing stress (τ) is much greater, roughly speaking, by a factor of 10, in large part because of the much higher density in the potassium turbine compared to the back end of the steam turbine. The increase in friction factor (C_f) is associated with the reduction in boundary layer thickness.

3.3 Blade Wake Calculation

Downstream wakes may be calculated from the boundary layer properties at the trailing edge of blades by methods as in NACA-TN 3771[9]. By these procedures, the downstream properties of turbulent, low-speed wakes are specified by theoretical and empirical relations. While the experimental data is largely for isolated airfoils, there is reasonable agreement with limited cascade data. An outline of the calculation procedure is as follows:

Given:

1) Boundary layer at blade trailing edge:

   $(\theta, H)_{pressure}$, $(\theta, H)_{suction}$

2) Blade exit angle $\alpha_{t.e.}$ and solidity, σ .

Calculational method:

Calculations are performed on slices of the wake for the suction and pressure sides of the

TABLE C-6

Two-Stage Potassium Turbine Boundary Layer Properties at the Trailing Edge of the Blade*

		θ/ℓ	H	δ^*/ℓ	δ/ℓ	δ-in	n	Re_θ	C_f	τ-ppsf
2nd stator blade 3/4 blade ht. position	pressure side	0.000533	1.21	0.0006449	0.006787	0.007669	9.524	148.3	0.00975	6.42
where D = 9.177"; ℓ = 1.13" $Re_\ell = 2.78 \times 10^5$	suction side	0.00244	1.53	0.003733	0.01782	0.02014	3.774	680.	0.00392	2.58
	Total	0.002973		0.004378	0.02461	0.02781				

where:

$Re_\ell = V\rho\ell/\mu$; $n = 2/(H-1.)$; $Re_\theta = V\rho\theta/\mu$; $C_f = \dfrac{\tau}{\frac{1}{2}\rho V^2} = 2. \times .123 \times 10^{-.678H} \times Re_\theta^{-.268}$

θ, δ^* and δ are the momentum thickness, displacement thickness, and full thickness of the boundary layer at the trailing edge of the blade.

*All values are point values for the trailing edge position; e.g., C_f is the local skin friction coefficient at the trailing edge position.

blade at selected downstream locations. The general procedure is:

1) Define H as a function of (x/ℓ) by empirical expression:

$$H_{x/\ell} = \frac{\left(\frac{x/\ell + 0.025}{0.025}\right)^{1/2}}{\left(\frac{x/\ell + 0.025}{0.025}\right)^{1/2} - \left(\frac{H_{te} - 1.}{H_{te}}\right)}$$

where x/ℓ is the referred downstream distance based on the chord length of the blade
$H_{te} = H_{x/\ell} = 1.$

2) $\hat{\theta}_{x/\ell} - \left(\frac{\theta}{\ell}\right)_{x/\ell} \frac{\sigma}{\sin \alpha_{x/\ell}} \approx \theta$/throat opening, where α is the flow angle with respect to the tangential direction.

3) The wake properties downstream of the blade are specified by:

$$F_1 \left(\hat{\theta}_{x/\ell}, H_{x/\ell}\right) = 0$$

$$F_2 \left(\alpha, \hat{\theta}_{x/\ell}, H_{x/\ell}\right) = 0$$

The change in form factor (H) with downstream distance is defined by an empirical expression based on isolated airfoil and cascade data due in large part to Spence-1952[10]. The referred momentum thickness of the wake ($\hat{\theta}$ = momentum thickness/throat opening) and direction of flow (α) with respect to downstream distance is specified by analytical expressions based on continuity, energy and momentum expressions, incompressible flow, and boundary conditions at the trailing edge of the blade. These expressions can be programmed for the computer, but, in these turbine calculations, values of $\hat{\theta}$ and α were extrapolated from curves in NACA TN 3771. This approximation is justified by the small increase in $\hat{\theta}$ and α with downstream distance (roughly 2% and 0.2 degree in the Yankee turbine).

There is a small decrease in mainstream velocity, V (x), with downstream distance due to the mixing of the wake. The downstream value of V(x) for values of $x/\ell \geq 0.10$ is estimated from the trailing edge displacement thickness (δ^*) as:

$$V = \left[V_{te}\right]\left[1 - \sigma\ (\delta^*/\ell)/\ (O/s)\right],$$

where σ and O/s are the solidity and gauging and V_{te} is trailing edge velocity.
V(x) for x/ℓ between 0.0 and 0.10 is determined by interpolation.

Calculational results for the eighth rotor and ninth stator of the Yankee steam turbine are given in figures C-1 and C-2, respectively. Results for the second stator of the two-stage potassium turbine are shown in figure C-3. As shown, the wake properties (H, α, θ) quickly change downstream of the trailing edge, whereby there is little change beyond 0.1 to 0.2 x/ℓ. Note also that while the wake thickness (δ) continues to increase beyond 0.1 to 0.2 x/ℓ, the velocity within the wake (V (y)) is nearly the same as that of the full stream since:

$$V(y) = V(x) \left(\frac{y}{\delta}\right)^{\frac{1.}{n}} \quad \text{where } n \sim 6.$$

Thus, the downstream flow is roughly axisymmetric from about 20% of the chord length distance downstream of the blade by this assessment of the process. As might be expected because of the relative size of the two turbines, the thickness of the wake from the steam turbine blades is an order of magnitude greater than from the potassium turbine blades.

While the incompressible flow assumption made in carrying out the calculations was not investigated, it is improbable that it has an important effect in well ordered turbines with thin boundary layers and hence only a small percentage increase in momentum thickness downstream of the blade is expected.

Of possible greater importance is the effect of the wheel speed on the wake velocity profile, turbulence, and mixing of wake downstream of the rotor blade. Due to the trigonometric effect of the wheel speed on the boundary layer profile, the velocity profile downstream of the blade (in the absolute frame of reference) is not colinear and is by no means the same as on the blade surface. The calculation ignores this effect in using the blade surface value of form factor (H) for the trailing edge wake. It is probable that the non-colinearity promotes turbulence, mixing of wake, and affects the transport and size of the droplets.

An important effect not considered in the results of figures C-1, C-2, and C-3 is the sheltered zone immediately downstream of the blade trailing edges provided by a finite trailing edge thickness. This wake information may be plotted in a different manner as shown in figures C-4 and C-5. Figure C-4 is a plot of the pressure side wake of the ninth stator of the steam turbine, and figure C-5, a similar plot for the pressure side wake of the second stator of the potassium turbine. The chief use of the wake information in the erosion model is to allow the calculation of the atomization and acceleration of the collected liquid between

x/ℓ	H	$\hat{\theta}$	α^{θ} deg	θ-in.	n	$\hat{\theta}$-in.	V(x) fps	V(y) fps
	Item 1 Expres'n	Item 2 Expres'n	F_2 Expres'n	$\frac{\hat{\theta}\ell \sin\alpha}{o}$	$\frac{2}{H-1}$	$\frac{\theta(1+n)(2+n)}{n}$		
Pressure side								
0 (t.e.)	1.41	0.01017	91.1	0.008475	4.88	0.07034	456	
0.05	1.20	0.01028	91.3	0.008556	10.	0.1129	451	
0.10	1.15	0.010.8	91.3	0.008556	13.31	0.1412	444	
0.50	1.068	0.01028	91.3	0.008556	29 40	0 2781	444	
0.979 (Stator Inlet)	1.045	0.01028	91.3	0.008556	44 45	0.4064	414	
Suction side								
0 (t.e.)	1.55	0.033037	91.1	0.02752	3.64	0 1976	456	
0.05	1.26	0.033763	91.3	0.02812	7.70	0.3079	451	
0.10	1.19	0.033763	91.3	0.02812	10.50	0.3852	444	
0.50	1.083	0.033763	91.3	0.02812	24.10	0.7649	444	
0.979 (Stator Inlet)	1.06	0.033763	91.3	0.02812	33.33	1.021	444	

$V(y) = V(x)\ (y/\delta)^{1/n}$

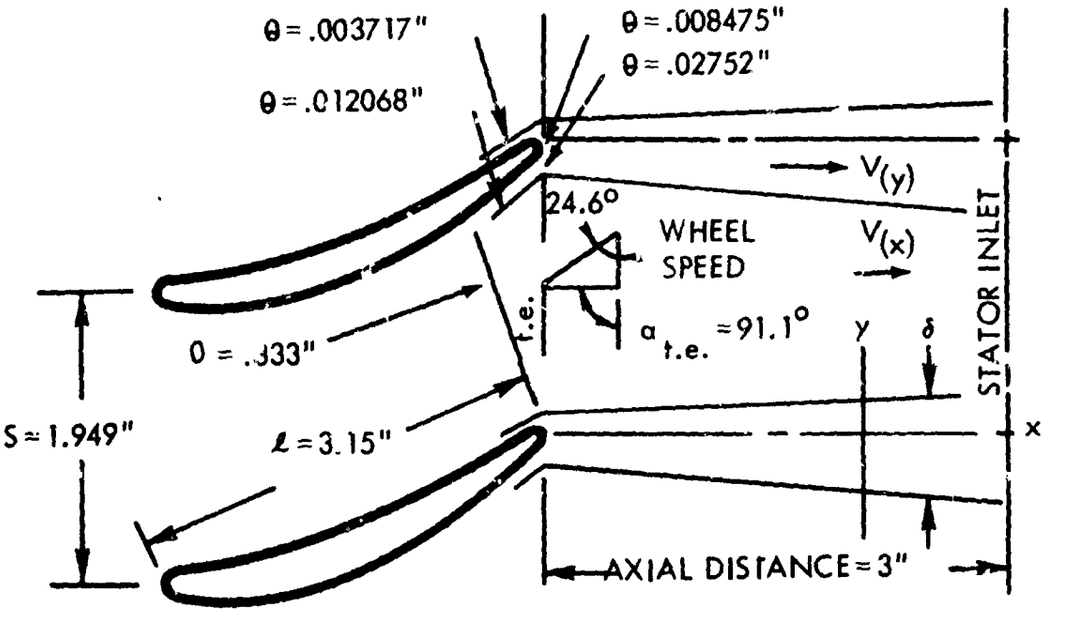

Figure C-1. Results of Blade Wake Calculation for Eighth Rotor Blade at 3/4 Height Position, Yankee Turbine

x/ℓ	H	$\hat{\theta}$	α-deg	θ-in.	n	δ-in.	V(x) fps	V(y) fps
	Item 1 Expression	Item 2 Expression	F_2 Expression	$\frac{\hat{\theta}\ell \sin\alpha}{\sigma}$	$\frac{2}{H-1}$	$\frac{\theta(1+n)(2+n)}{n}$		
Pressure side								
0 (t.e.)	1.41	0.00369	25.3	0.009196	4.88	0.0763	955	
0.05	1.202	0.00372	25.2	0.00927	9.90	0.1212	948	
0.1	1.15	0.00372	25.2	0.00927	13.35	0.153	935	
0.2	1.107	0.00372	25.2	0.00927	18.70	0.202	935	
0.358 (Rotor Inlet)	1.08	0.00372	25.2	0.00927	25.0	0.260	935	$V(y) = V(x)(y/\delta)^{1/n}$
Suction side								
0 (t.e.)	1.51	0.01206	25.3	0.03003	3.92	0.223	995	
0.5	1.24	0.01222	25.1	0.0304	8.34	0.352	948	
0.1	1.177	0.01222	25.1	0.0304	11.30	0.440	935	
0.2	1.127	0.01222	25.1	0.0304	15.80	0.575	935	
0.358 (Rotor Inlet)	1.095	0.01222	25.1	0.0304	21.10	0.735	935	

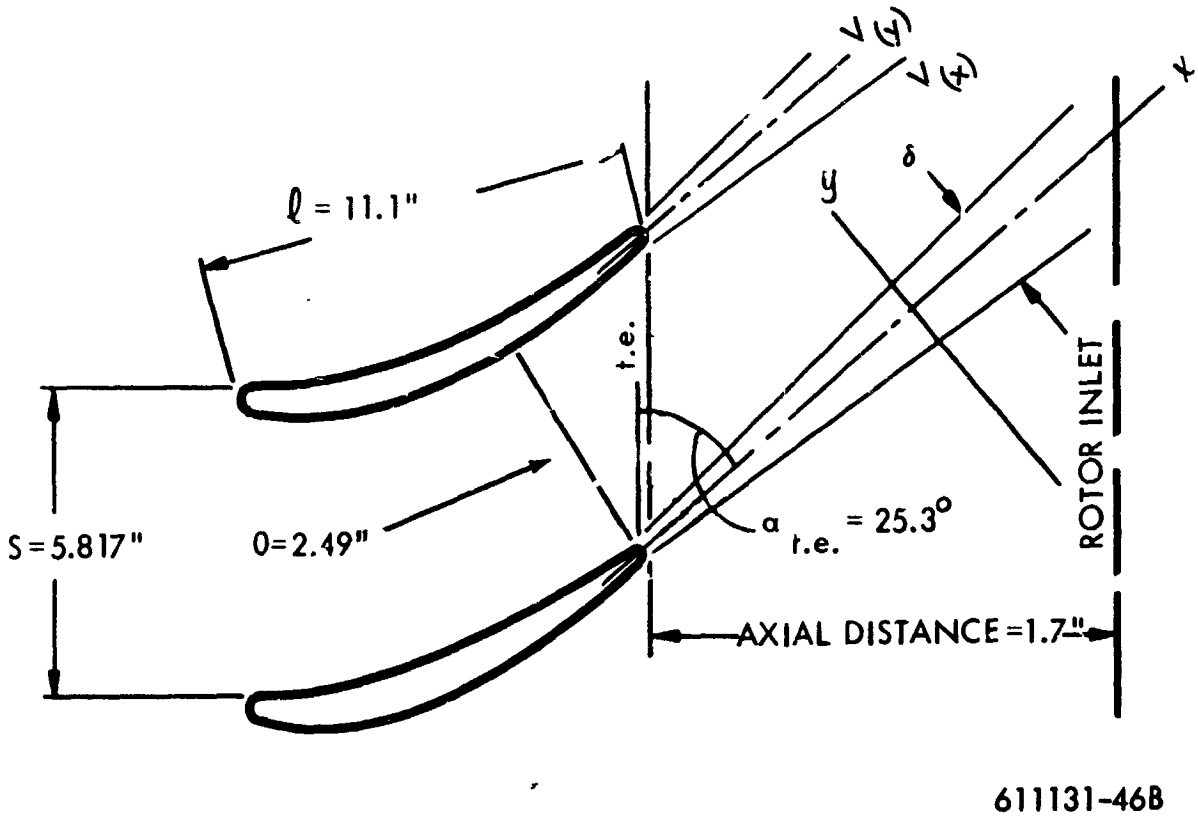

Figure C-2. Results of Blade Wake Calculation for Ninth Stator Blade at 3/4 Height Position, Yankee Turbine

x/ℓ	H	$\frac{\ell}{o}$	α-deg	δ-in.	n	$\frac{2}{H-1.}$	δ-in. $\frac{\theta(1+n)(2+n)}{n}$	V(x) fps	V(y) fps
Pressure side									
0. (t.e.)	1.210	0.00248	22.3	0.000603	9.524		0.00767	1105	
0.0443	1.113	0.0025		0.000610	17.70		0.01268	1098	
0.0885	1.088	↓		↓	22.70		0.0157	1090	
0.177	1.064				31.20		0.0208	1088	
0.266	1.053				37.70		0.0248	1088	
0.354	1.048				41.60		0.0272	1088	
0.496 (Rotor Inlet)	1.039	↓	20.95	↓	51.25		0.03305	1088	$V(y) = V(x)\ (y/\delta)^{1/n}$
Suction side									
0. (t.e.)	1.530	0.01134	22.3	0.00276	3.774		0.0202	1105	
0.0443	1.262	0.01150		0.00280	7.630		0.0304	1098	
0 0885	1.192	↓		↓	10.40		0.038	1090	
0.177	1.140				14.28		0.0487	1088	
0.266	1.112				17.82		0.0586	1088	
0.354	1.098				20.40		0 0657	1088	
0.496 (Rotor Inlet)	1.080	↓	20.95	↓	25.00		0.0784	1088	

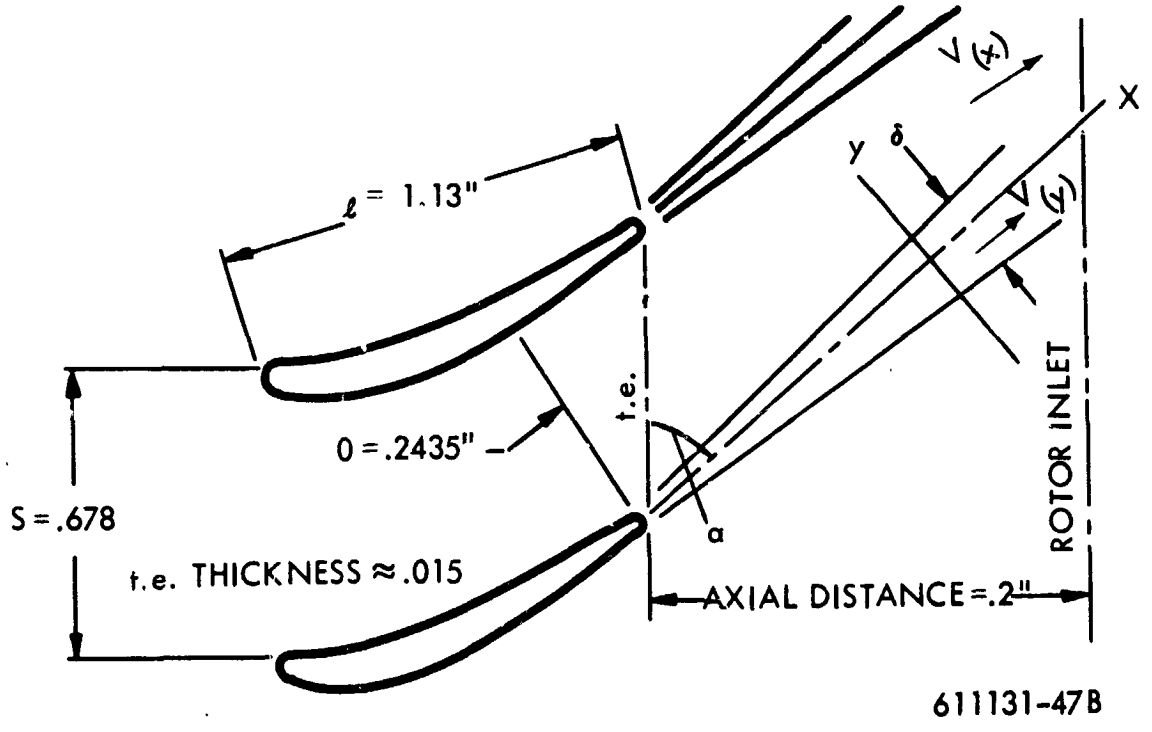

Figure C-3. Two-Stage Potassium Turbine; Results of Blade Wake Calculation for Second Stator Blade at 3/4 Blade Height Position

stator and rotor. Mathematically the effect of finite thickness of trailing edges of actual turbines on the collected liquid trajectory calculations was treated as a zero velocity space extending 4.8 trailing edge thicknesses downstream of the trailing edge and joined to a wake corresponding to a zero thickness trailing edge by a discontinuity. This discontinuity is represented by the vertical lines in figures C-4 and C-5. This procedure gave reasonable agreement with some cascade test results (See Vol. II, Section D).

Possibly, another weakness in the analysis is in regarding the downstream portion of the wake as a viscous process associated with the trailing edge boundary layer. Generally, this is only correct for near zero trailing edge thickness as in the Lieblein report. In actual turbines, the wake from the trailing edge of the blade can be like the separated vortex flow downstream of a circular cylinder. Investigations by Heskestad - 1960[11], as well as current Westinghouse tests, show that the downstream wake depends to a large extent on the detailed geometry of the trailing edge. Strong vortex streets are associated with thick, cylindrical trailing edge shapes. At the other extreme, there is evidence of unseparated flow downstream of tapered trailing edges shapes. In all, further work is required in this area.

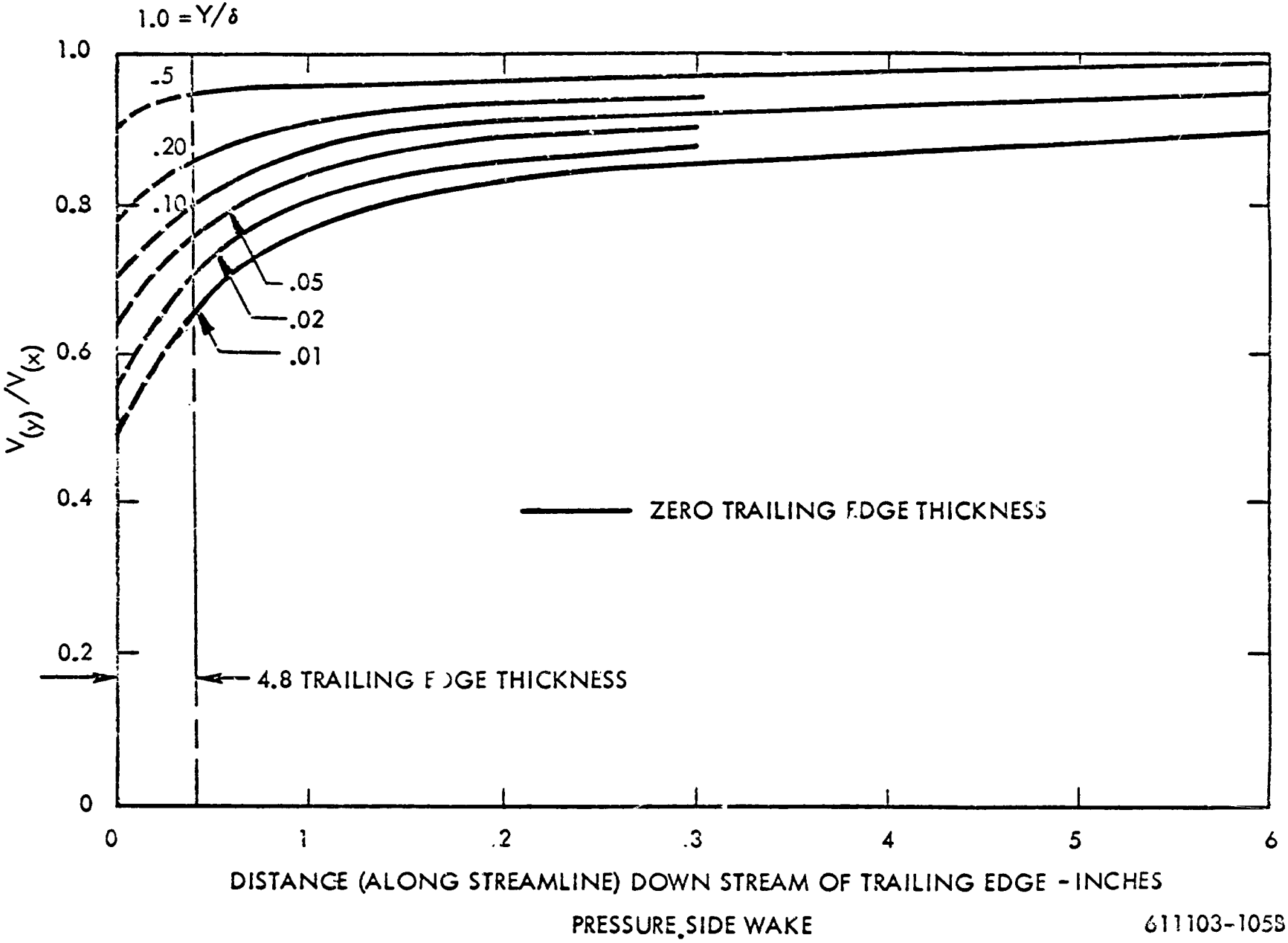

Figure C-4. Wake Pressure Side Velocities; Ninth Yankee Stator

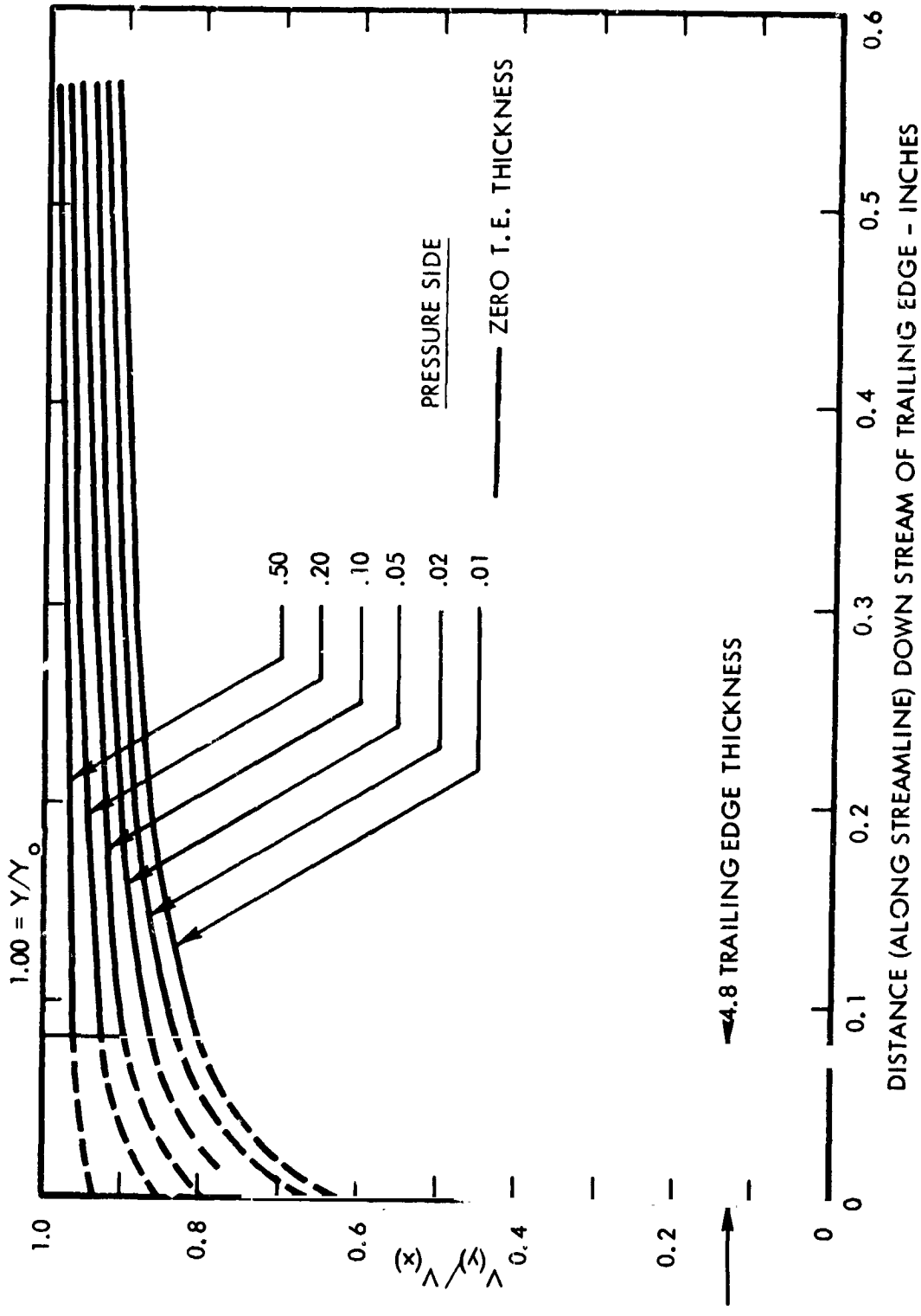

Figure C-5. Second Stage Potassium Turbine;
Wake Velocity Second Blade Row - 3/4 Blade Height Position Pressure Side

4.0 DEPOSITION OF MOISTURE ON THE SURFACE OF BLADES

The deposition of moisture is considered from the standpoint of:

1) The deposition on the inlet edge (nose) of the blades

2) The deposition on the concave face of the blades

The mechanism of deposition of moisture on blade surfaces is considered to be that of inertial impaction based on the macroscopic application of the laws of motion. In this we have followed Gyarmathy[5]. While deposition by diffusion of particles (Brownian motion and/or eddy diffusion) is recognized as a possible factor, inertial impaction is thought to warrant first consideration. Even between inertial impaction calculations, as between Gyarmathy and Brun et al[4], there is substantial difference in numerical values which we have been unable to resolve.

4.1 Deposition on the Inlet Edge of the Blades

The analysis considers the nose of the blade as a circular cylinder. Thus the impingement of moisture particles is specified by the path of the particles when acted upon by the potential flow about a circular cylinder.

The path and impingement of particles with respect to circular cylinders, based on two-dimensional trajectory calculations and suitable drag coefficients, is given in a number of reports. NACA Report 1215 by Brun, et al [4] was used in this analysis. Here the data are shown by a non-dimensional plot in terms of the conventional inertia parameter (K), a Reynolds Number parameter, and the collection efficiency. (Collection efficiency is the ratio of the width of the free stream capture stream tube, within which all particles strike the cylinder, to the diameter of the cylinder.)

As the flow about the miniature moisture drops is often in the slip flow regime, it is necessary to correct the NACA data for the reduction in drag due to slip flow. Correction was made by multiplying the report value of the inertia parameter by the ratio ($C_{D,\ slip\ flow}/C_D$) where C_D is the conventional drag coefficient for continuum flow. This correction is specified by an empirical expression in terms of Knudsen Number[12]. As shown in figure C-6, Gyarmathy's expres-

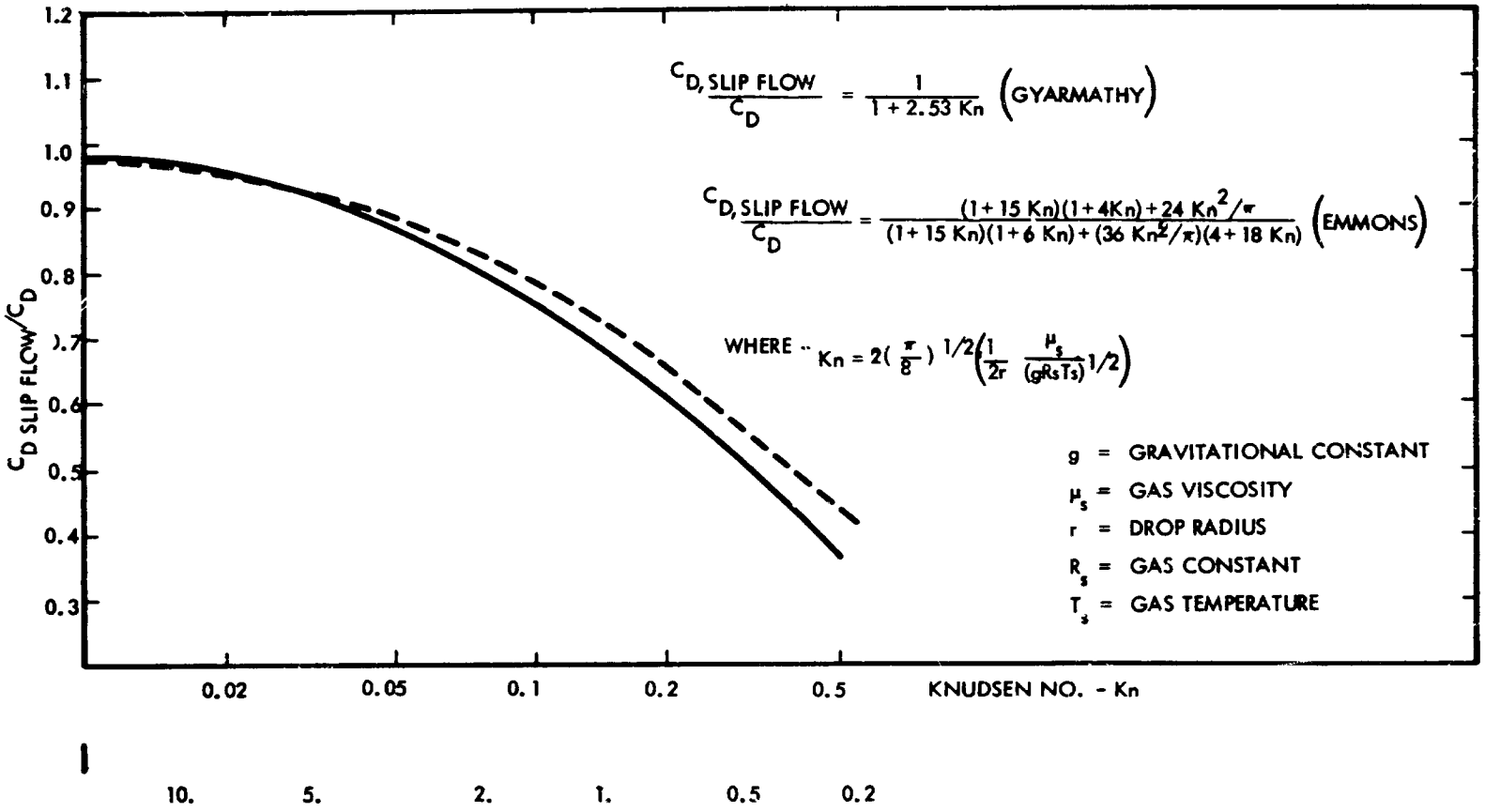

SLIP FLOW CORRECTION FOR THE DRAG COEFFICIENT OF SPHERES

Figure C-6. Knudsen Number Corrections

$$\frac{C_{D,\ slip\ flow}}{C_D} = \frac{1}{1 + 2.53\ K_n},$$

sion, is a simple approximation to the above expression. As also shown by this curve, the drag on 0.4 μ radius drops under these turbine conditions is only 45% of the continuum drag. In fact, the drag on particles will only approach continuum values at approximately 15 μ or greater radius.

By these data, the collection efficiency was calculated for the nose of the ninth stator blade row, 3/4 blade height position of the Yankee steam turbine, and is shown by figure C-7. For comparison, the efficiency is also shown by Gyarmathy's data. These data give a higher collection efficiency throughout the range of moisture drop size. This difference cannot be explained by the fact that the NACA data account for the increase in Stoke's law drag with Reynolds Number as in this instance, the fluid properties are nearly coincident with the NACA curve for zero Reynolds Number ($\alpha = 0.$). Possibly, the difference could be explained by differences in the trajectory calculation, but this calculation is not qualified in Gyarmathy's report.

By the NACA curve, drops less than 0.3 μ radius do not collect on the nose of the blade, but, by Gyarmathy's curve, the collection efficiency is roughly 15% for 0.4 μ estimated drop radius.

The portion of drops collected on the inlet edge is shown in figure C-8. The portion is with respect to the total number of drops and, as shown by the curve sketch, depends on the collection efficiency and the size of the inlet edge. By the NACA curve: the portion collected is 0.2% for 0.4 μ radius estimated size; drops less than 0.3 μ radius are not collected. But by Gyarmathy's curve, the portion collected is 0.9% for 0.4 μ drop size.

A similar situation exists with respect to the collection calculations on the blade noses of the two-stage potassium turbine. The results of the calculations are shown on figures C-9 and C-10. Figure C-9 gives the collection efficiency of the second stator and rotor. Figure C-10 gives the portion collected on the same stator and rotor. The portion collected is with respect to the total number of drops and, as shown by the curve, depends on the collection efficiency and the size of the inlet edge. The large inlet edge on the stator blade accounts for the larger portion of moisture collected in the range of drop size > 1.4 μ. By the NACA curve (figure C-10): drops $< 0.5\mu$ radius are not collected on the stator nose and drops $\geq 0.2\mu$ radius are not collected on the rotor nose.

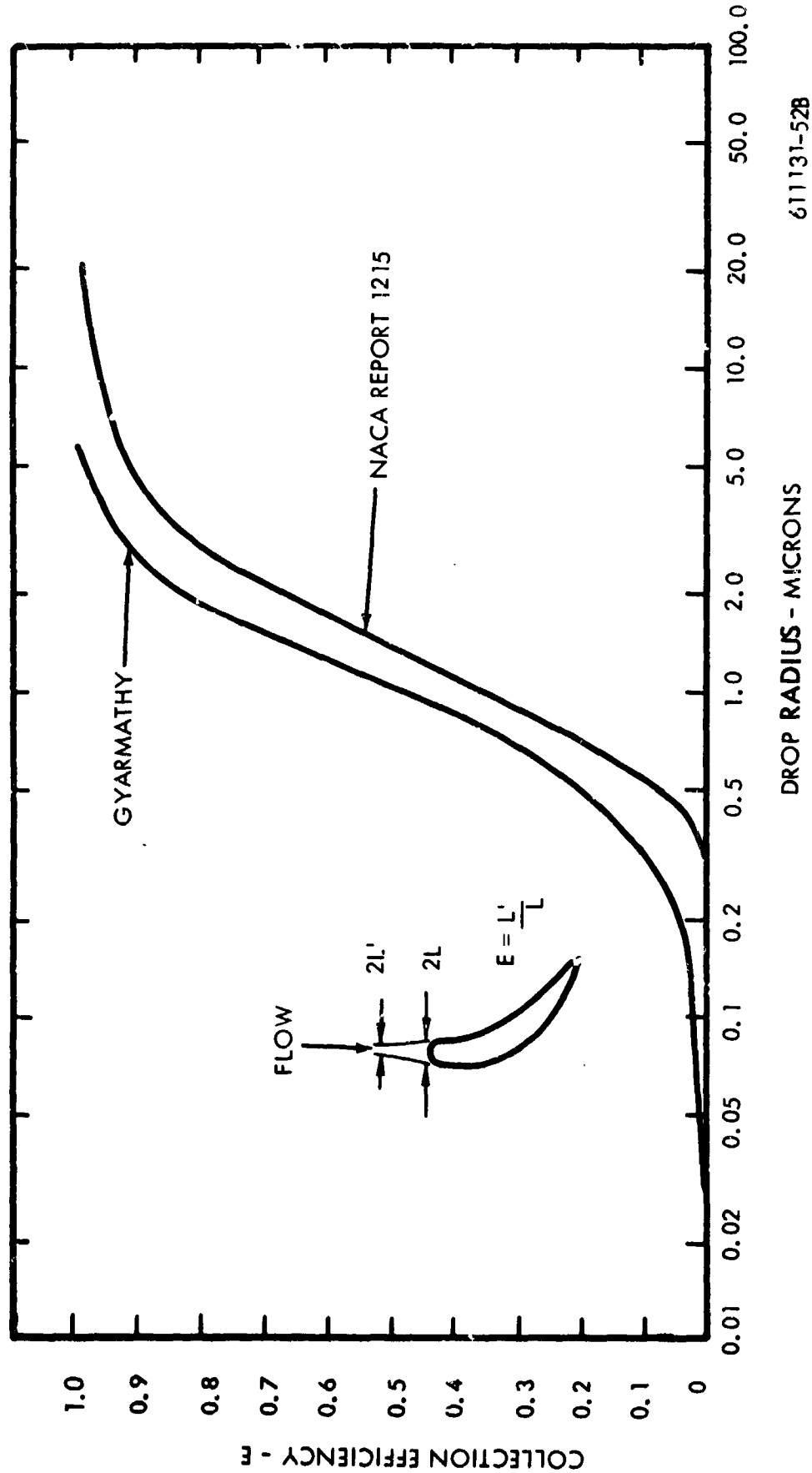

Figure C-7 Collection Efficiency Ninth Stage Stator Nose Yankee Turbine

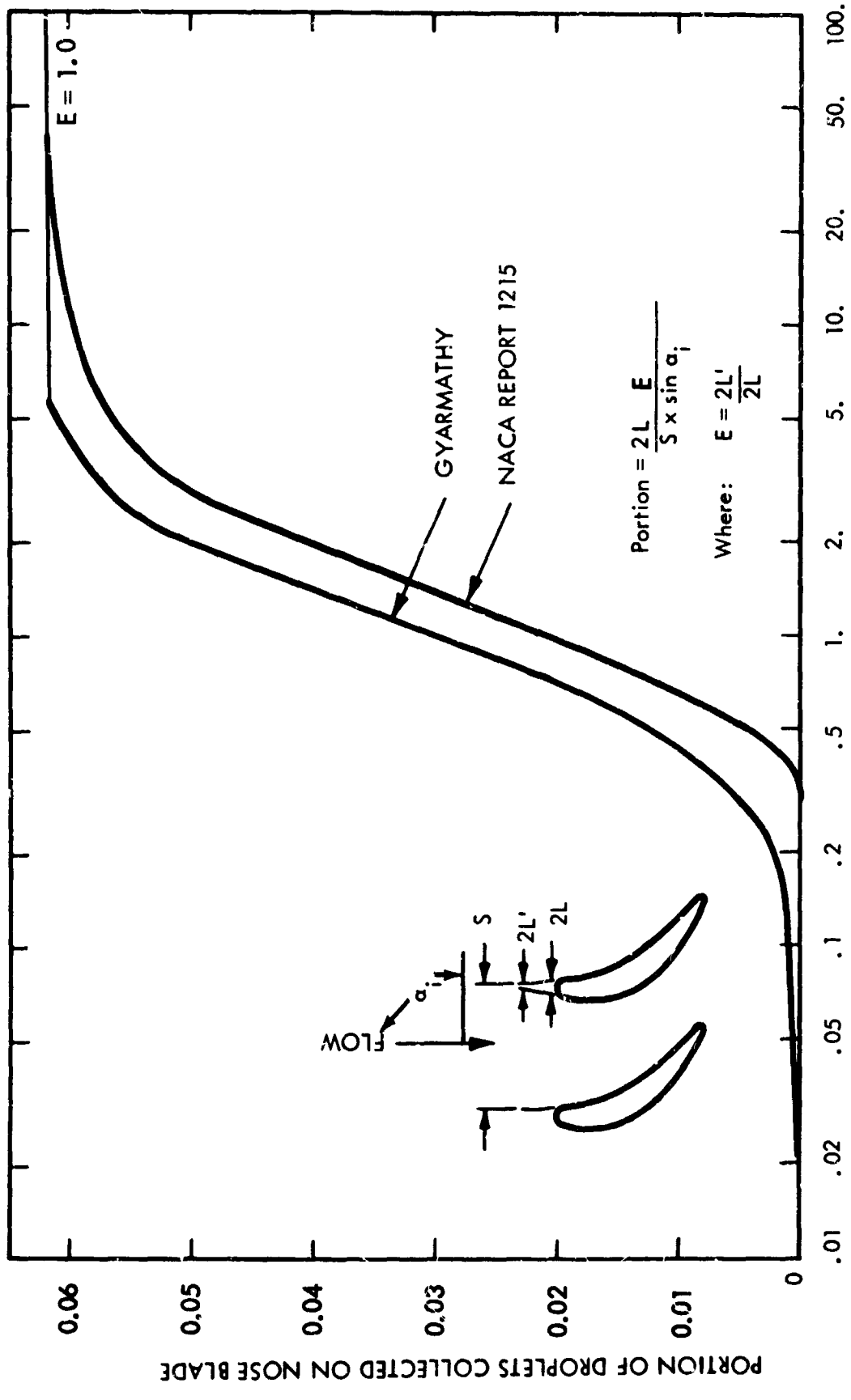

Figure C-8. Portion Collected Ninth Stage Stator Nose Yankee Turbine

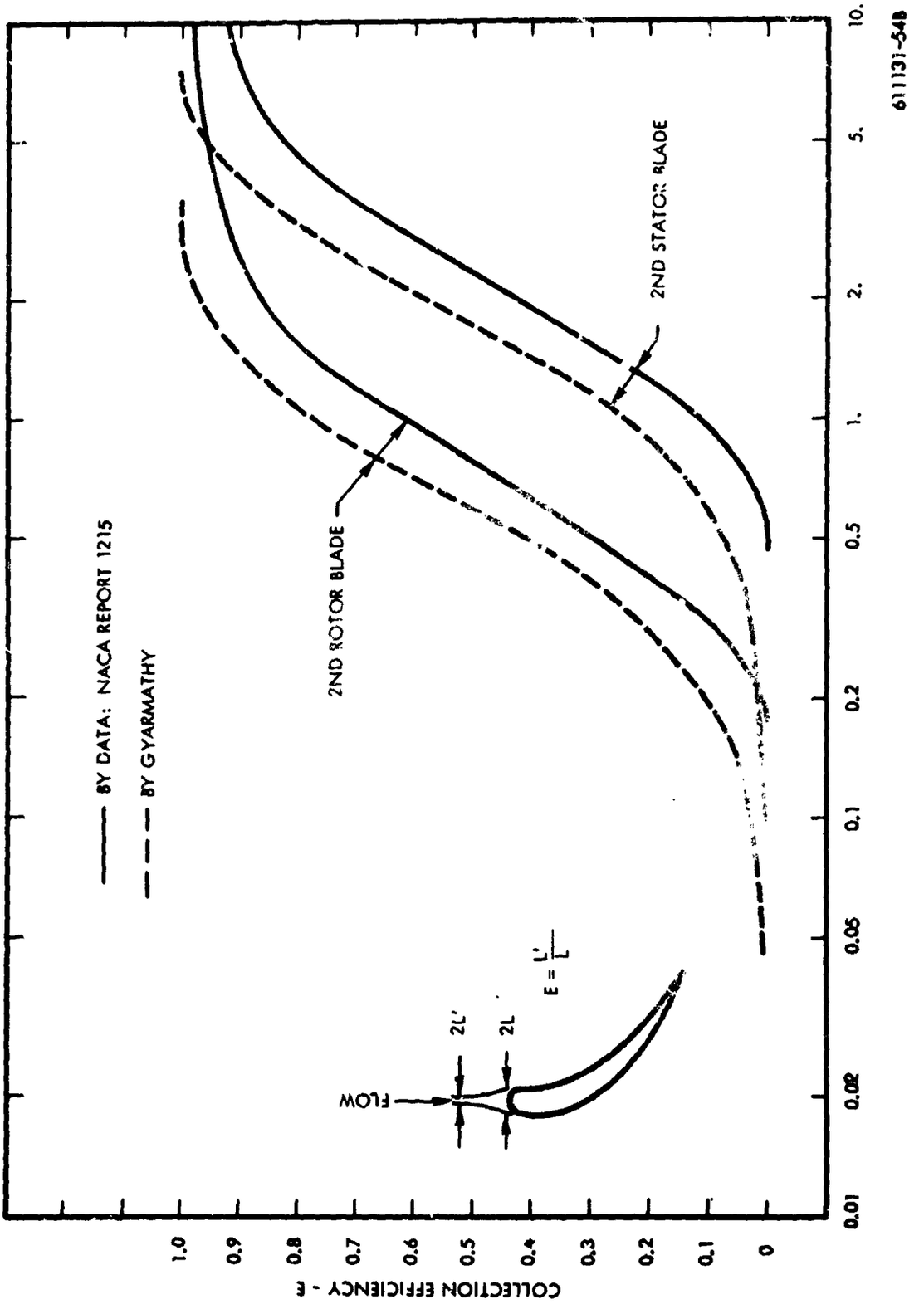

Figure C-9. Two-Stage Potassium Turbine; Collection Efficiency, Blade Nose

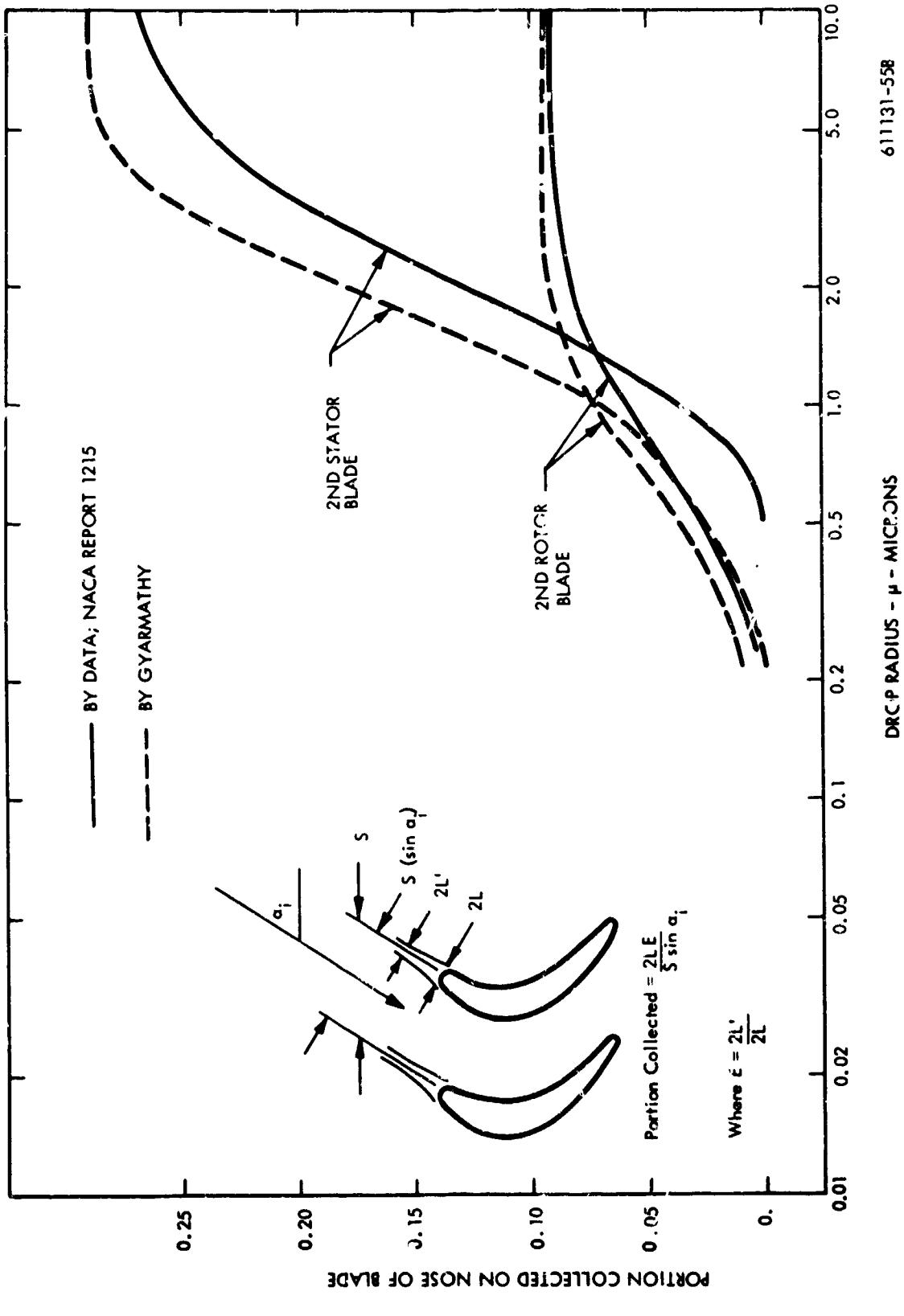

Figure C-10. Two-Stage Potassium Turbine; Portion Collected on Blade Nose

Hence, the drops in the turbine flow, 0.12 μ radius estimated size, are not collected. A larger collection is shown by Gyarmathy's curve, but the portion collected is near zero for 0.12 μ estimated size.

While the density of liquid potassium, about 2/3 that of water, tends to reduce the collection on the inlet edge, the greater part of the difference between the steam and potassium turbine is accounted for by the size of the inlet edge.

4.2 Deposition of Moisture on the Concave Face of the Blade

Generally, the analysis was performed along the lines of approach in Gyarmathy's report. The contour of the blade surface was approximated by a polynomial expression. The path of the vapor corresponds to the blade contour and the path of the particles, acted upon by the drag of the vapor, was calculated by trajectory equations. The drag on the particles is by Stokes' law with correction for slip flow. By simplifying assumptions of constant vapor velocity with respect to the distance between blades and equal and constant moisture-particle axial velocity, the particle acceleration was described by a linear differential equation. By further assumptions as to boundary conditions, the integrated equation gives the width of the band at the blade inlet, within which all moisture particles impinge on the blade surface. Finally, the ratio of band width to the space between blades gives the amount of the collection with respect to the total moisture approaching the blades.

Thus, by the above assumptions, the collection of moisture is specified by closed form calculation. Since this treatment of the process is not covered in the literature, a detailed account of the equations is given in Appendix 3. This includes the development of the equations and an example calculation.

Calculation results for the Yankee steam turbine are shown in figure C-11. This figure gives the portion of moisture collected as a function of drop size. As shown by the curve sketch, the portion collected is specified by the inlet width of the band (ζ), within which all particles impinge on the blade with repsect to the blade pitch. The band width cannot exceed the space between blades (pitch minus inlet edge blockage) which accounts for the break in the curve at 93-1/2%. Collection by Gyarmathy's data is 20% less in the range <0.4 μ drop radius. The difference is due to the fact that Gyarmathy specifies the blade shape by a quadratic expression

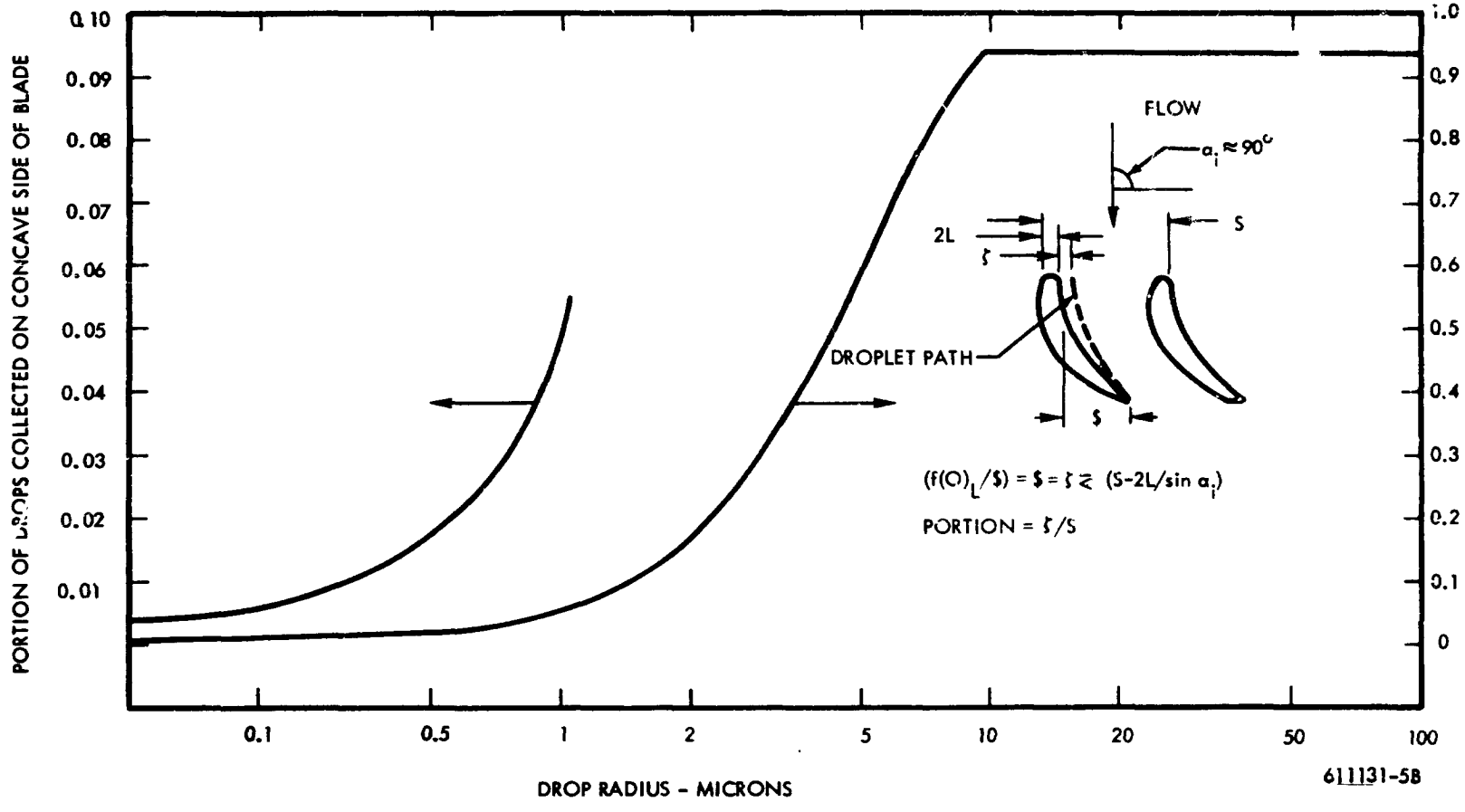

Figure C-11. Portion Collected; Concave Side, Ninth Stator Yankee Turbine

compared to a higher order curve fit which, in this instance, better matches the blade.

For 0.4 μ estimated drop radius: 1.3% of the drops are collected on the concave side of the blade; by Gyarmathy's data, the portion collected is 1.04%.

Similar calculations were carried out for the two-stage potassium turbine. Figure C-12 gives the portion of moisture collected on the concave side of the second stage stator and second stage rotor blade. The calculation assumes: a blade surface shape as by the average between a second and third degree polynomial and drag on the drops as by Stoke's law with correction for slip flow. Other assumptions as to constant and equal vapor, drop axial velocity, etc, are as in Gyarmathy's analysis.

As shown by the curve sketch, the portion collected is specified by the width of the band (δ), within which all particles impinge on the blade, with respect to the blade pitch. The band width cannot exceed the space between blades (pitch minus inlet edge blockage) which accounts for the break in the stator and rotor curve at 72 and 91%. Collection by Gyarmathy's data is nearly the same and is not shown.

For 0.12 μ radius drops: 0.3% of the drops are collected on the stator blade surface and 0.6% on the rotor blade surface. The larger collection on the rotor surface is due in large part to the passage shape (higher value of $/S). This compares to an approximate 0.4% collection in the Yankee steam turbine, same drop size. Here, the difference is again due in large part to the passage shape rather than fluid properties. (The inertia parameter is inversely proportional to the blade width and, hence, is much greater in the potassium turbine.)

An attempt was made to improve on the assumption of constant velocity in the space between blades to allow for the velocity gradient in the region of the boundary layer. Due to the non-linearity of the equations, the calculations could not be performed by closed form solution. In fact, the numerical solution of the equations was in effect a two-dimensional trajectory calculation. It therefore appears that a numerical solution will be required to improve upon the assumptions.

5.0 MOVEMENT OF MOISTURE ON BLADE SURFACES

The movement of collected moisture over the blade surfaces is not a critical part of the

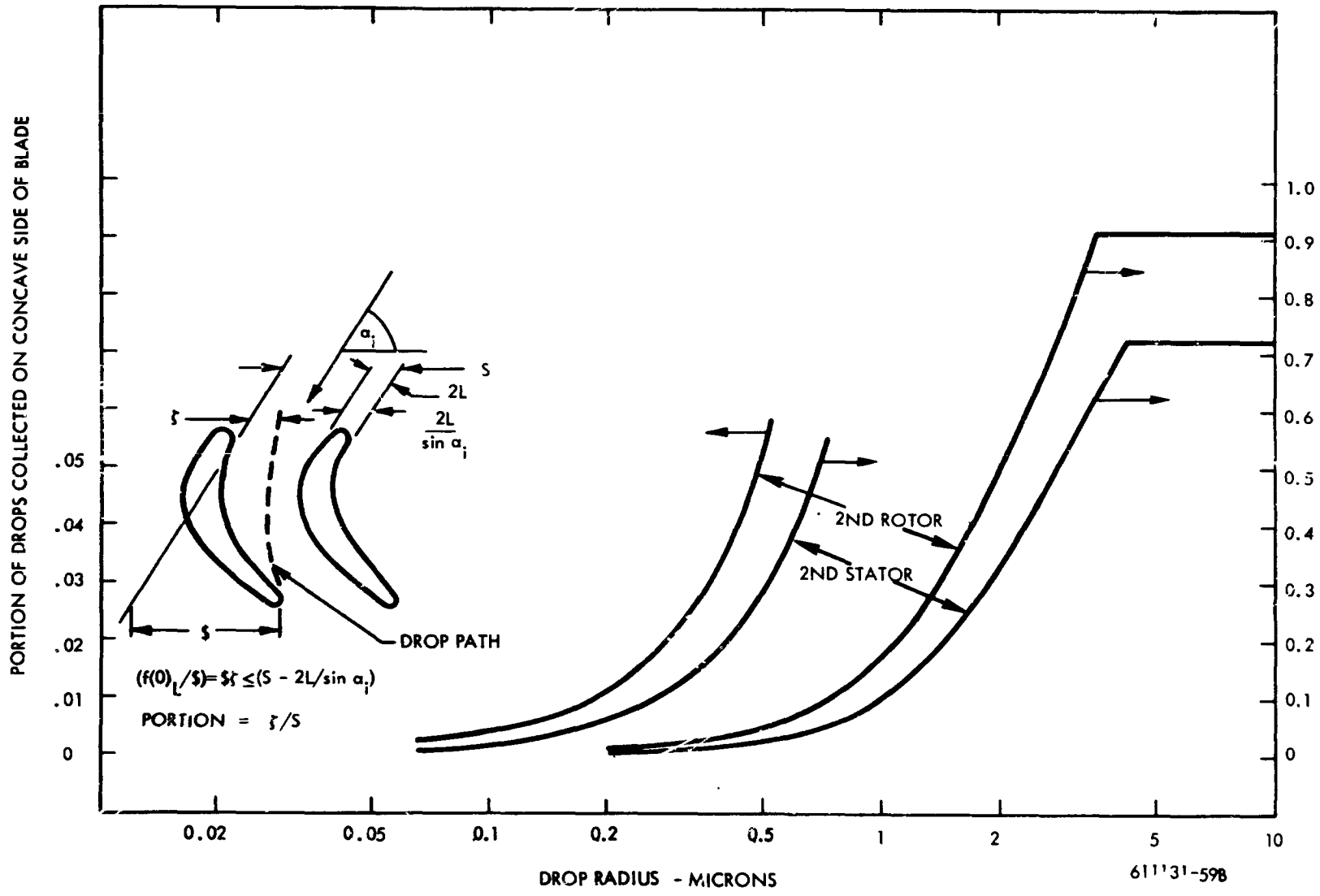

Figure C-12. Portion Collected; Concave Side Two-Stage Potassium Turbine

overall erosion model with respect to numerical precision. The main value of the analysis is in pointing out certain variables which may be neglected and in the added qualitative understanding of one of the sequences of events leading to turbine blade erosion. A most important conclusion which can be drawn from the analysis is that the carryover of collected moisture from stage to stage will be negligible in a well-drained turbine because the flow of liquid on the rotor blades is essentially radial. The liquid is therefore slung from tip against the outer casing and can be efficiently collected by suitable drain slots. Another conclusion is that the liquid flow on the stators is essentially along the vapor streamlines.

In this analysis, it is assumed that the collected moisture forms a continuous film controlled by the laws of viscous flow. Generally, the thickness and velocity of the moisture film is based on the force balance between the viscous shear of the film, vapor stream friction, and centrifugal force. The force on such a film from the radial pressure gradients in the turbines examined is small compared to the other forces mentioned. It is also assumed that the moisture collects only on the concave side of the blades for purposes of numerical calculation and collection on the convex sides through the action of secondary flows is neglected. This is a conservative assumption since it places a higher liquid load per unit of surface on the blade than is probably actually present. Since different procedures are involved for the stator and rotor blade calculations, the discussion is by separate topics.

5.1 Rotor Blade Moisture Transport Model and Results

The main equation, based on the Navier-Stokes equations, relates the centrifugal force to the viscous shear of the film. This assumes that the flow is in the radial direction and is only acted upon by the centrifugal force. The error in this assumption is shown by calculating the axial force on the film (due to steam friction) and the axial film velocity for the ninth stator of the Yankee turbine. Assuming 2% moisture collection, the axial velocity is 0.88 fps compared to 6.5 fps velocity in the radial direction, corresponding to a 7.8° angle of flow with respect to the radial direction. Assuming the flow is in the radial direction only and disregarding the low order terms, the Navier-Stokes equations reduce to:

$$F = -\mu \frac{\partial^2 u}{\partial y^2},$$

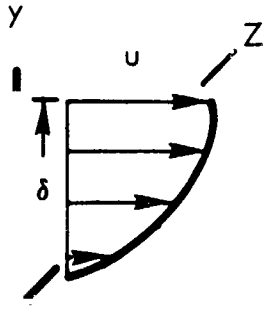

611131-56B

where the body force F is the centrifugal force.

Integration with boundary conditions as specified by a parabolic velocity distribution gives:

$$\frac{F y^2}{2} - F \delta y = - \mu u. \tag{1}$$

The mass flow and velocity are specified by continuity as:

$$\dot{m}_L = \rho_L Z u dy$$

$$u = \frac{1}{\rho_L Z} \frac{d\dot{m}_L}{dy} \tag{2}$$

Combining (1) and (2) and integrating force gives:

$$\frac{F \delta^3}{3} = \frac{\mu}{\rho_L Z} \dot{m}_L$$

Substituting for the centrifugal force: $F = \rho_L \omega^2 r$ gives the final expression for δ at the tip of the blade:

$$\delta = \left(\frac{3 \mu_L \dot{m}_L}{Z \rho_L^2 \omega^2 r} \right)^{1/3} \tag{3}$$

$$\bar{u} = \frac{\dot{m}_L}{\rho_L Z \delta} = \left(\frac{\dot{m}_L^2 \omega^2 r}{3 \rho_L Z^2 \mu_L} \right)^{1/3} \tag{4}$$

This assumes that the flow is uniformly distributed over the surface of the blade.

The calculation also assumes a parabolic velocity distribution with film thickness. The latter assumption is for calculation purposes and could be improved upon by detailed investigation of the amount and distribution of moisture. As to the width of the film, the film thickness and mass average velocity at the tip of the blade are inversely proportional to the 1/3 power and 2/3 power of the film width respectively; thus, the film thickness and mass average velocity would be 1.26 and 1.59 times the calculated values, for full width, if the film extended over half the width of the blade. In the case of radial distributions, with a triangular distribution of film thickness along the height of the blade, the centrifugal force F would be roughly 0.58, the film thickness 1.2, and the velocity 0.83 times the calculated values for constant radial thickness. As to the moisture flow ($\dot{m}_L$), the film thickness and velocity are directly proportional to the 1/3 power and 2/3 power of the flow.

Using the expressions just developed, parametric calculations for the eighth rotor of the Yankee steam turbine and the first rotor of the two-stage potassium turbine were carried out. The results are shown in tables C-7 and C-8, respectively. The parameter varied is the fraction (ϵ) of equilibrium moisture collected since this quantity depends upon inputs from the rest of the model. Note that the film velocity ($\bar{u}$) is the mass average at the tip of the blade.

TABLE C-7

Yankee Turbine, Eighth Rotor Liquid Flow

ϵ	$\dot{m}_L \times 10^4$ p-s/f	$\delta \times 10^5$ f	$\bar{u}$ fps	Re_L
0.005	0.215	1.59	2.58	7.65
0.010	0.43	2.02	4.11	15.3
0.020	0.86	2.52	6.49	30.6
0.050	2.15	3.44	12.0	76.5
0.100	4.30	4.31	18.9	153.0

TABLE C-8

Two-Stage Potassium Turbine, First Rotor Liquid Flow

ϵ	$\dot{m}_L \times 10^6$ p-s/f	$\delta \times 10^6$ f	$\bar{u}$ fps	Re_L
0.005	0.284	2.64	1.50	1.92
0.010	0.567	3.33	2.38	3.83
0.020	1.134	4.16	3.78	7.66
0.050	2.84	5.68	7.0	19.15
0.100	5.67	7.15	11.03	38.30

5.2 Stator Blade Moisture Transport Model and Results

The main equation, based on the viscosity expression, relates the viscous shear to the axial force due to the steam friction drag and the impingement of the moisture particles. It is assumed that there is a linear velocity distribution with film thickness and that the flow per unit blade height (at the 3/4 section) is the average unit flow along the height of the blade. This assumption could be improved upon by detailed investigation of the radial distribution. The viscous shear in the liquid film is given by:

$$\tau = \mu_L \frac{\partial u}{\partial y}$$

assuming a linear velocity distribution:

$$\tau = \mu_L \frac{u_{max}}{\delta} = \frac{2\mu_L \bar{u}}{\delta} \qquad (5)$$

where δ and $\bar{u}$ are the film thickness and mass average velocity. The flow of liquid is by continuity:

$$\dot{m}_L = \rho_L Z \delta \bar{u}$$

and

$$\bar{u} = \frac{\dot{m}_L}{\rho_L Z \delta} \qquad (6)$$

at the blade exit position assuming that the flow is evenly distributed over the distance Z (see sketch next page)

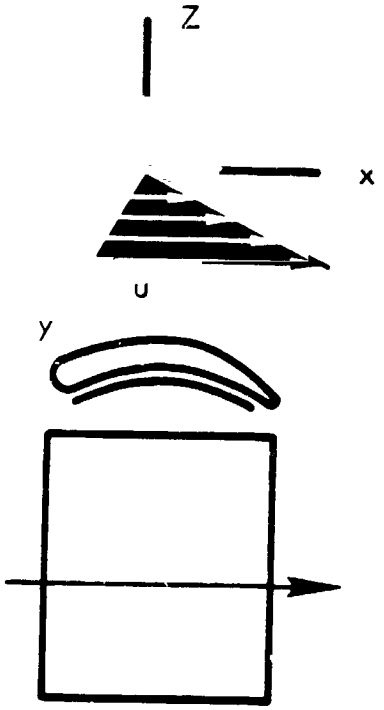

611131-57B

Combining (5) and (6) gives:

$$\delta = \left(\frac{2 \dot{m}_L \mu_L}{\rho_L Z \tau} \right)^{1/2} \tag{7}$$

The viscous shear on the film is due to the drag of the steam and the force of the impinging drops, i.e.:

$$\tau = C_f \rho_S \frac{V_S^2}{2} + \frac{\dot{m}_L}{ZX} V_S \tag{8}$$

where the boundary layer friction coefficient (C_f) in the region of the trailing edge is specified as:

$$C_f = 2 \times 0.123 \times 10^{-0.678 H} \left(\frac{V \theta \rho}{\mu} \right)^{-0.268} \quad \text{(Schlichting)} \tag{9}$$

where θ and H are boundary layer parameters.

Equations (7) and (8) may be combined to give:

$$\delta = \left(\frac{2 \dot{m}_L \mu_L}{\rho_L Z} \; \frac{1}{\tau + \frac{\dot{m}_L V_S}{X Z}} \right)^{1/2} \tag{10}$$

The film Reynolds Number is by definition:

$$Re_L = \bar{u} \, \delta \rho_L / \mu_L \tag{11}$$

Note that the axial force by the drag of the vapor is specified by the wall shearing stress of the boundary layer. The axial force due to the momentum of the impinging drops depends on the amount of the collection: for 1/2, 2, and 10% collection, the momentum force is roughly 5, 20, and 100% of the vapor drag force (τ).

As the amount of moisture collected depends on inputs from the other parts of the program, calculated film properties are with respect to the amount of equilibrium moisture collected, designated as ϵ. Results for the two turbines examined are given in tables C-9 and C-10 following. As shown, the film thickness and velocity are roughly proportional to the square root of ϵ, when ϵ is less than 0.05. The velocity ($\bar{u}$) is the mass average value at the trailing edge of the blade.

TABLE C-9

Yankee Steam Turbine, Ninth Stator Liquid Flow

ϵ	$\dot{m}_L \times 10^4$ p-s/f	$\delta \times 10^5$ f	$\bar{u}$ fps	Re_L
0.005	0.63	2.58	0.404	1.55
0.010	1.26	3.56	0.585	3.1
0.020	2.53	4.81	0.869	6.23
0.050	6.30	6.75	1.54	15.5
0.100	12.6	8.22	2.54	31.0

TABLE C-10

Two-Stage Potassium Turbine, Second Stator Liquid Flow

ϵ	$\dot{m}_L \times 10^6$ p-s/f	$\delta \times 10^6$ f	$\bar{u}$ fps	Re_L
0.005	0.615	0.795	0.868	0.32
0.010	1.23	3.27	3.88	5.9
0.020	2.46	4.54	5.60	11.8
0.050	6.15	6.93	9.18	29.5
0.100	12.30	9.18	13.60	59.0

From limited data (Gardner [6]; Baker [13]) it appears that there are ripples on the surface of the film when the film Reynolds Number (Re_L) is greater than 4, corresponding to ϵ greater than roughly 1%. These ripples probably affect the size of the drops from the blades as discussed in Section D under atomization.

PART D

ATOMIZATION AND TRAJECTORIES OF DAMAGING LIQUID

W. D. Pouchot and J. D. Milton

1.0 INTRODUCTION AND SUMMARY

As discussed in some of the preceding sections, a small percentage of the condensate particles passing through a turbine collect on the stator vanes. This collected moisture is carried to the rear of the stator vanes by the drag forces of the main stream. At and near the trailing edge of the stators this liquid is detached from the surface and ultimately forms into a spray of relatively large drops. This detachment process from the stators is labeled "primary atomization" in conformity to the usual terminology for gas-atomized sprays.

The drops from the primary atomization process are caught in the decaying wake of the stator or into the bulk stream. In either case, most but not all of the primary drops are subjected to air forces which are sufficient to disrupt them further. This additional fracturing of the collected liquid is labeled "secondary atomization" in conformity with gas-atomization terminology. In previous excellent studies of the overall erosion process by Gardner[1] and Gyarmathy[2], the simplifying assumption is made that all the drops formed by the primary atomization processes undergo secondary breakup before impacting the turbine rotor. This study differs importantly from these previous studies in that an attempt is made to trace the history of the relatively small percentage (about 20%) of the primary drops which do not undergo secondary breakup. Unfortunately, from the point of view of model simplification, these big unbroken primary drops cause damage disproportionate to the percentage of damaging liquid involved.

Before, during and subsequent to the secondary atomization process, if time is available, the drops are accelerated along the vector of the gas stream. These drops then arrive at the inlet of the following turbine rotor in a variety of sizes and with a dispersion of velocities relative to the nose and leading edge of the rotor blades. It is, of course, the impacting of these drops on the rotor blades which causes the erosion damage of concern in this analytical model.

To calculate the erosion of damaging form, caused by this liquid, it is necessary to know the size, relative velocity and number and location of impacts on the rotor blades as a function of time. There are at least four different mechanisms of primary atomization, and two for secondary atomization which have been observed experimentally under conditions related to those in turbine stators. There is, as well, a variety of accelerational paths provided by the velocity profiles in the stators' trailing edge wakes. To trace the history of all these possible paths and processes would be a formidable, if not impossible, task. Because of this, the approach taken here (to estimate distribution of drop sizes and drop velocities of impact) involves substantial simplification through the gross description of droplet classes based in part on empirical correlations from gas-atomization studies.

The focus of attention in this atomization investigation was on the processes as they might apply in the Yankee Atomic Plant low-pressure steam turbine and, in particular, to the last stage of that turbine. Nonetheless, it is felt that the observations in the steam turbine are applicable to a broader spectrum of turbine working fluids (such as the liquid metals) of low liquid viscosity and substantial surface tension*.

The calculational procedure used to estimate the drop sizes approaching the turbine rotor inlet involved six steps. The first of these steps was to estimate an average primary drop size. The model chosen for this purpose was the classical one of a sheet of liquid ruffled under the impress of aerodynamic forces, the ripples developing into ligaments, and the ligaments in turn collapsing into drops. The derivation of the numerical expressions used is given in Section 2.0.

Observations in an actual turbine are reported in Reference 4 and in turbine-like stationary cascades in References 4 and 3. Mechanisms of primary atomization reported

---

*Wetability of the liquid with respect to surfaces does not seem to be an important factor. Experiments reported in Reference 3 seem to indicate that under the impress of aerodynamic forces (even where good wetting would occur in the absence of such forces) liquids tend to become non-wetting. This is reasonable since the ground state of a liquid mass in the absence of external forces such as gravity is a sphere and perturbations from aerodynamic sources would tend to allow films and rivelets to "ball up".

are: (1) stripping of masses of liquid or sheets from liquid puddles, (2) stripping or tip bursting of oscillating pendant drops attached to the stator trailing edge, (3) eye-dropper like tearing of individual drops from the stator trailing edge and (4) direct formation of individual drops on the convex surface of stator by some mechanism giving results similar to a drop of water on a hot stove.

In none of these references is there quantitative information on the relative volumes of liquid involved in the observed processes. It seems reasonable that the tearing of masses or sheets of liquid from the stators involves a more important part of the total liquid available than the other observed mechanisms of detachment. The sheet atomization model is on this basis the logical tool for estimation of average primary drop sizes. As the information available is not conclusive, the pendant modes may be more important than assumed. A discussion of pendant atomization in addition to that on sheet atomization is given in Appendix 2.

An estimate of the primary drop size distribution was obtained by applying the well known empirical drop size distribution function of Nukiyama and Tanasawa[9] to the average primary drop size. The distribution function was applied assuming that the average drop size estimate represented the condition of maximum rate of creation of spray volume. This latter assumption is consistent with the assumption that the sheet model is volume-wise the most important of the primary atomization processes occurring in a turbine. It should be pointed out that using an empirical distribution function to some extent allows for the other possible process of primary atomization since they too will be expected to produce a distribution of drop sizes and may well have been present in the studies of gas atomization of liquids to which the Nukiyama-Tanasawa function has been applied as a correlating parameter.

To distinguish between primary drops which are stable from origin to rotor impact and primary drops which undergo secondary atomization, a parametric time history analysis of drops in the stator wake was carried out. (Section 3.0.) The parameters used were drop size and wake streamline path. It was assumed that the primary drops become entrained by a given wake streamline and the liquid represented remains with that streamline until rotor impact. The criteria for disruption of a primary drop was taken as the exceeding of a drop Weber Number of the order of 22 at some point along the path between detachment from the stator to impact with the rotor.

From such parametric calculations, it was determined that primary drops up to at least 350 microns in diameter would impact the Yankee ninth rotor without undergoing secondary atomization. On the basis of the primary distribution estimate, drops under 350 microns make up about 12% of the damaging liquid flow. The remaining 88% of the damaging liquid is then assumed to undergo secondary atomization to produce a mass mean drop diameter according to the Wolfe and Anderson equation [13] with the mass distributed among various size drops in accordance with the Nukiyama and Tanasawa distribution function. The former equation is theoretically derived and has limited experimental confirmation. The residual of the primary drop distribution was then added to the secondary drop distribution to give the drop size distribution arriving at the plane of the following rotor.

All of the preceding calculations were carried out across a tangential slice of the stator wake mid-way between hub and tip.

Since there is a substantial change in state conditions from hub to tip of a turbine, an approximate correction to the parametric trajectory calculations was incorporated when using the parametric information to establish the dispersion of velocities impacting the turbine rotor. It was assumed (Volume III) that the damaging component of the drop impact velocities is that normal to a blade surface. In the Yankee turbine last rotor it is assumed that these surfaces are the nose of the blade and the leading (convex) edge of the blade. The maximum impact velocities normal to the leading edge are substantially lower than the maximums normal to the nose at the vapor stagnation point according to these calculations. The nose stagnation point normal impact velocity calculated for a 350 micron drop is 915 ft/sec at the blade tip.* This maximum velocity falls to 750 ft/sec, 5 inches from the tip of the 40-inch long blade. At the tip of the last stage the rotor blade speed is 1246 ft/sec and the nozzle exit vapor velocity is 866 ft/sec.

---

*Higher calculated normal impact velocities were found for the nose radius between the stagnation point and the convex leading edge. (See Volume I, fig. B-20)

It can be said that the results of the trajectory and atomization calculations are in qualitative agreement with the sparse experimental information available. The erosion in the Yankee turbine is on the nose of the blade over the last two inches at the tip. There is fair quantitative agreement between the calculated drop velocities and those observed in a CERL of Great Britain stationary cascade[4] under state conditions similar to those in the Yankee turbine. In addition, there is an approximate agreement as to maximum size of primary drop which can escape secondary atomization as between these calculations and reported maximum size of drops observed impacting the rotor of an actual English steam turbine[5]. Also, the range of drop sizes seen departing from stators as reported by CERL[4] and the Rocketdyne Division of North American Aviation[3] (Contract NAS 7-391) appears to be about those calculated here.

However, to obtain an adequate check on this or any model of atomization, acceleration, and impingement of damaging moisture requires much more extensive and complete sampling of the total spray produced under turbine-like conditions than has been done to date. The reported experimental work to date has involved selective examination of a few drop trajectories and atomization processes rather than a comprehensive summation in numerical terms that describe the total spray. Such a total summation is required for erosion calculations.

In conclusion then, the model of damaging liquid history from stator to rotor, proposed here, bears a substantial resemblance to reality in spite of numerous simplifications and assumptions. The quantitative degree of validity of the model cannot be determined from the reported experimental data available. It is recommended that experiments be conducted to provide numerical values of the total characteristics of turbine sprays rather than the selective observations carried out to date.

2.0 PRIMARY ATOMIZATION IN TURBINES

In turbines, atomization of collected moisture from stators can occur in either one or two stages. First, some relatively large drops are detached at or near the trailing edge of the stator vanes under the influence of the gas forces present. This is shown schematically

in figure D-1 and is labeled "primary atomization". In this figure the straight line represents a top view of the trailing edge of the stator and one possible succession of steps in primary drop formation is indicated. Most of these primary drops will escape the wake of the stator blades and be caught up in the bulk flow and further atomized possibly as depicted in the part of figure D-1 labeled "secondary atomization". A substantial fraction may not escape the wake, however, and will remain at the size formed during primary atomization. These will impinge upon the following rotor without further breakup.

The process of primary atomization from the trailing edge of stator vanes bears a resemblance to the atomization from whirling disc or drum atomizers for spray formation. However, the process is much more straightforward in whirling atomizers because the centrifugal force creating the spray is of easily determined magnitude and direction in most cases. Even in whirling atomizers, however, there are three modes of atomization reported in the literature, which depend upon flow rate. In trailing edge air atomization because of the additional degrees of freedom available and the rather smaller force levels, there are many more possibilities.

There are few experimental observations on primary atomization as such and even fewer in turbines or under turbine-like conditions. Some direct observations in a turbine were reported at the British Royal Society Meeting of May 27, 1965[5]. In the published summary of these observations, the observed drop sizes from the trailing edge of the stator are reported as being between 150 and 450 microns in diameter. The conditions of geometry and operation of the turbine which produced the drops are not reported in sufficient detail in the summary to allow a quantitative analysis of the information.

Among the available experimental observations of primary atomization under turbine-like conditions are those recently reported by Hays[4] on some CERL results he obtained on a trip to Great Britain. In this report information on atomization and moisture flow is given both for an actual steam turbine and a simple steam turbine-like cascade. More recently information on primary atomization in a turbine-like cascade has been reported by Degner[3].

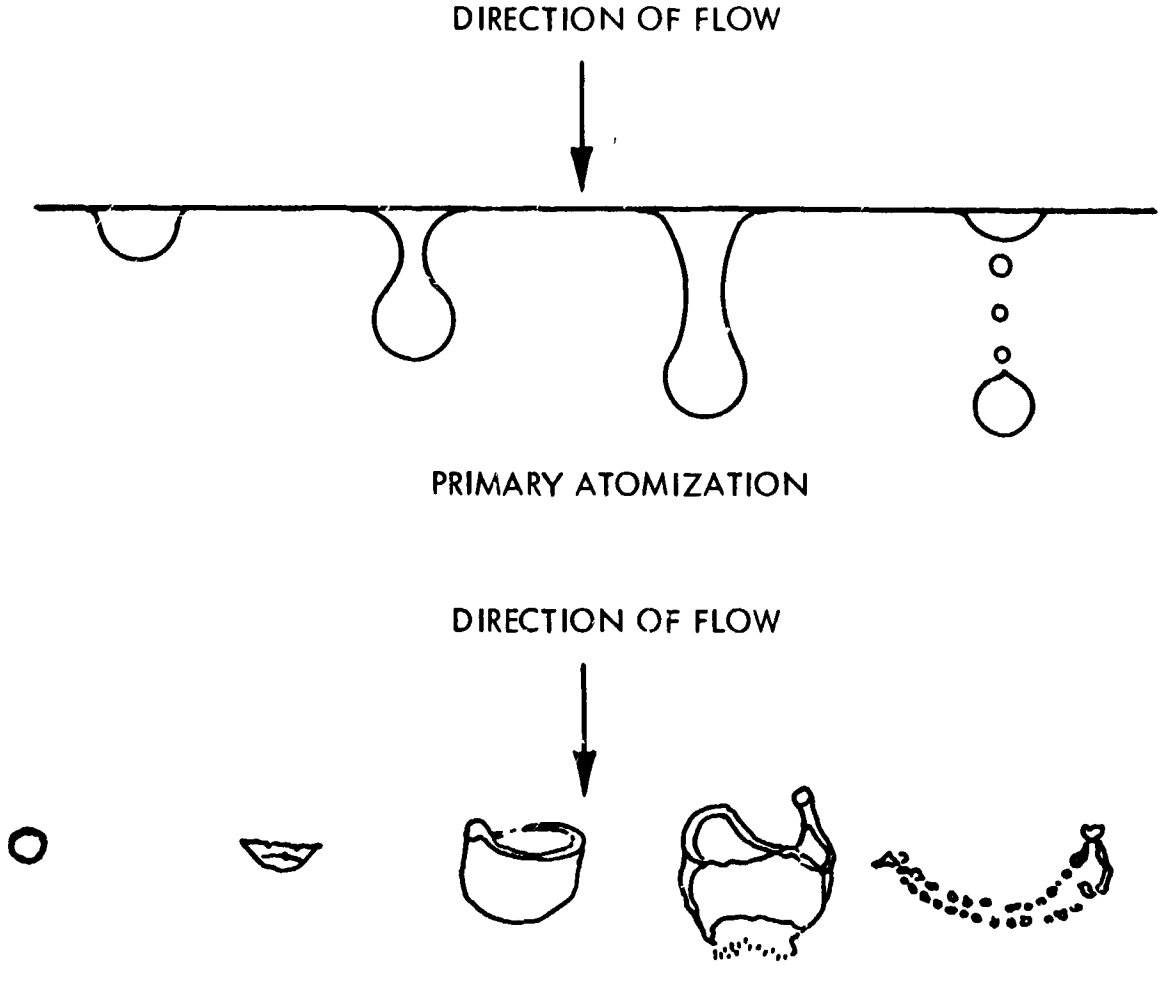

Figure D-1 Stages of Atomization

Mechanisms of primary atomization reported are: (1) stripping of masses of liquid or sheets from liquid puddles, (2) stripping or tip bursting of oscillating pendant drops attached to the stator trailing edge, and (3) eye-dropper-like tearing of individual drops on the convex surface of the stator by some mechanism giving results similar to a drop of water on a hot stove.

Unfortunately, none of the referenced work gives quantitative information on the relative volumes of liquid involved in the observed processes. It seems reasonable that the tearing of masses or sheets of liquid from the stators involves a more important part of the total liquid available than the other observed mechanisms of detachment. The sheet atomization model is on this basis the logical tool for estimation of average primary drop sizes. As available information is insufficient for definitive conclusions, the pendant modes may be more important than assumed. Sheet atomization is discussed in the text that follows and pendant atomization is discussed in Appendix 2.

2.1 Nomenclature - Primary Atomization

Symbol	Definition
a	Spray distribution constant
b	Spray distribution constant
B	Ligament diameter
C_f	Stator wall friction drag coefficient
d	Drop size
$\bar{d}$	An average drop size
g	Gravitational constant
H	Stator boundary layer form factor
$\dot{m}_L$	Mass flow rate per unit of stator edge length-(lb/sec/ft)/g

Symbol	Definition
n	Spray distribution constant
N	Number of drops
υ	Gamma function parameter
U_s	Bulk steam velocity
V	Volume rate of spray formation
V_{tot}	Total volume rate of spray formation
X	Stator chord length
x	Gamma function parameter
z	Drop size
β	Drag coefficient
δ	Stator liquid film thickness
θ	Stator boundary layer form factor
λ	Wave length of ripples in liquid film
λ_B	Wave length of varicosities in ligaments
$(\bar{\lambda})$	Most probable wave length
ρ_L	Density of liquid
ρ_s	Density of vapor (bulk)
σ_L	Liquid surface tension
τ_s	Stator wall friction drag per unit area
μ_L	Liquid viscosity
μ_s	Vapor viscosity

2.2 Sheet Atomization

Based on actual turbine observations such as those reported by Hays[4], the flow of collected moisture over stator vane surfaces is far from uniform. The flow gathers in rivelets or puddles which feed separated atomization sites.

In an actual turbine, the location of the atomization points is probably influenced by surface and vapor flow irregularities. However, even with a perfectly uniform surface, a distribution of attachment points can be expected. Under such uniform surface conditions it is to be expected that the fluid would initially start to collect in the wake of the stator trailing edge as a roll of liquid with a cross-sectional diameter of approximately the width (W) of the trailing edge. As is well known, such a slender cylinder of liquid is unstable in the presence of surface tension forces and develops varicosities along its length. The pitch of these varicosities would then determine the atomization sites. The pitch (or length) of the varicosities would not be uniform but would have a distribution of pitches. Numerically as given by Green[6] after Rayleigh, the minimum pitch of a cylindrical instability is π W and the most probable pitch is 4.5 W. Other pitches than these, of course, have a statistical probability of existence[7].

If the distance between the atomization sites becomes fairly large, the local liquid flow rates at the site will be many times that of a uniformly distributed flow. This high local flow rate results in a thickening of the local liquid boundary layer and an opportunity for the development of sufficient liquid boundary layer momentum with ripples to give sheet type atomization rather than pendant atomization. This sheet type atomization is analogous to the stage 3-type of whirling cup atomization which takes place at high rates of liquid feed to cup or disc atomizers[6]. In this example of the whirling disc atomizer, the flow rate on a uniform basis is high enough to produce sheet atomization. Such sheet atomization could obviously also take place from wet turbine stators on a uniform or nearly uniform film basis if the liquid flow rate is high enough. In the case of the Yankee Atomic turbine low pressure end, sufficient collection of moisture on the ninth (and wettest) stator to produce uniform film sheet atomization does not seem likely. Sheet type atomization is probably a result of local flow rates greater than average.

Average Droplet Size from Sheet Atomization

Schematically, the process of sheet atomization is assumed to be as follows:

1) The liquid film of average depth (δ) flowing towards the stator trailing edge (as a result of air drag forces) develops ripples of wave length (λ).

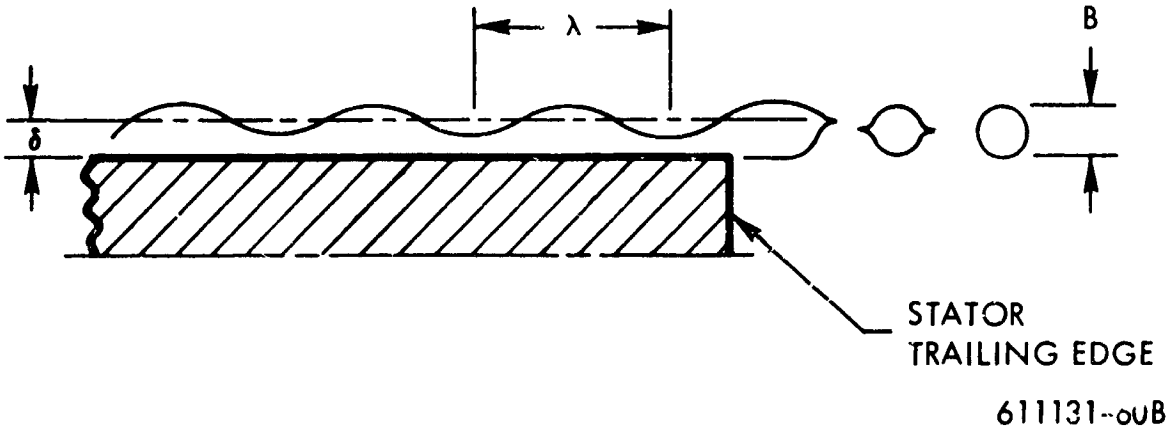

2) This rippled film is then blown from the trailing edge of the stator and collapses into ligaments of cross-sectional diameter B strung out parallel to the trailing edge. The cross-sectional area of the ligament is approximately equal to the product of the average film thickness times the ripple wave length or

$$B = \sqrt{\frac{4}{\pi}\ \delta\ \lambda}\ . \qquad (1)$$

3) The ligament so formed in turn develops instabilities of wave length (λ_B) along its length and collapses into drops of diameter (d).

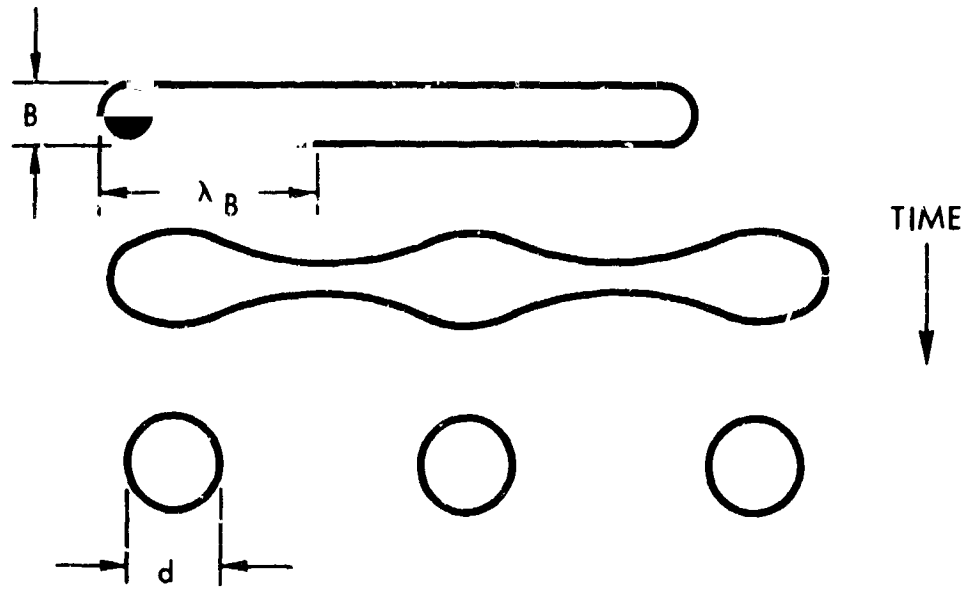

611131-61B

The volume of the drop being approximately equal to a cylindrical section of diameter B of length λ_B or:

$$\frac{\pi}{6} d^3 = \frac{\pi}{4} B^2 \lambda_B$$

$$d = (3/2\ B^2\ \lambda_B)^{1/3} \qquad (2)$$

As previously quoted from Green[6], the most probable value of λ_B is:

$$\lambda_B = 4.5\ B$$

and

$$d = \frac{3\ B}{\sqrt[3]{4}} \qquad (3)$$

Substituting for B from equation 1 into equation 3 gives:

$$d = 2/14 \sqrt{\delta \lambda} \qquad (4)$$

The average liquid boundary layer thickness at the trailing edge of the Yankee Atomic turbine low pressure end, ninth stage stator, is given by: (eq.10, Section C 5.2)

$$\delta = \left[\frac{2 \dot{m}_L \mu_L}{\rho_L \left(\tau_s + \frac{\dot{m}_L}{X} U_s \right)} \right]^{1/2} \qquad (5^*)$$

where

$$\tau_s = \frac{C_f \rho_s}{2} U_s^2$$

and

$$C_f = (2)\ (.123)\ (10^{-.678 H})\ \left(\frac{U_s \theta \rho_s}{\mu_s} \right)^{-0.268} \qquad (*)$$

An analysis by Jefferys of wind-generated gravity waves has been developed by Mayer[8] to predict the most probable capillary wave length in a windblown sheet. Mayer's expression gives:

$$\bar{\lambda} = 9\pi \sqrt[3]{16} \left(\frac{\mu_L \sqrt{\sigma_L / \rho_L}}{\beta \rho_s U_s^2} \right)^{2/3} \qquad (6)$$

Considering the expression $\beta/2\ \rho_s U_s^2$ as the effective drag force per unit area of film, it may be written in terms of the boundary layer calculations (neglecting for particle impact momentum) as:

*The equation is incorrect as shown in the Second Quarterly Progress Report Contract NAS 7-390, Westinghouse Electric Corp., Report WANL-PR(DD)-007, Feb. 9, 1966. Also note that $\dot{m}_L$ is defined as weight flow per second per unit of trailing edge length divided by the gravitational constant "g" when English units are used.

$$\beta \rho_s U_s^2 = C_f \rho_s U_s^2 = 2 \tau_s$$

or

$$\bar{\lambda} = 9\pi \sqrt[3]{16} \left(\frac{\mu_L \sqrt{\sigma_L / \rho_L}}{2 \tau_s} \right)^{2/3} \qquad (7)$$

Substituting in equation 4 from equations 6 and 7 results in an expression for an "average" drop size:

$$\bar{d} = 17.0 \left(\frac{\dot{m}_L \mu_L}{\rho_L \left(\tau_s + \frac{\dot{m}_L U_s}{X} \right)} \right)^{1/4} \left(\frac{\mu_L}{\tau_s} \sqrt{\frac{\sigma_L}{\rho_L}} \right)^{1/3} \qquad (8)$$

In Figure D-2 "average" drop sizes from equation 8 are presented. It may be noted that the drop size predicted by equation 8 appears to become independent of flow rate at the higher values of flow rate examined. This suggests that a simplified expression such as equation 9 will be adequate for predicting the "average" drop size in many instances.

$$\bar{d} = 17.0 \left(\frac{\mu_L X}{\rho_L U_s} \right)^{1/4} \left(\frac{\mu_L}{\tau_s} \sqrt{\frac{\sigma_L}{\rho_L}} \right)^{1/3} \qquad (9)$$

Numerical evaluation of equation 9, inserting the same values for the independent variables, as used in evaluating equation 8 (figure D-2) gives:

$\bar{d}$ = 630 microns.

Examining equation 9, it will be seen that the average drop size predicted varies slowly with most of the variables except U_s. Setting $\tau_s :: U_s^2$ gives the variation with respect to U_s as:

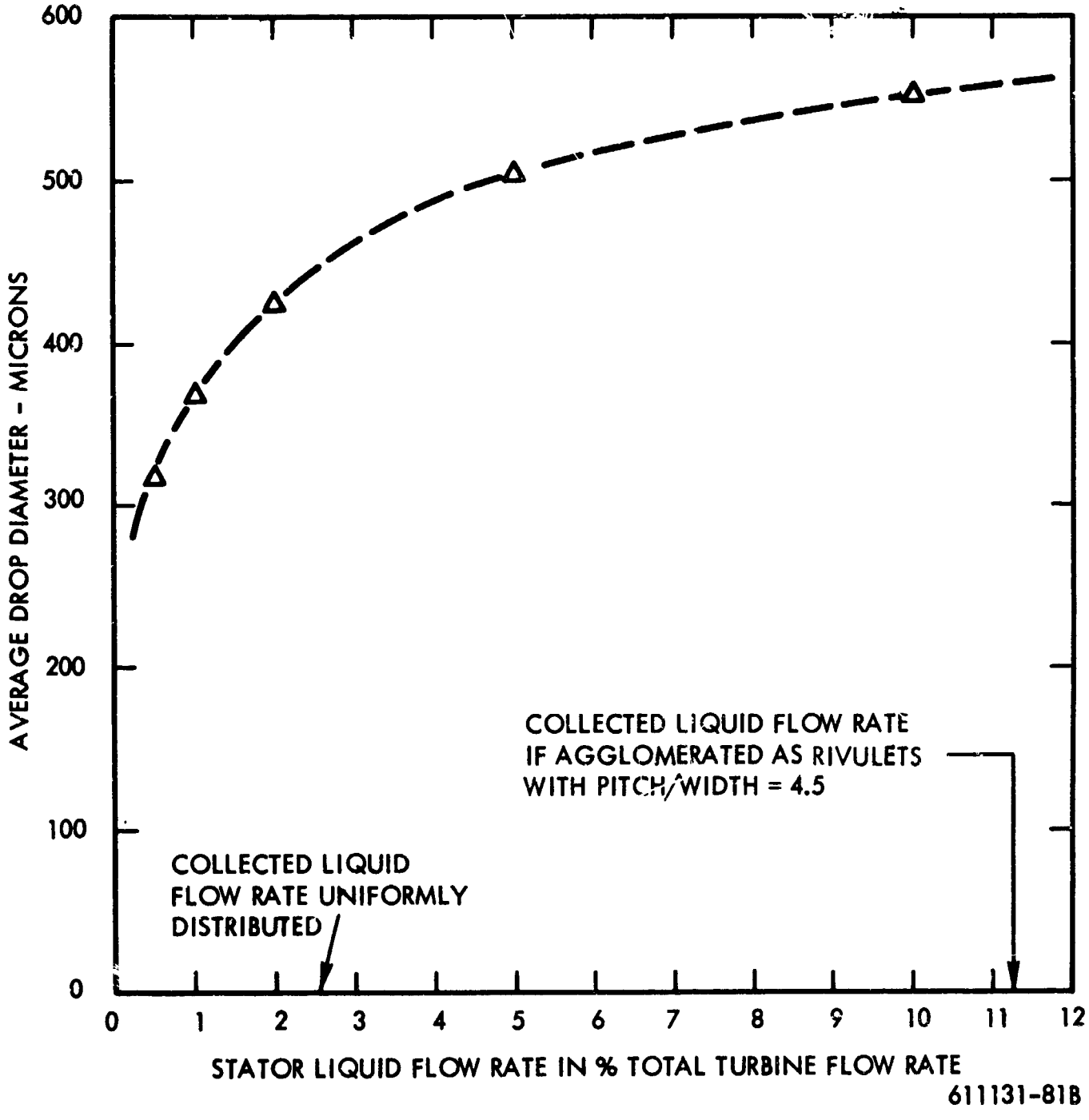

Figure D-2. Average Drop Size, Primary Atomization

$$d :: U_s^{-.92}$$

Sheet Atomization Drop Size Distribution

There is a distribution of drop sizes resulting from sheet atomization (in fact from almost any atomization process). There is the distribution of sites (inflow rates) along the trailing edge, the distribution of atomization wave lengths (λ) in the direction of flow, and the distribution of cylindrical wave lengths (λ_B) producing the final primary drops. A distribution function could be developed from the Rayleigh[7] cylindrical instability function and the Jefferys-Mayer[8] capillary wave length function. However, an overall empirical distribution function due to Nukiyama-Tanasawa is easier to use:

$$\frac{dN}{dz} = a z^2 e^{-b z^n} \qquad (10)$$

Quoting from Putnam[9], "Two Japanese investigators, S. Nukiyama and Y. Tanasawa, obtained extensive data on drop sizes in sprays by air atomization, and sought to correlate these data ----------n". Their investigations indicated that a value of 2 for the exponent of (z) effected a good correlation of the experimental data in every case, and that exponent (n) varied but little from unity.

While other investigators, including the writer, have found that the value of the exponent (n) may fall as low as 1/4, a numerical case can be made for the Yankee turbine to consider this exponent as having a value of unity. An exponent of the order of unity is required to get a reasonable fit between an upper size limit on drops (order of 1500 to 2000 microns) resulting from the size of the trailing edge thickness and an unspecified kind of average drop size from figure D-2 of the order of 500-600 microns.

Using n = 1 and writing equation 10 in terms of volume rather than number of drops gives:

$$\frac{dV}{dz} = \frac{\pi a}{6} z^5 e^{-bz} \qquad (11)$$

This equation contains two undetermined constants, (a) and (b). Constant (a) may be determined from the total volume of the spray using the continuity relationship once constant (b) has been found. In connection with constant (b), it may be observed that if a value of the "average" drop size corresponding to the most probable flow rate of figure D-2 is selected, the rate of change of volume of spray produced is a maximum with respect to this average drop size (z_{av}) or,

$$\frac{dV}{dz} = \left(\frac{dV}{dz}\right)_{max.}$$

and

$$\frac{d^2V}{dz^2} \equiv 0 = \frac{\pi a}{6} \left(e^{-bz}\right) z^4 (5 - zb)$$

or, $b = 5/z_m$

where z_m is z_{av} at $\left(\frac{dV}{dz}\right)_{max.}$ (12)

Substituting from equation 12 in equation 11 gives:

$$\frac{dV}{dz} = \frac{\pi a}{6} z^5 e^{-5} \frac{z}{z_m} \qquad (12a)$$

If the substitution, $x = 5\, z/z_m$ is made in equation 12a, it becomes:

$$dV = \frac{\pi a}{6} \left(\frac{z_m}{5}\right)^6 x^5 e^{-x}\, dx \qquad (13)$$

$$V_x = \frac{\pi a}{6} \left(\frac{z_m}{5}\right)^6 \int_0^x x^5 e^{-x}\, dx = \frac{\pi a}{6} \left(\frac{z_m}{5}\right)^6 \Gamma_x(6) \qquad (13a)$$

also $$\frac{V_x}{V_{tot}} = I(u, 5) \qquad (14)$$

where $u = x/\sqrt{6} = \frac{5\ z}{z_m \sqrt{6}}$

and I (u, 5) is a form of the incomplete gamma function as tabulated in Reference 10. The ratio of cumulative liquid volume to total liquid volume of a spray is given as a function of drop size in table D-1 for the ninth stator of the Yankee turbine.

TABLE D-1

Spray Liquid Volume Distribution Versus Drop Size

Drop Size (z) (microns)	V_z/V_{tot}
100	0.0004
175	0.007
250	0.0356
350	0.12
525 = z_m	0.38
750	0.72
1050	0.93
1575	0.997

A small amount of data on stator primary atomization, obtained from the British CEGB, has been reported by Hays[4]. This information is reproduced in table D-2 for conditions which more or less bracket the conditions at the ninth stator of the Yankee Turbine. This data cannot be said to confirm the model of primary atomization used here because of the low number of drops sampled. A comparison between tables D-1 and D-2 is encouraging, however.

TABLE D-2

Data On Stator Primary Atomization

Static Pressure (psia)	Bulk Steam Velocity (ft/sec)	No. of Drops	Max. Size (microns)	Min. Size (microns)
1.61	976	5	1080	460
1.72	1180	4	620	360

3.0 DROP TRAJECTORIES AND SECONDARY ATOMIZATION (DOWNSTREAM OF STATORS)

3.1 Introduction

The large drops formed at the trailing edges of the stators during the primary atomization process undergo an acceleration and in most cases further break-up before entering the succeeding rotor passages. It is the purpose of this section to show how the aerodynamic forces accelerate and additionally breakup these droplets so that when they impact on a rotor, the level of impact can be determined.

The subject matter is presented in the following order: the mathematical model used, application to the ninth stage of the Yankee turbine with a discussion of the results. The processes mathematically described are the force balance resulting in acceleration and breakup of the primary drops, the average time to secondary breakup, the criterion for secondary breakup, the average size of drops resulting from secondary breakup, the distribution of normal impingement velocities on the nose and leading edge of the rotor blades, the distribution of sizes resulting from secondary breakup.

3.2 Nomenclature

Symbol	Definition
A_d	Cross sectional area of droplet
a	Distribution function parameter
b	Distribution function parameter
C_D	Drag coefficient
D_b	Diameter of blade
D_d	Diameter of droplet
D_{3-0}	Mass mean diameter of the stripped droplets
F_d	Aerodynamic force on droplet
We_d	Droplet Weber number
V	Spray volume rate
V_b	Veolcity of blade
V_d	Velocity of droplet
$V_{d_{N1}}$	Normal component of droplet velocity relative to blade leading edge
$V_{d_{N2}}$	Normal component of droplet velocity relative to blade nose stagnation point
V_g	Velocity of gas (steam)
V_{rel}	Relative velocity
W_i	Droplet weight
x	Length downstream of the trailing edge of the stator
y	Direction perpendicular to x
y_o	Width of wake at x

Symbol	Definition
y/y_o	Position of droplet in wake at x
z	Drop diameter
α	Angle of steam and droplet velocity to axial direction
μ_d	Droplet viscosity
μ_g	Gas viscosity
ρ_d	Density of droplet
ρ_g	Density of gas
σ_d	Droplet surface tension
g	Gravitational acceleration
h_b	Blade height
Re_d	Droplet Reynolds number
t	Time
t'	Time to start the stripping of a droplet
U	Gas velocity of wake at the point $(x, y) = V_g$
U_o	Gas velocity of free stream boundary at the point (x, y_o)
U/U_o	Ratio of gas velocity in wake to free stream gas velocity

3.3 MATHEMATICAL MODEL

Forces

In the following analysis spherical drops are assumed with a C_D correction.

The aerodynamic force F_d on a droplet is given by the relation:

$$F_d = C_D \frac{\rho g}{2g} (V_{rel})^2 A_d \qquad (15)$$

where the cross sectional area is $A_d = \frac{\pi D_d^2}{4}$ and the (16)

relative velocity is $V_{rel} = V_g - V_d$ (17)

The drag coefficient C_D for distorted droplets as given in Reference 11 is:

For $0 \leq Re_d < 80$ $C_D = 27\ (Re_d)^{-0.84}$ (18a)

For $80 \leq Re_d \leq 10^4$ $C_D = 0.271\ (Re_d)^{+0.217}$ (18b)

For $Re_d > 10^4$ $C_D = 2.0$ (18c)

A plot of drag coefficient (12) versus Reynolds Number is shown in Figure D-3.

In general the range of Reynolds Number encountered in this type of problem are such that Equation (18b) is applicable.

The droplet Reynolds Number is given by the expression:

$$Re_d = \frac{\rho_g V_{rel} D_d}{\mu_d} \quad (19)$$

Newton's second law can also be used to express the accelerating force. So if the droplet mass remains constant, then:

$$F_d = \frac{W_d}{g} \frac{dV_d}{dt} \quad (20)$$

The weight of a droplet is:

$$W_d = \frac{\pi}{6} D_d^3 \rho_d \quad (21)$$

Combining Equations (15), (16), (20), and (21) gives:

$$F_d\ C_D \frac{\pi}{8g} D_d^2 \rho_g (V_{rel})^2 = \frac{\pi}{6g} D_d \rho_d \frac{dV_d}{dt} \quad (22)$$

$$\frac{dV_d}{dt} = \frac{3}{4} C_D \frac{\rho_g}{\rho_d} \frac{(V_{rel})^2}{D_d} \quad (23)$$

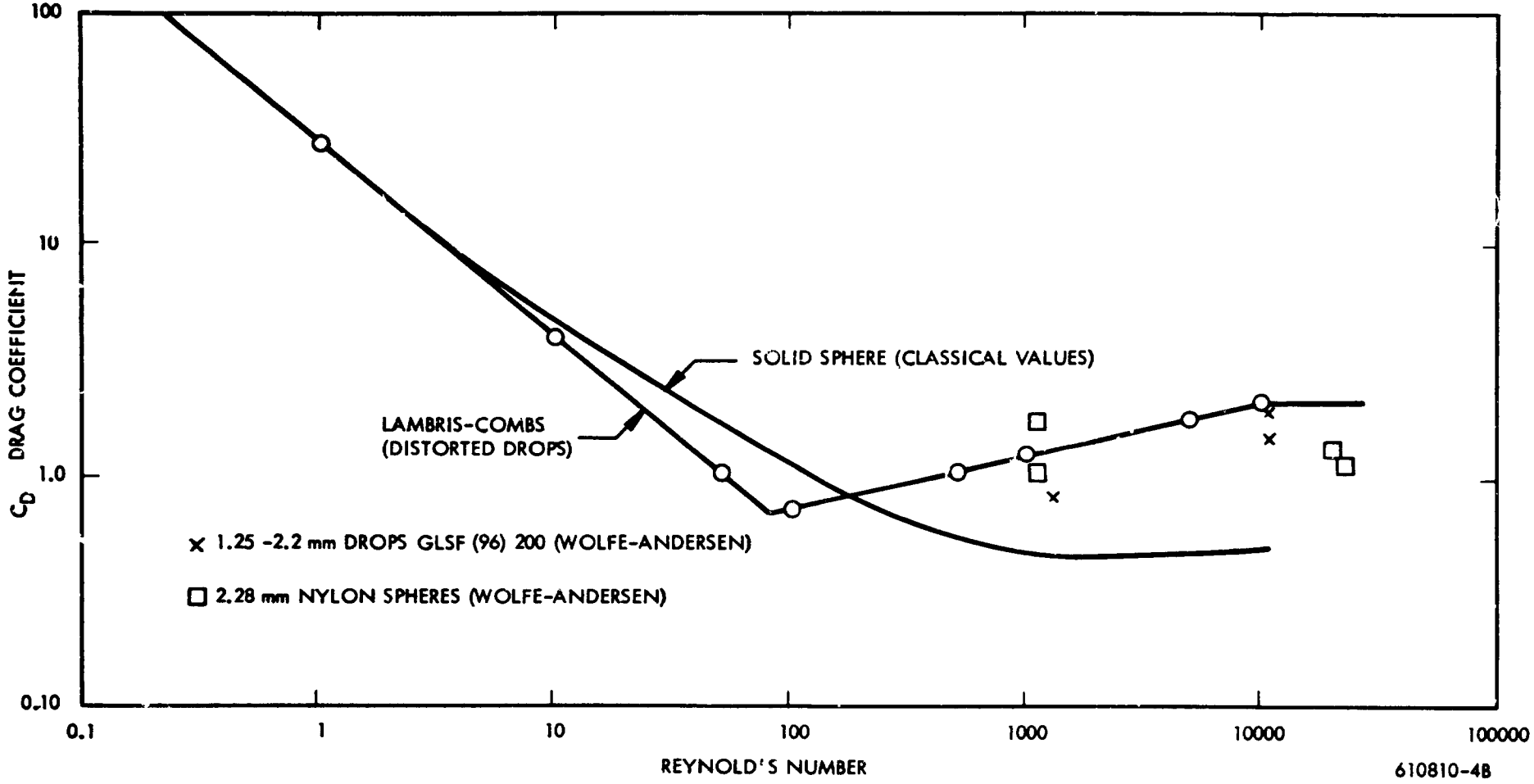

Figure D-3 Drag of Spheres and Liquid Droplets

Since the second derivative of the distance x traveled with respect to time t is equal to the droplet acceleration or the first derivative of the droplet velocity with respect to time, then:

$$\frac{d^2 x}{dt^2} = \frac{d V_d}{dt} = 0.75 \; C_D \frac{\rho_g}{\rho_d} \frac{(V_{rel})^2}{D_d} \qquad (24)$$

Equation (24) is a second order, nonlinear, ordinary differential equation with variable coefficients and is best solved by numerical integration techniques. ANALOG-ALGOL was used to obtain rapid results for a number of cases. (See Appendix 4 for computer program discussio

Secondary Breakup Criterion. The Weber number is indicative of droplet stability[1,2]. It is calculated by:

$$We_d = \frac{\rho_g (V_{rel})^2 D_d}{g \sigma_d} \qquad (25)$$

When the Weber number exceeds a critical value (of the order of 13-22), the drop will start to break up into smaller droplets.

Time to Disruption. An expression for the time t' to the start of the disruption of water drops as derived from Reference 13 information is:

$$t' = 1.1 \left(\frac{D_d}{V_{rel}} \right) \sqrt{\frac{\rho_d}{\rho_g}} \qquad (26)$$

Mean Diameter Secondary Drops. The mass mean diameter D_{3-0} of the secondary drops which are stripped from the primary drops of diameter D_d during $t > t'$ is taken from Wolfe and Andersen[13] as:

$$D_{3-0} = \left[\frac{136 g^{3/2} \mu_d \sigma_d^{3/2} D_d^{1/2}}{\rho_g^2 \rho_d^{1/2} V_{rel}^4} \right]^{1/3} \qquad (27)$$

Secondary Drop Size Distribution. The secondary drop size distribution was determined using the empirical relationship of Nukiyoma and Tanasawa[9] for gas atomized liquids:

$$\frac{dV}{dz} = \frac{\pi a}{6} z^5 \; e^{-bz^n} \tag{28}$$

The value of n was taken equal to 1.0 on the same basis as previously discussed in connection with primary atomization.

Normal Impacts on Rotor Blades. According to knowledgeable opinion such as Reference 14 (also Volume III) it is the normal component of the impacting drop velocity against the rotor blade which causes erosion and the tangential component can be neglected. Hence, if the drops have been accelerated to the free stream velocity, little erosion should be expected as turbine blading is usually designed so that the vapor slices along the blades cleanly.

Since in most turbine designs, there is not sufficient space between rotor and stator to allow complete acceleration of the liquid torn from the stator, the drops have damaging velocity components normal to the nose and leading edge of the rotor blades.

In Reference 1 Gardner gives the following expression for droplet impact velocity normal to the leading edge of the rotor blade:

$$\frac{V_{d_{N1}}}{U_o - V_d} = \frac{\cos \alpha}{\left[\left(\frac{U_o}{V_b}\right)^2 - 2\left(\frac{U_o}{V_b}\right)\sin \alpha + 1\right]^{1/2}} \tag{29}$$

A similar expression for droplet impact velocity normal to the nose of the rotor blade at the stagnation point is:

$$\frac{V_{d_{N2}}}{V_d} = \frac{V_b}{U_o}\sqrt{\left(\frac{U_o}{V_b}\right)^2 - 2\left(\frac{U_o}{V_b}\right)\sin \alpha + 1} \tag{30}$$

3.4 Application of Model to Yankee Turbine Ninth Stage

The mathematical expressions of the model have been used in conjunction with the wake information of the previous section to calculate a set of values of the drop sizes and velocities of the damaging liquid impacting the Yankee ninth rotor blades.

The wake information used is given in figures D-4, D-5, and D-6. As discussed in Section C, the thickness y_o of the wake from the trailing edge of a stator is a function of x as shown in figure D-4. The ratio (U/U_o) of the steam velocity in the wake to the free steam velocity is plotted versus x for the pressure and suction sides with y/y_o as a parameter in figures D-5 and D-6.

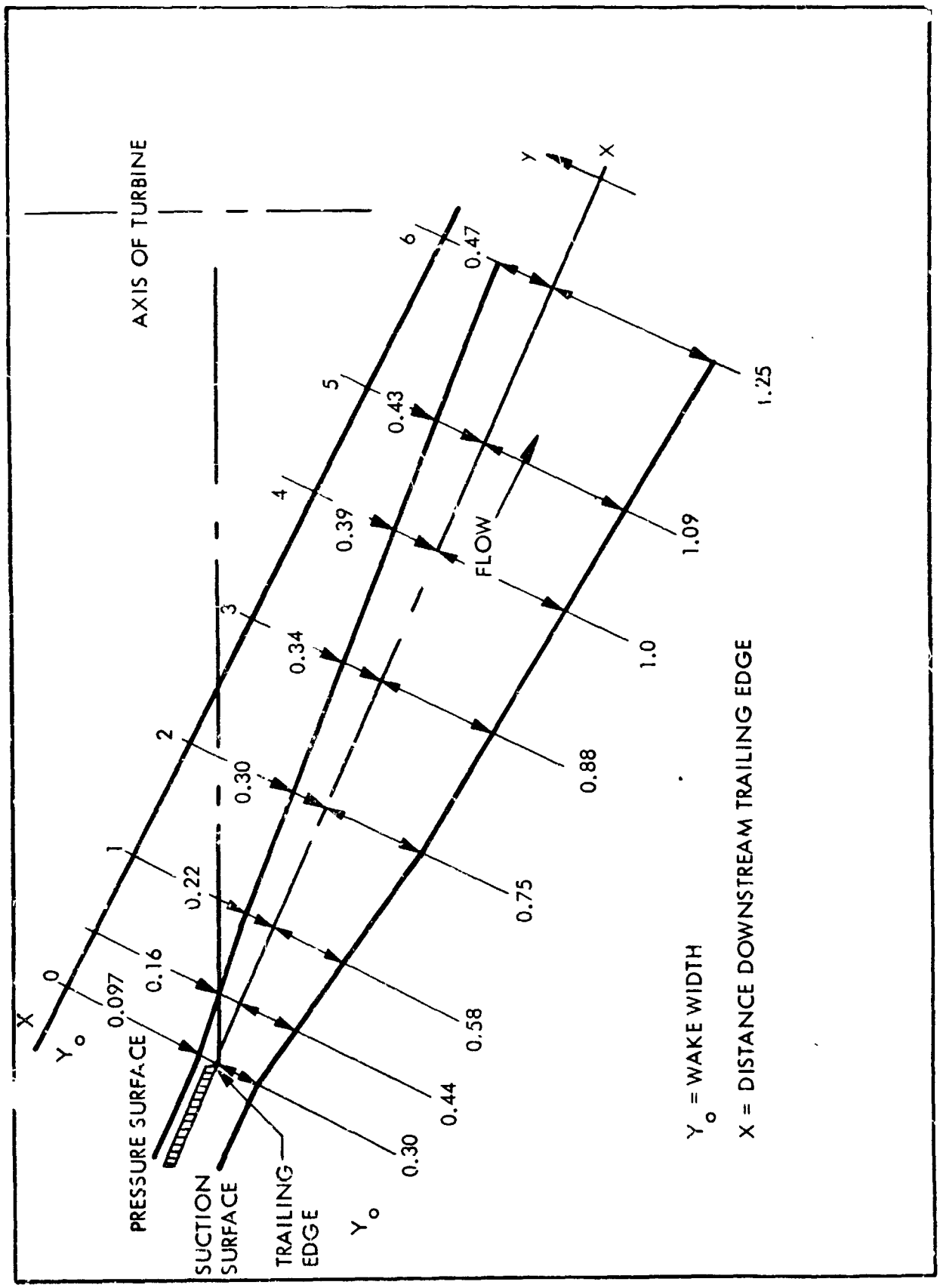

Figure D-4. Ninth Stage Stator Wake, Yankee Turbine

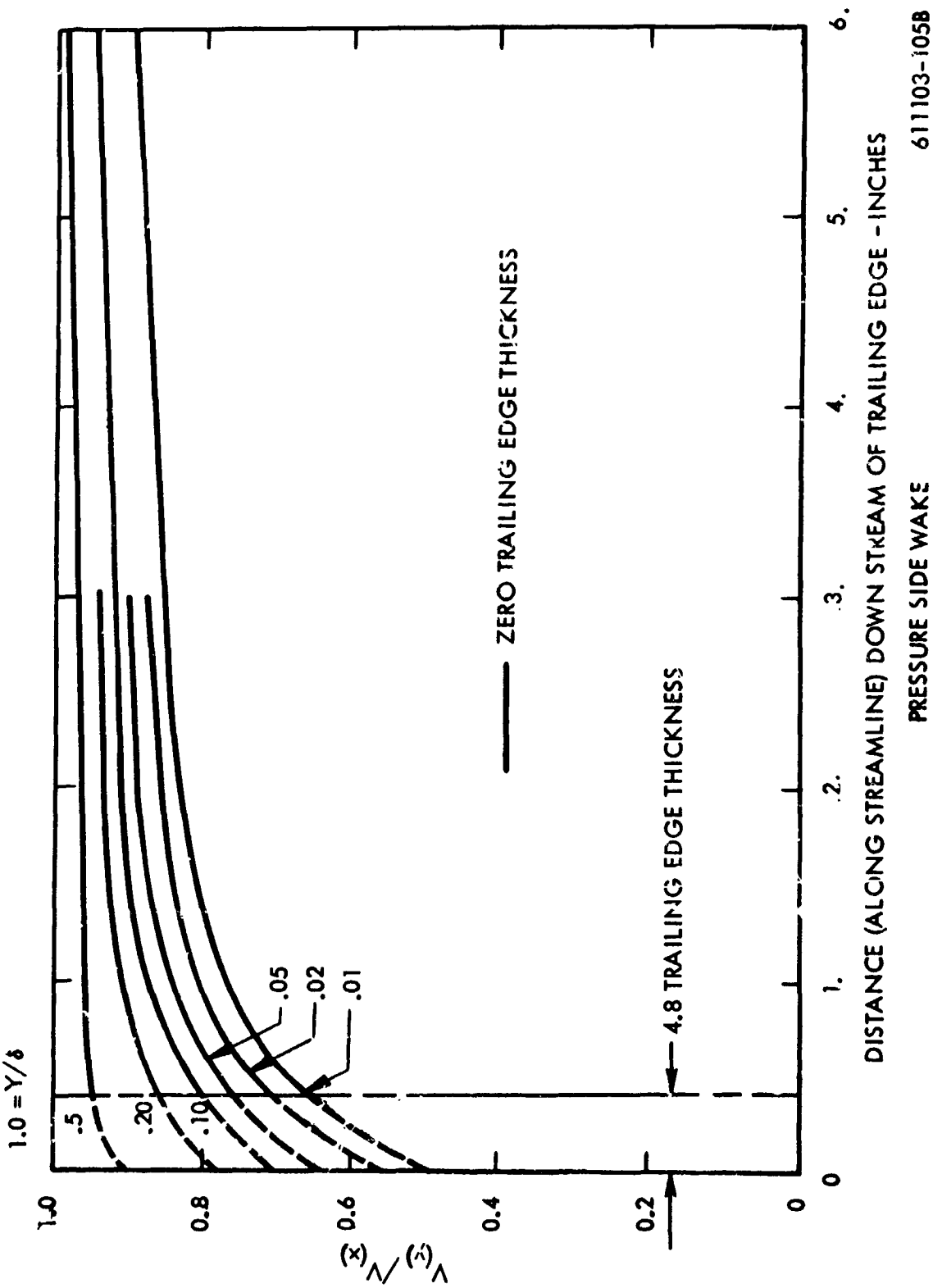

Figure D-5. Wake Pressure Side Velocities, 9th Stator Yankee Turbine

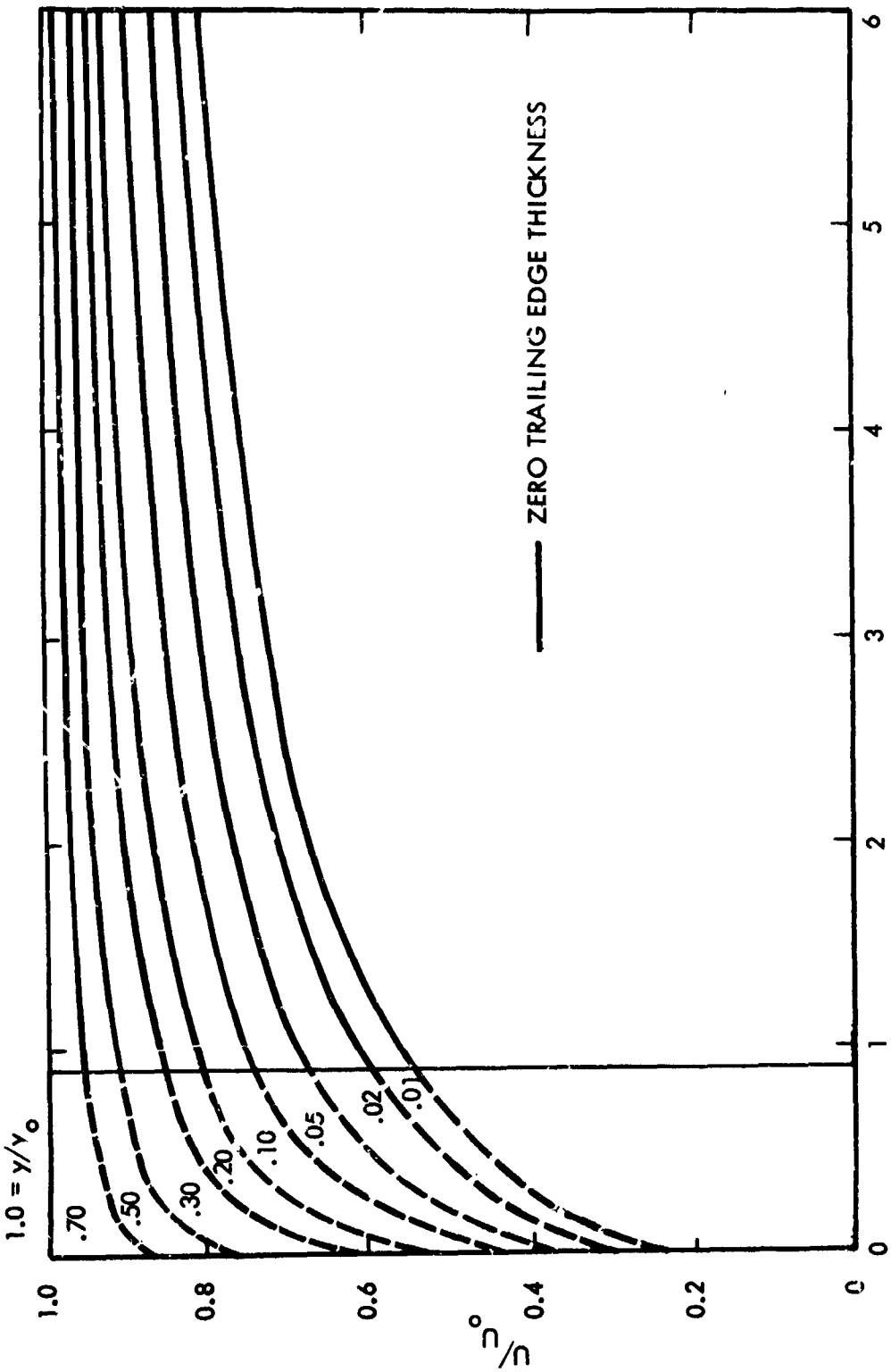

Figure D-6. Wake Suction Side Velocities, Ninth Stator Yankee Turbine

Trajectory Calculations. In performing the computations, it was assumed that the droplets (once torn off the stator) were to migrate in the wake until they arrived at a position of x=3/8" with a downstream velocity of essentially zero. Then they were accelerated by the aerodynamic forces along a constant y/y_o path. Three values of y/y_o were chosen as representative droplet paths for both the pressure and suction sides: 1.0, 0.2, and 0.01. To reduce technician plotting time, a computer printout is in some instances selected to display plots of: droplet velocity, Reynolds Number, Weber Number, and $(U_o - V_d)$ versus distance x traveled and x versus time. It should be realized that since a line printer can not "half-space", the resulting points may be slightly in error--but the overall trend is usually quite apparent. All calculations are for the exit conditions of the ninth stator of the Yankee Atomic Turbine.

Initially, seven droplet diameters were chosen and the symbols "1", "2", "3", "4", "5", "6", and "7" correspond to droplet diameters of 100, 200, 300, 400, 600, 1000, and 1400 microns, respectively. Figures D-7 through D-11 show typical plots of droplet velocity, vapor velocity minus drop velocity, Reynolds Number, and Weber Number versus distance x traveled and x versus time t of travel for various values of y/y_o.

A comparison of the calculated droplet velocity and size with experimental CERL data in Reference 4 from a steam tunnel shows fair agreement even though the test conditions are only approximately equivalent to those of the Yankee Atomic Turbine ninth stator exit. Figure D-12 indicates that perhaps a better initial starting point for the droplets would be 1/4 inch rather than the 3/8 inch as was assumed. However, it should be noted that the trailing edge thickness of the ninth stator of the Yankee Atomic Turbine is 0.077 inch, whereas the CERL blade was approximately 1/16 inch.

From these plots (and others not shown) the following may be concluded for the droplets torn off the ninth stator:

1) Smaller droplets are accelerated faster than are larger droplets.
2) Droplet Reynolds numbers ranged from approximately 100 to 3500.
3) Droplet Weber numbers ranged from approximately 1 to 174.

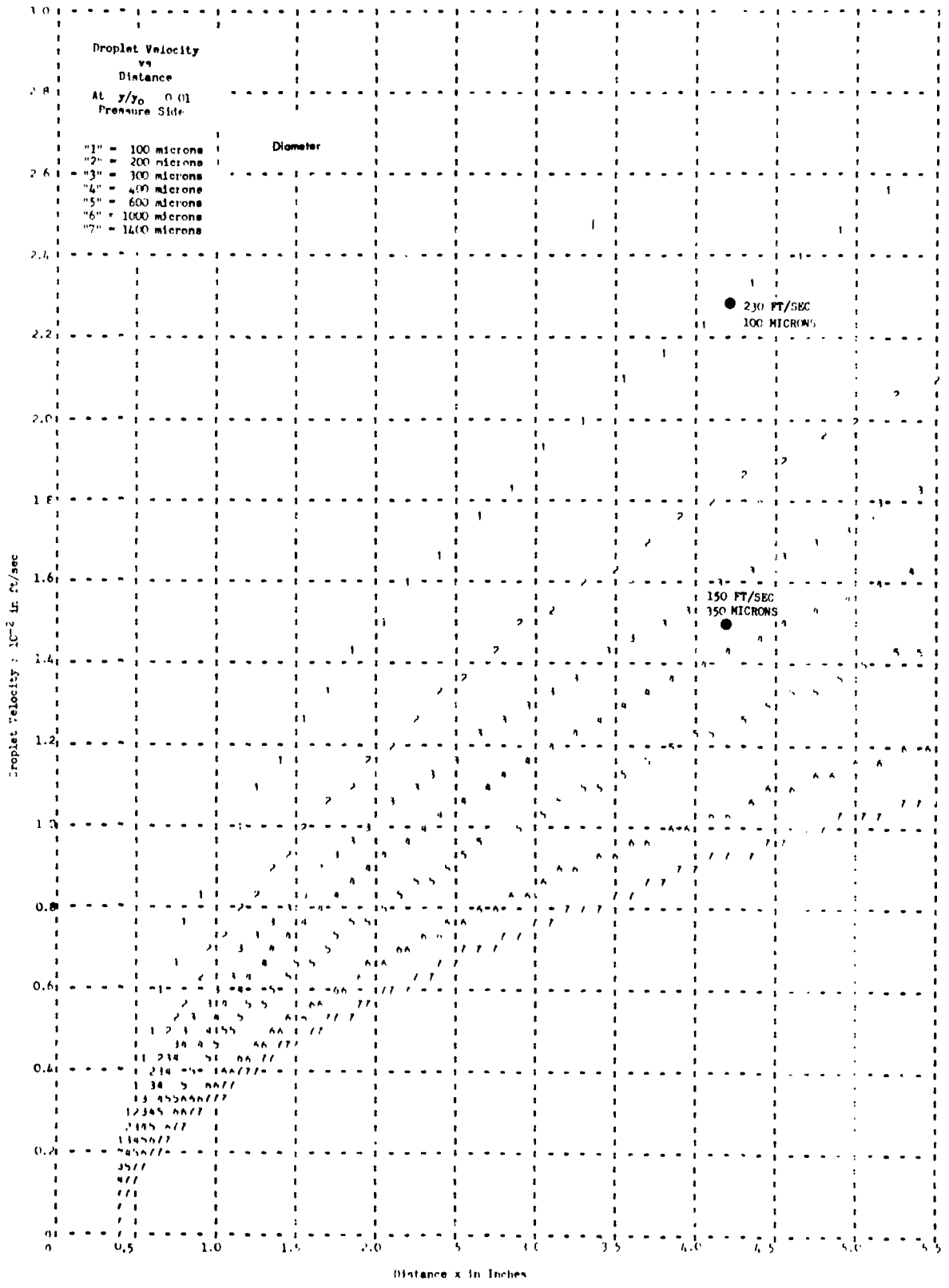

Figure D-7. Droplet Velocity Versus Distance

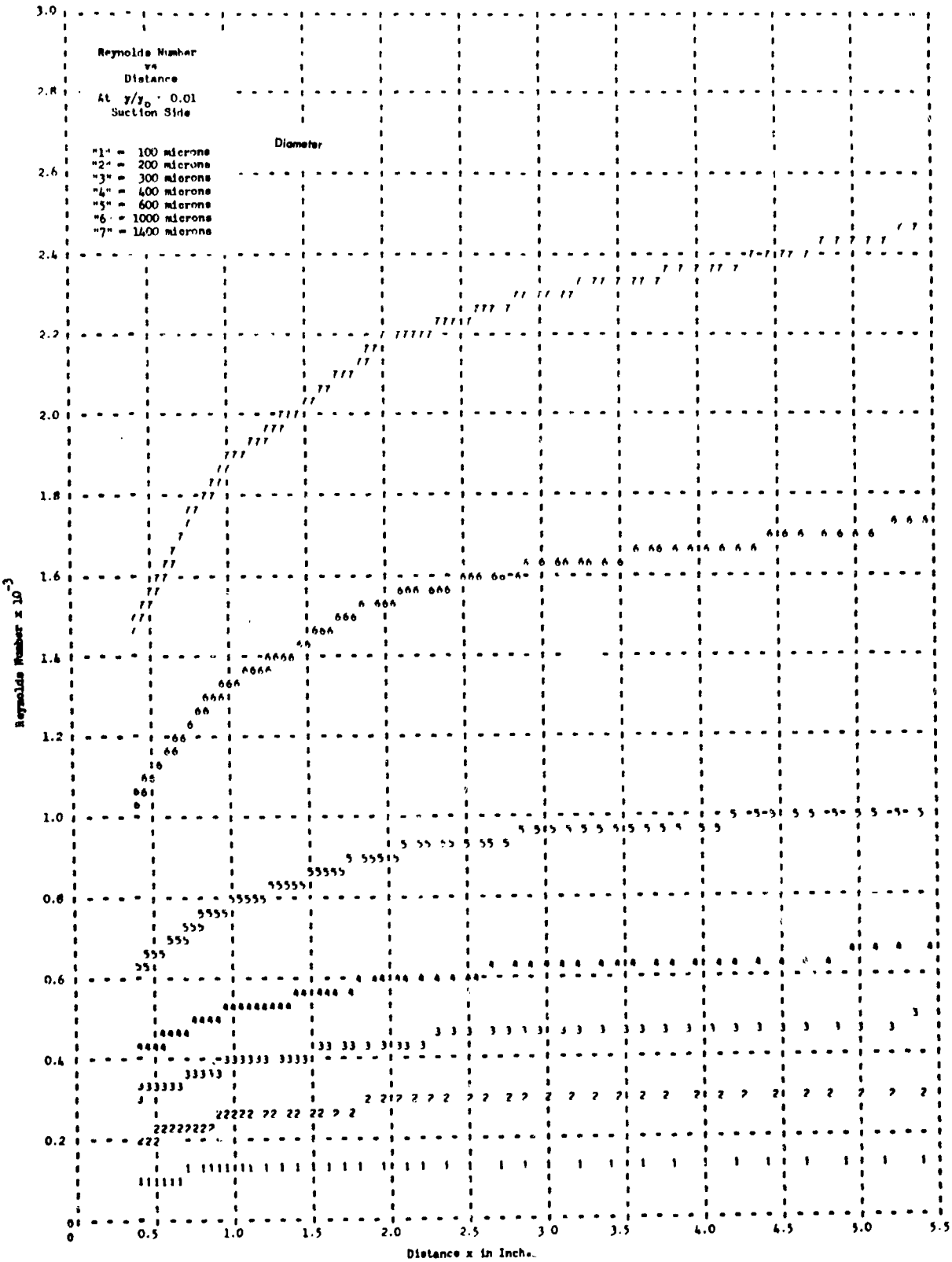

Figure D-8. Reynolds Number Versus Distance

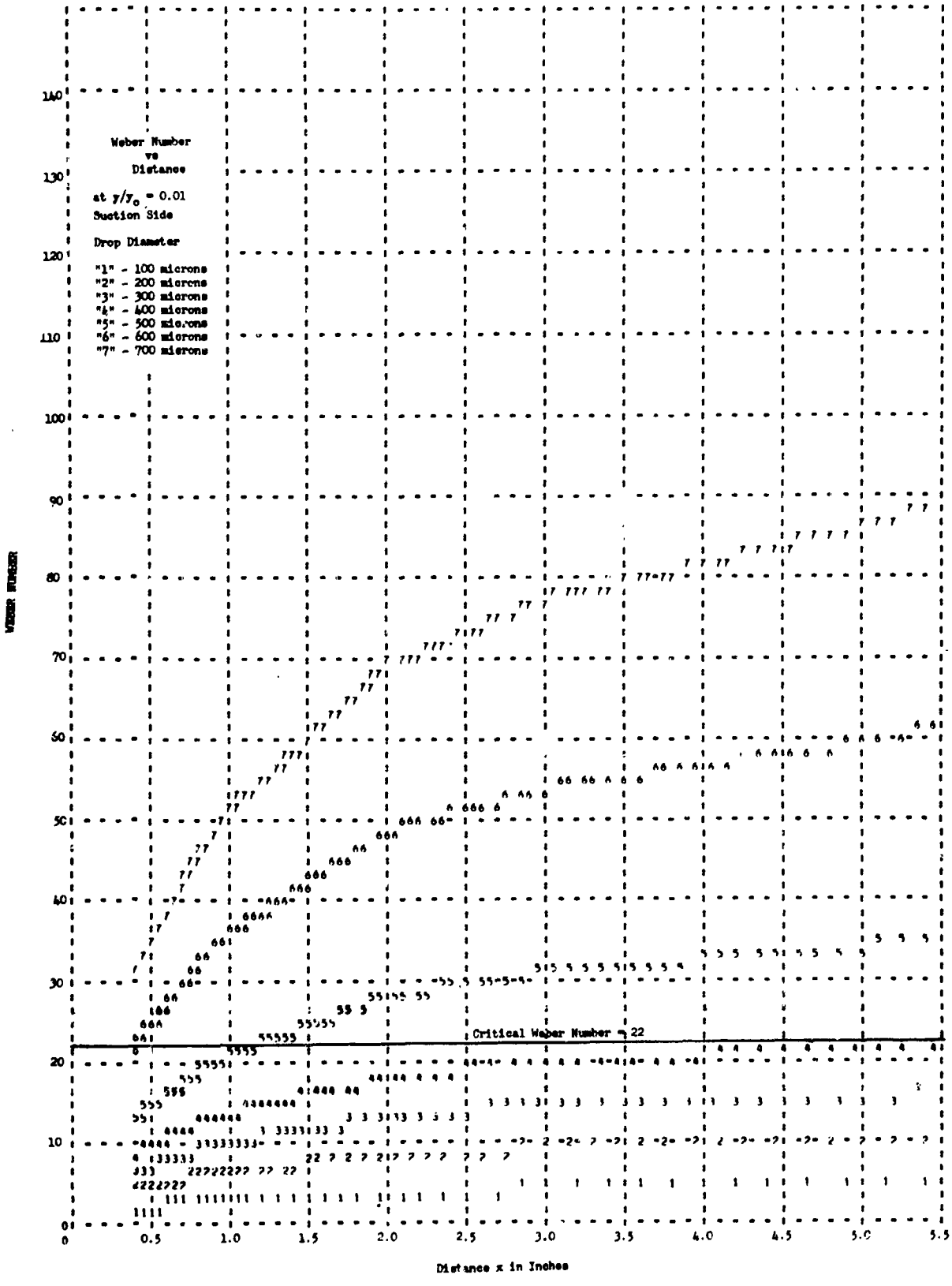

Figure D-9a. Ninth Yankee Stator Wake, Weber Number versus Distance at y/y_o = 0.01 Suction Side

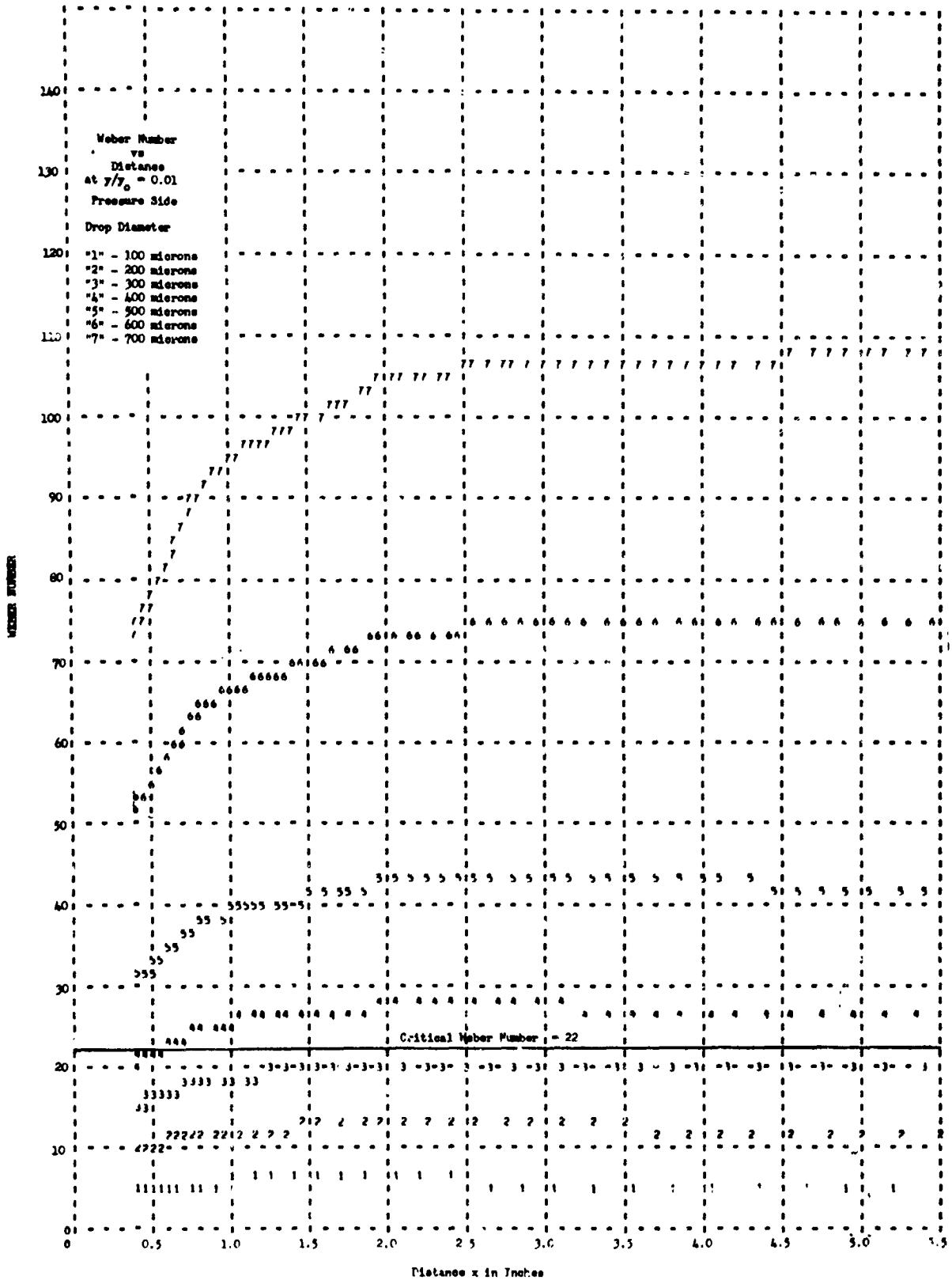

Figure D-9b. Ninth Yankee Stator Wake, Weber Number versus Distance at y/y_o - 0.01 Pressure Side

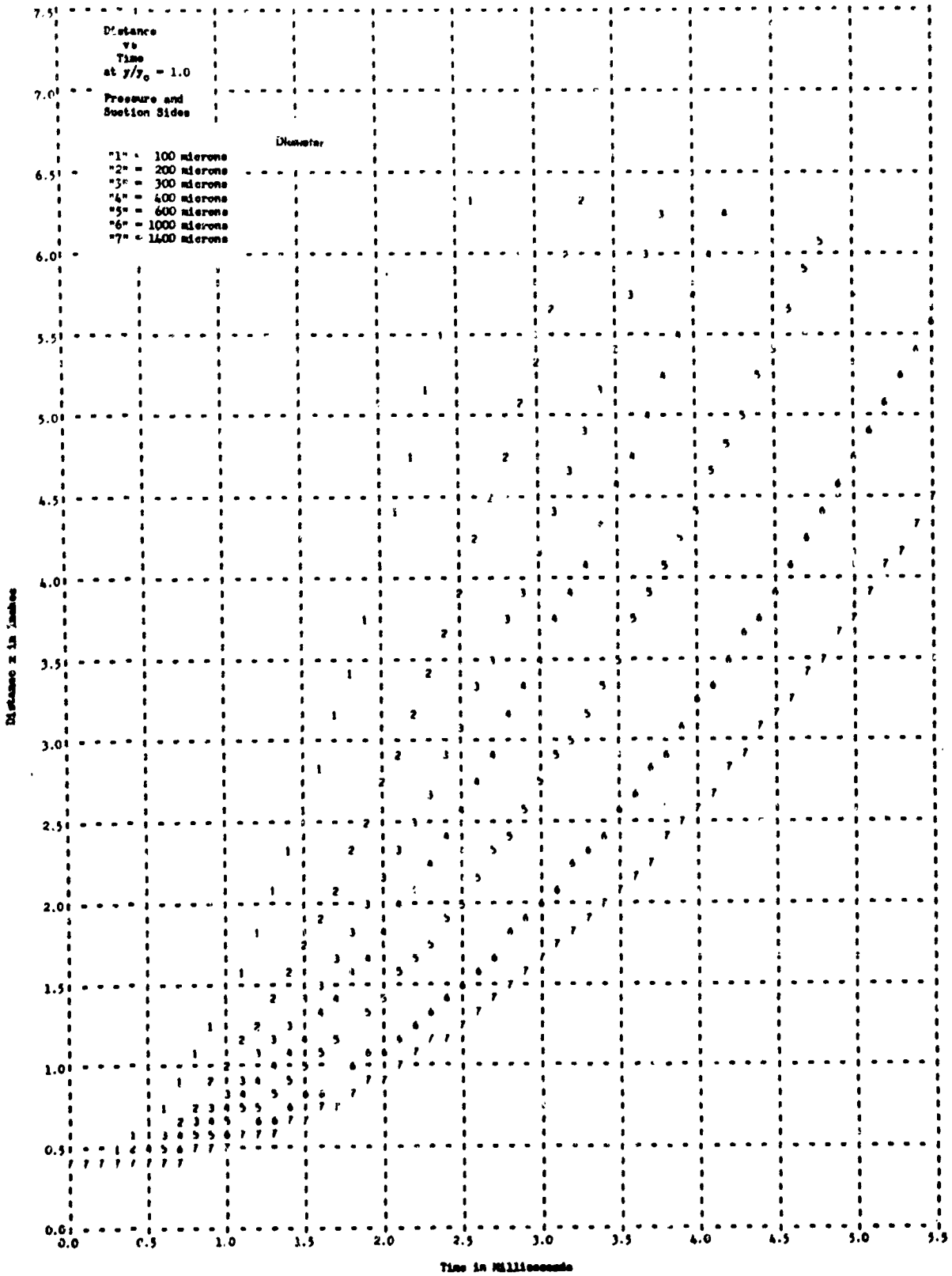

Figure D-10 Distance Versus Time at y/y_o = 1.0

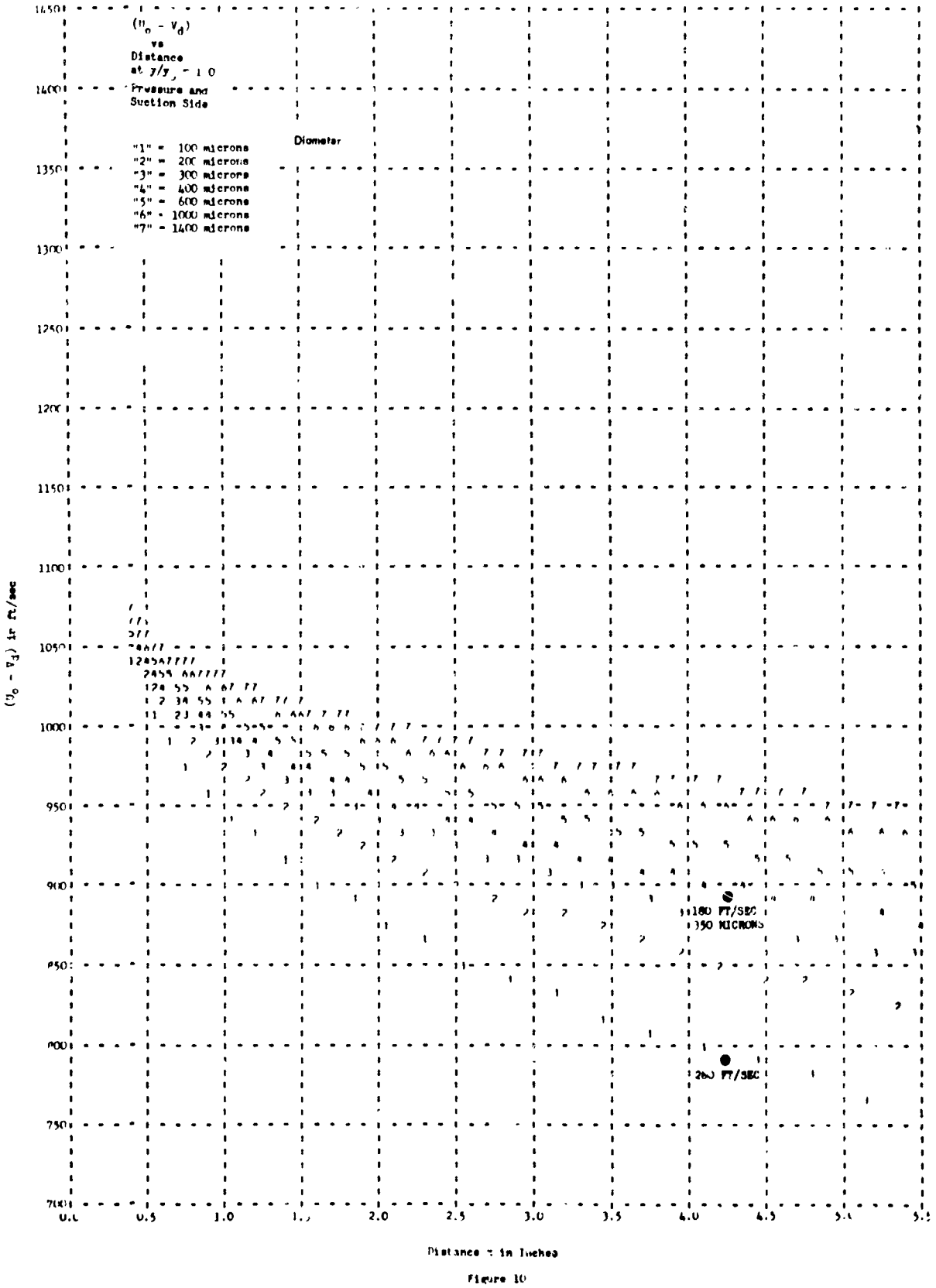

Figure 10

Figure D-11. $(U_o - V_d)$ Versus Distance at $y/y_o = 1.0$

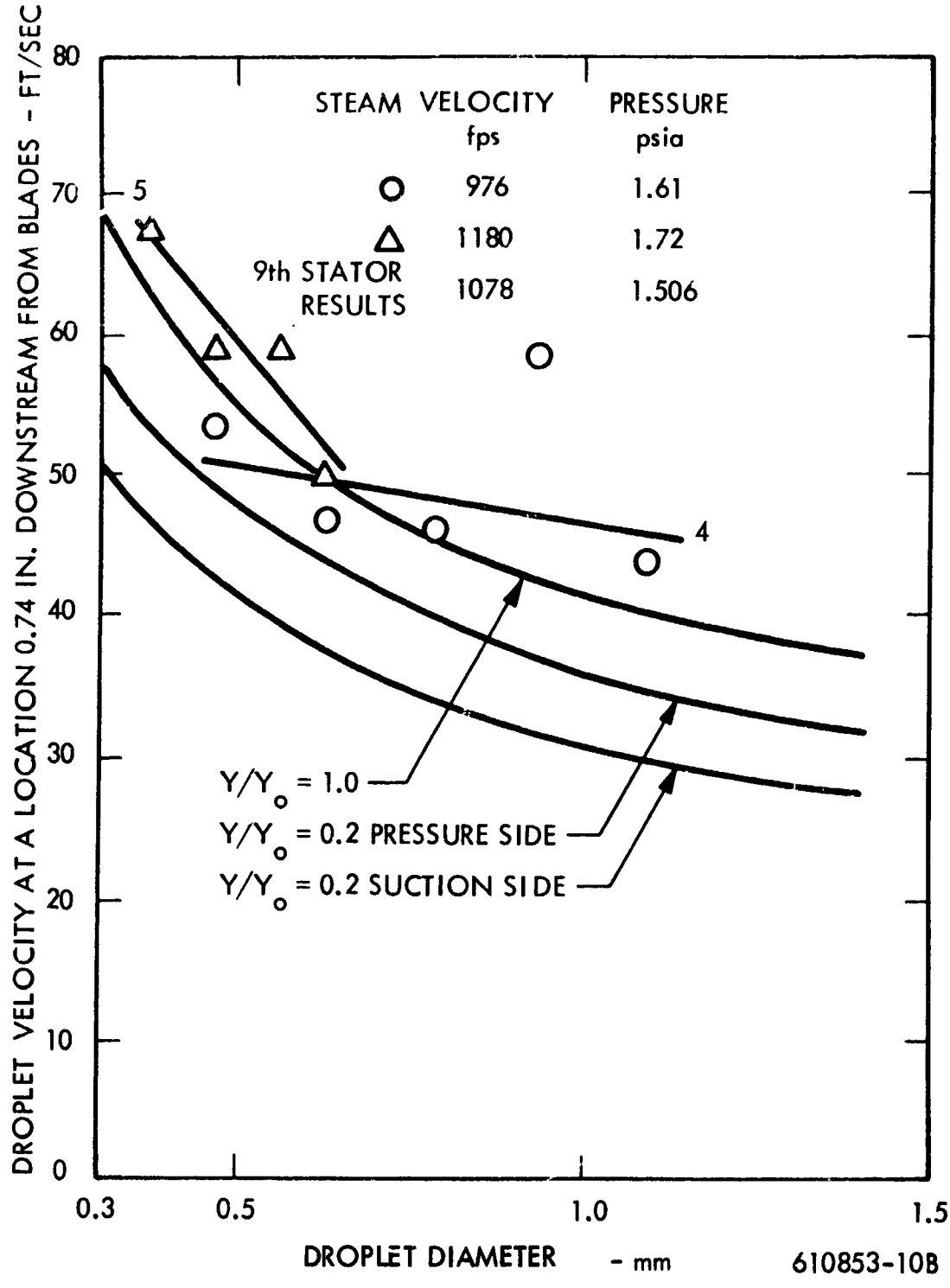

Figure D-12. Drop Velocity

4) Assuming a critical Weber number of 22, the maximum stable droplet diameter appears to be 300 - 400 microns depending on the position (y/y_o) in the wake.

5) In order for droplets from the ninth stator to hit the ninth rotor, they must travel through a distance of about 4.25 inches. For a 350 micron diameter droplet it would take from 3.2 to 6.7 msec to reach the rotor. The time t' to initiate stripping as calculated using Equation 26 varies from 0.15 to 0.20 msec. The reason for the variations is due to the position from which the droplet started in the wake. It is estimated that stripping (if it occurs) would be essentially complete by 2.5 t'. It is therefore concluded that stripping will decrease the droplet size so that the largest diameter hitting the ninth rotor will be of the order of 350 microns.

6) The mass mean diameter of the droplets produced by the aerodynamic breakup of a liquid drop of diameter >350μ varies from 22.5μ to 80μ, depending upon the initial diameter before stripping and its relative velocity (which in turn depends upon the initial starting point in the wake). Equation 27 is used for these calculations. An upper bound on the diameter of drops torn off the stator is assumed to be 1600μ. Hence, if stripping occurs, it will be complete before approximately 0.5 msec have elapsed. During this short interval, the droplets will not be accelerated appreciably, therefore, $V_{rel} \cong U$.

Conclusion 6 allows a simplification in model calculations. It indicates that from a practical view of the impact velocities of various drops with the following rotor that all drops can be considered to have originated at the same time and axial locations. Using the assumption and the parametric drop trajectory calculations plus Equations 29 and 30, the normal velocities of damaging impact, $V_{d_{N1}}$, $V_{d_{N2}}$, with the following rotor have been calculated.* These results are displayed in figures D-13 and D-14. Figure D-13 gives the calculated minimum velocity of impact and figure D-14, the calculated maximum velocity of impact for various drop sizes as a function of rotor blade length measured from the hub. The possible velocities of impact for a given drop size vary depending upon the particular streamline followed by the

---

* The maximum impact normal to the blade surface is on the nose radius between the nose stagnation point and the convex side leading edge. This velocity is equal to $\sqrt{(V_{d_{N1}})^2 + (V_{d_{N2}})^2}$.

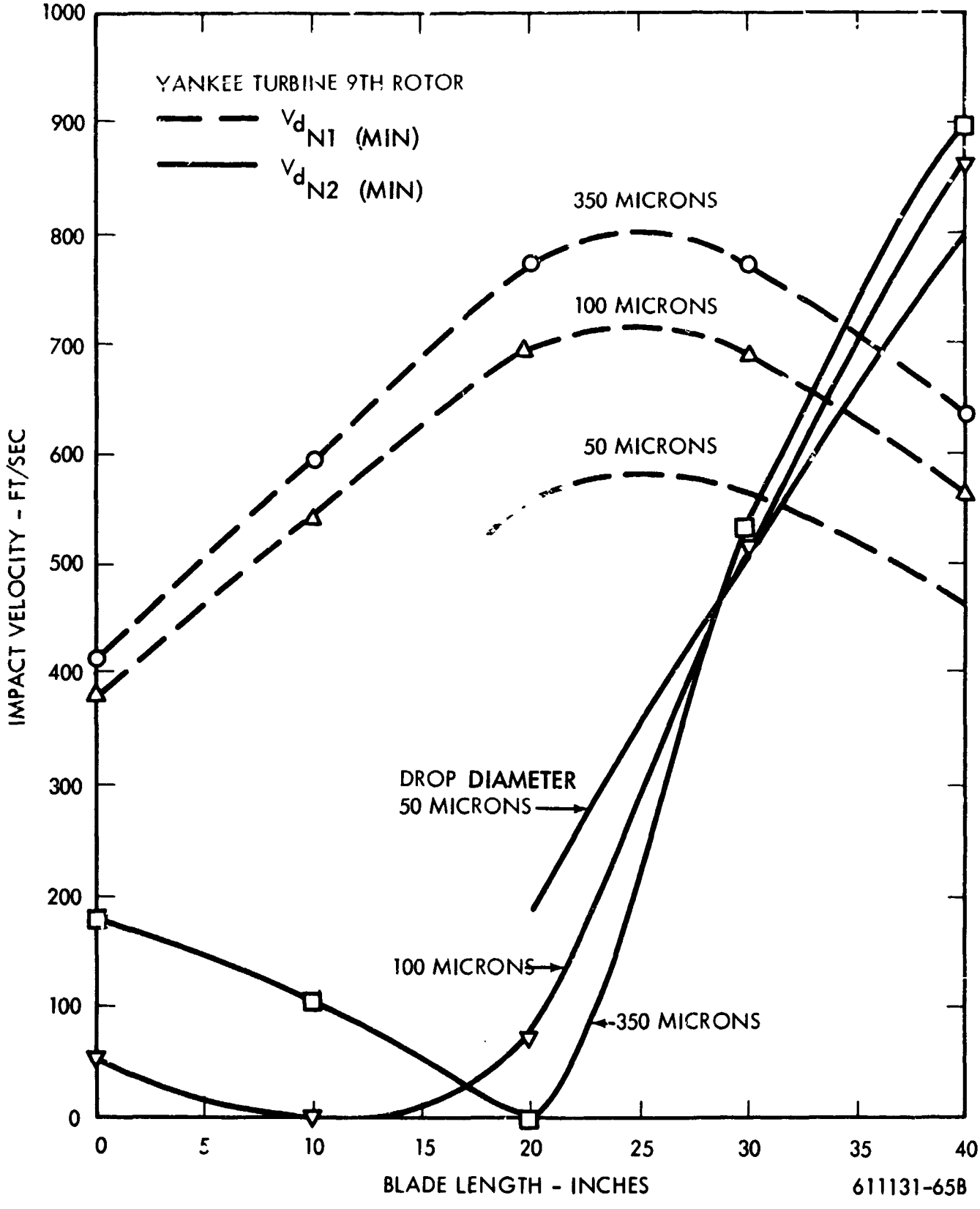

Figure D-13. Damaging Drops Normal Impact Velocities (Minimum)

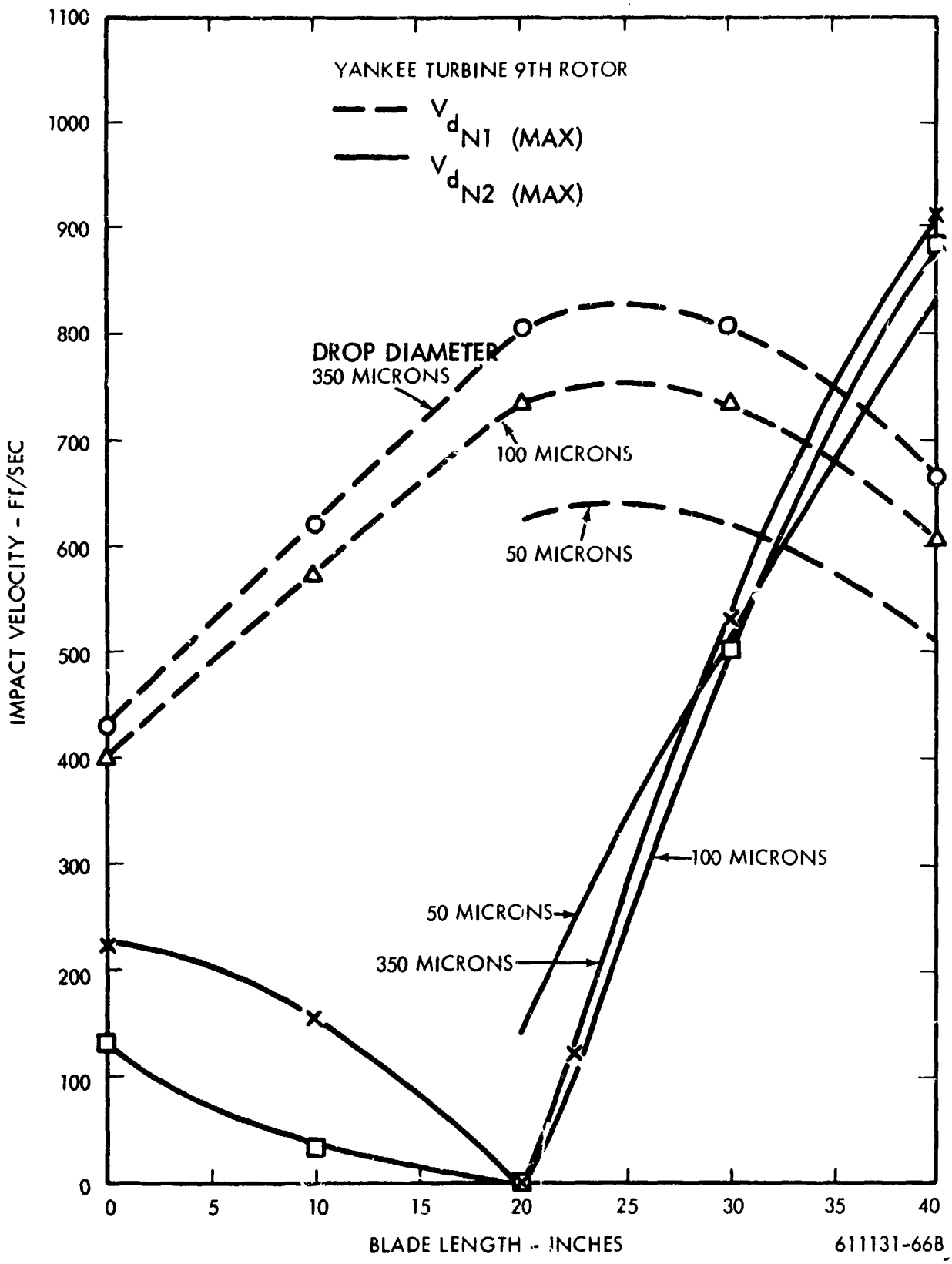

Figure D-14. Damaging Drops Normal Impact Velocities (Maximum)

drop with respect to the wake of the stator. The information presented in figures D-13 and D-14 accurately reflects the changes in bulk stream velocity and rotor blade speed along the blade length from the standpoint of equations 29 and 30. However, the parametric drop trajectory calculations were only carried out at mid-span of the blade. The final drop velocities at other spanwise locations were obtained by correcting the mid-span values in the ratio of the square roots of the initial accelerating forces. This is a reasonable procedure since the large drops of interest are always substantially below vapor stream velocity. No corrections were made for three dimensional effects such as a blade tip vortex.

The calculated maximum and minimum axial length of the convex surface of the rotor over which the drops impact is shown in figures D-15 and D-16. The qualifying remarks made with respect to the normal impact velocities also apply to the axial impact length calculations.

Drop Size Distribution at Turbine Rotor. On the basis of the trajectory calculations it was concluded that almost all the drops formed by primary atomization above 350 microns would undergo further breakup if the critical Weber Number is taken at 22.* From table 1 of the primary atomization discussion (Section D), these larger drops are 88 % by weight of the total damaging liquid flow and have a mass average** diameter of 640 microns ($2.1\ (10^{-3})$ft).

Applying the Wolfe and Anderson expression (equation 27) for secondary atomization to this diameter of 640 microns yields a mass mean diameter after secondary atomization of 48 microns. The state conditions used in the calculation were those at mid-span of the outlet of the ninth stator. In addition the value of V_{rel} was assumed, on the basis of an intuitive examination of figures D-3 and D-4, to be $0.78\ U_o$. This value agrees with the intuitive judgement of Gardner.

Applying the Nukiyama-Tanasawa distribution function, equation 28, to the mass mean diameter and adding the secondary distribution to the residual of unbroken drops from the primary atomization process ($D_p < 350$ microns) gives a drop size distribution approaching the ninth rotor. The distribution obtained is shown in figure D-17.

---

* The results of erosion calculations where 400μ drop diameter was taken as the upper limit are reported in Vol. I as well as these calculations. The 400μ diameter calculations give better agreement with the observed erosion. However, 350μ diameter is a better average size between suction and pressure side wake calculations. (see figures D-9a and D-9b.)

* 50 % of the 88% is in drops larger than the "average" diameter.

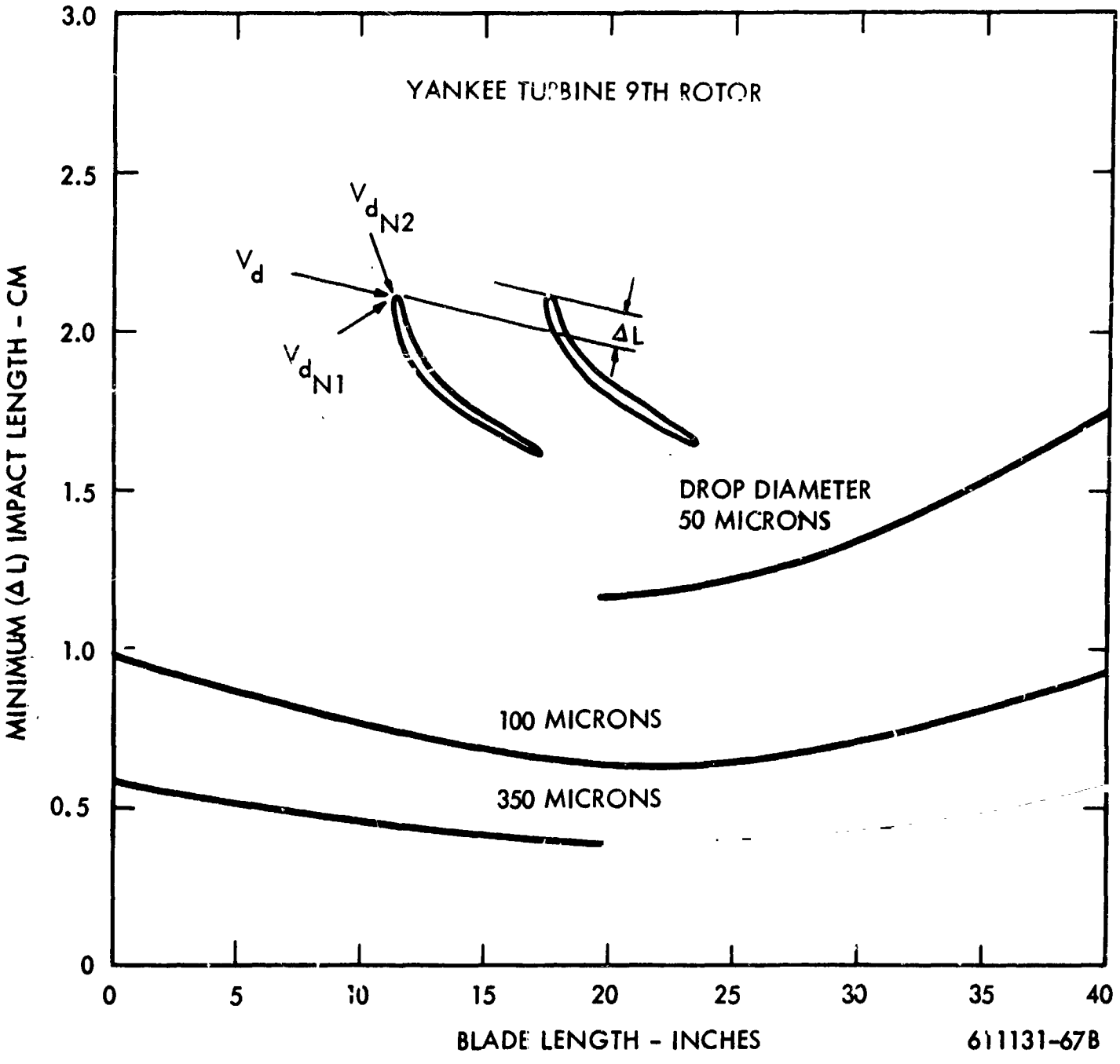

Figure D-15. Axial Length Impacted (Minimum)

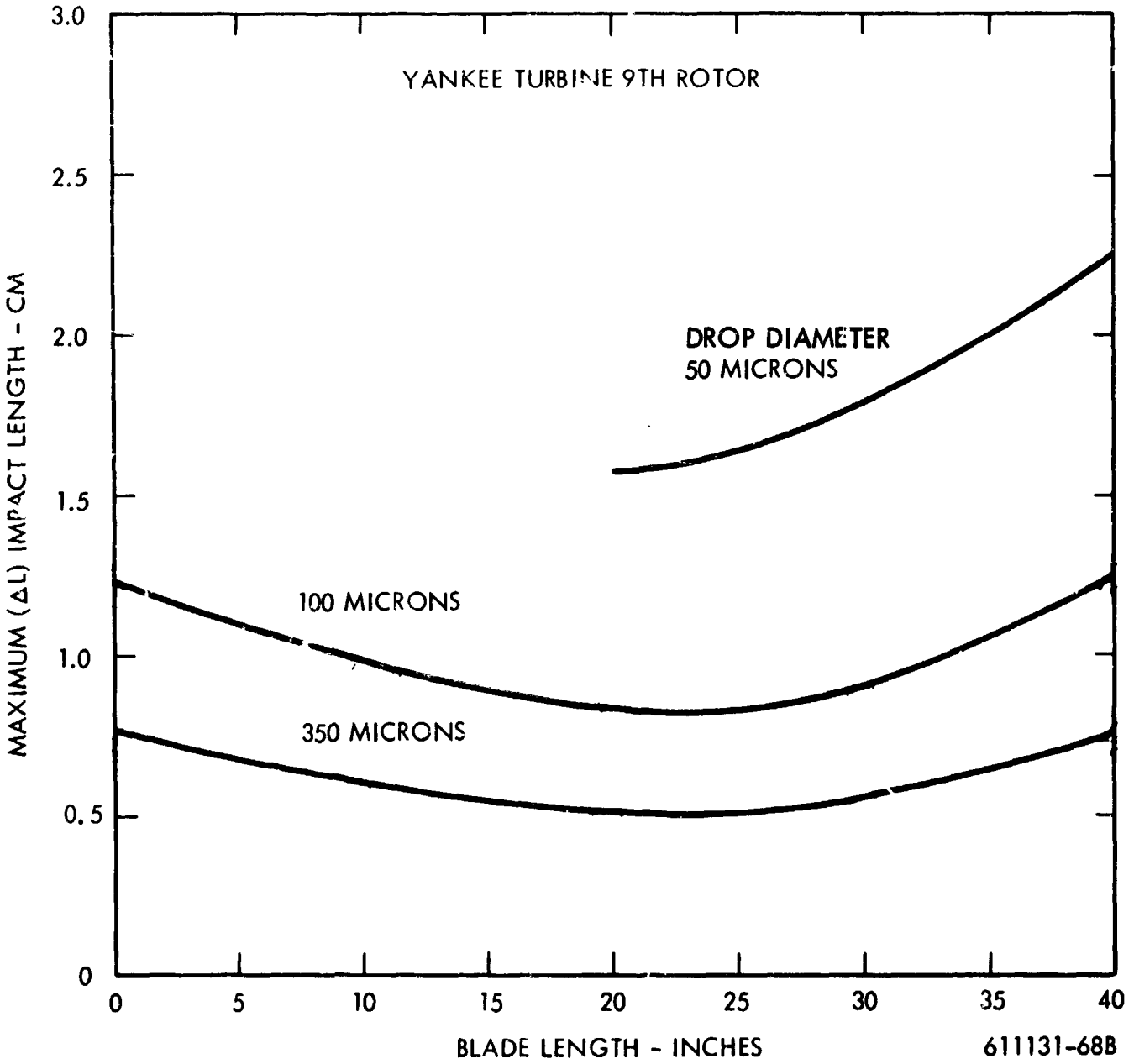

Figure D-16. Axial Length Impacted (Maximum)

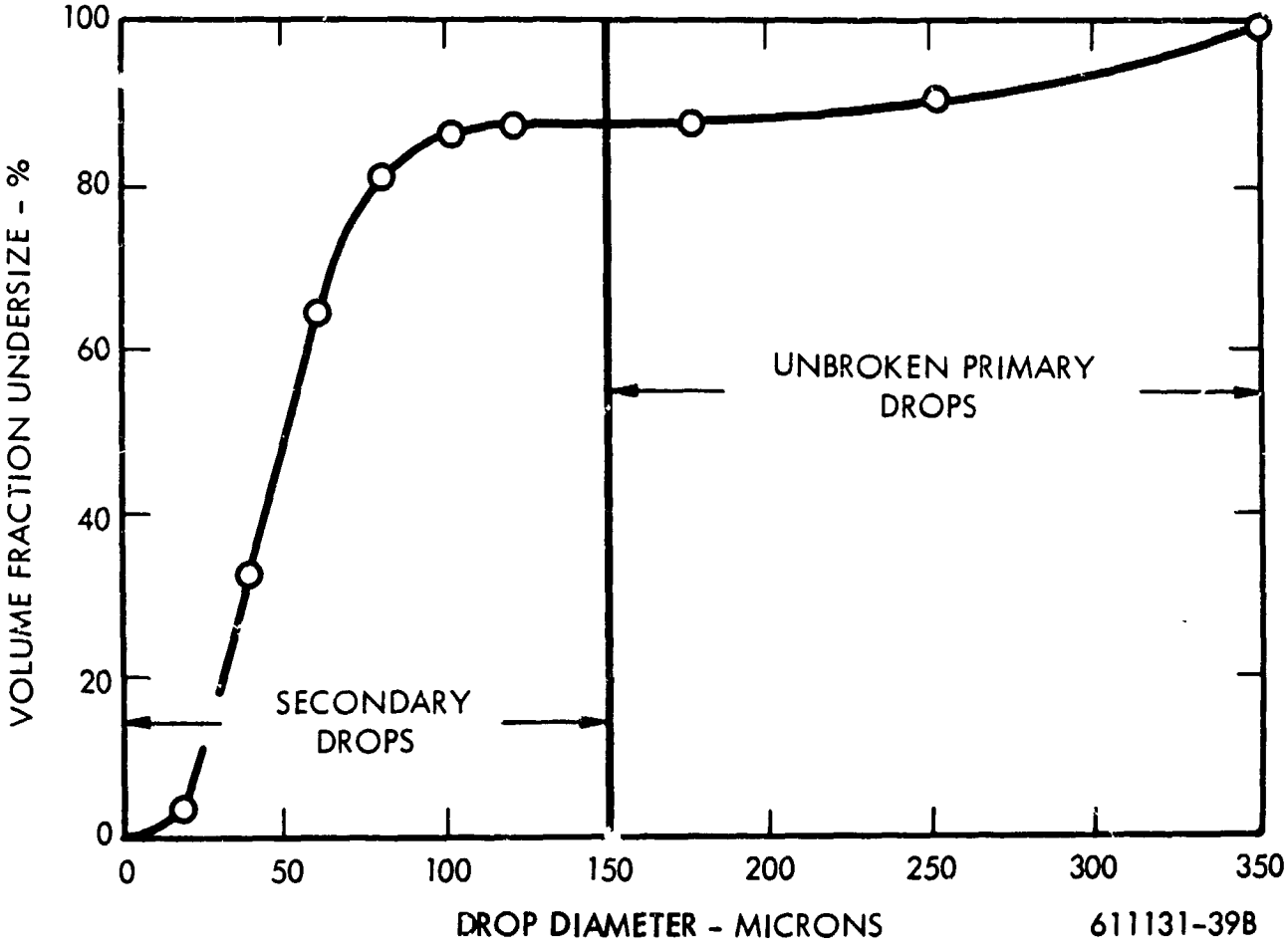

Figure D-17. Impacting Drop Size Distribution

BLANK PAGE

APPENDIX 1A

REFERENCES FOR PART A

1. Truckenbrodt, E., NACA-TM-1379, May 1955.
2. Gyarmathy, G., Juris-Verlag, Zurich 1962.
3. Gardner, C. G., Proc Inst. Mech Engrs 178, Pt 1, No. 23, pp. 593 to 623, 1963-1964.
4. Brun, R. J., W. Lewis, P. J. Perkins, J. S. Serafini, NACA Report 1215, 1955.

APPENDIX 1B

REFERENCES FOR PART B

1. Oswatitish, K. Z., Ver. deut. Ing., 86, p. 702, 1942.
2. Gyarmathy, G., Grundlagen Einer Theorie der Nassdampturbine, Juris-Verlag, Zurich, 1962.
3. Katz, J. L., H. Saltsburg, and H. Reiss, Nucleation in Associated Vapors, North American Aviation Science Center, SCPP-65-32, May 18, 1965.
4. Stever, H. G., Condensation Phenomena in High-Speed Flows, Fundamentals of Gas Dynamics, Princeton, Princeton Univ. Press, 1958.
5. Courtney, W. G., Recent Advances in Condensation and Evaporation, A.R.S. Journal, 31, pp. 751 to 756, June 1961.
6. Glassman, A. J., Analytical Study of the Expansion and Condensation Behavior of Alkali-Metal and Mercury Vapors Flowing through Nozzles, NASA-TND-2475, September 1964.
7. Hill, P. G., H. Witing, and E. P. Demetri, Condensation of Metal Vapors During Rapid Expansion, Trans. ASME (Heat Transfe `, Vol. 85, Part C, pp. 303 to 314, November 1963.
8. Frenkel, J., Kinetic Theory of Liquids, (Oxford), pp. 366 to 426.
9. Kantrowitz, A., Nucleation in Very Rapid Vapor Expansions, J. Chem. Phys., Vol. 19, No. 9, pp. 1097 to 1100, Septembe: 1951.
10. Head, R. M., Investigations of Spontaneous Condensation Phenomena, Ph. D. Thesis, Calif. Inst. Technol., 1949.
11. Tolman, R. C., The Effect of Droplet Size on Surface Tension, J. Chem. Phys., Vol. 17, pp. 333 to 337, 1949.
12. Gyarmathy, G. and R. Meyer, Spontane Kondensation, Ver. Deut. Ingr Forschungsh, No. 508, p. 21, 1965.
13. Gardner, G. C., Events Leading to Erosion in the Steam Turbine, Proc. Inst. Mech. Engrs, Vol. 178, Pt. 1, No. 23, 1963 and 1964.
14. Frisch, H. L and C. Willis, The Kinetics of Phase Transitions Involving Dimer Reactions, J. Chem. Phys., 22, No. 2, pp. 243 and 244, Feb. 1954.
15. Goldman, L. J. and S. M. Nosek, Experimental Determination of the Expansion and Flow Characteristics of Potassium Vapor through a Nozzle, unpublished as of Oct. 1, 1965.

APPENDIX 1C

REFERENCES FOR PART C

1. Schnetzer, E. (Ed.), Two Stage Potassium Test Turbine Quarterly Progress Report No. 15, (Nov. 8, 1964 - Feb. 8, 1965), Missile and Space Division, General Electric Co., NASA Contract NAS-5-1143.
2. Rossbach, R. J., Space-Vehicle Rankine-Cycle Power Plant Potassium - Turbine Development, Space Power and Propulsion Section, General Electric Co., ASME Paper 63-WA-326.
3. Joyce, J. P., Contract NAS-5-1143, Two-Stage Potassium Vapor Turbine, NASA Lewis Research Center, Nuclear Power Technology Branch, Letter 9212, March 15, 1966.
4. Brun, R. J., W. Lewis, P. J. Perkins, and J. S. Serafini, Impingement of Cloud Droplets on a Cylinder and Procedure for Measuring Liquid-Water Content and Droplet Sizes in Supercooled Clouds by Rotating Multicylinder Method, NACA Report, 1215-1955.
5. Gyarmathy, G., The Basis for a Theory of the Wet Steam Turbine, Juris-Verlag, Zurich, 1962.
6. Gardner, G. C., Events Leading to Erosion in the Steam Turbine Proc. Inst. Mech. Engrs., 178, Pt 1, No. 23, pp. 593 to 623, 1963-1964.
7. Truckenbrodt, E., A Method of Quadrature for Calculations of the Laminar Boundary Layer in Case of Plane and Ratationally Symmetrical Flow, NACA-TM-1379, May 1955.
8. Preston, J. H., The Minimum Reynolds No. for a Turbulent Boundary Layer and the Selection of a Transition Device, Journal of Fluid Mech., Vol. 3, pp. 373, 1957-1958.
9. Lieblein, S., and W. H. Roudebush, Low-Speed Wake Characteristics of Two-Dimensional Cascade and Isolated Airfoil Sections, NACA-TN-3771, October 1956.
10. Spence, D. A., Growth of the Turbulent Wake Close Behind an Airfoil at Incidence, C.P. No. 125, British ARC, 1952.
11. Heskestad, G., and D. R. Olberts, Influence of Trailing-Edge Geometry on Hydraulic-Turbine-Blade Vibration Resulting from Vortex Excitation, Trans. ASME, Jo. Eng. Power, pp. 103, April 1960.
12. Emmons, H. W., Fundamentals of Gas Dynamics, Vol. III, Sect. H., Princeton University Press, Princeton, N. J., 1958.
13. Baker, O., Simultaneous Flow of Oil and Gas, The Oil and Gas Jour., July 26, 1954.
14. Schnetzer, E., Two-Stage Potassium Test Turbine, Quarterly Progress Report No. 1B, August 8-November 8, 1965, Contract NAS-5-1143, January 10, 1966, NASA-CR-54917.

APPENDIX 1D

REFERENCES FROM PART D

1. Gardner, G. C., Events Leading to Erosion in the Steam Turbine, Proc. Inst. Mech. Engrs., Vol. 178, Part 1: No. 23: pg. 593 to 623, 1963-1964.
2. Gyarmathy, G., The Bases for a Theory of the Wet Steam Turbine, Juris-Verlag, Zurich, 1962.
3. Degner, V. R., Quarterly Status Letter No. 3, Contract NAS7-391, Investigation of Variables in Turbine Erosion, North American Aviation Inc., Rocketdyne Division 66RC5335.
4. Hays, L. G., Turbine Erosion Research in Great Britain, NASA, Jet Propulsion Lab C.I.T. Tech. Memo No. 33-271.
5. Christie, D. G., G. W. Hayward, Observations of Events Leading to the Formation of Water Droplets which Cause Turbine Blade Erosion, Meeting of the British Royal Society, May 27, 1965.
6. Green, H. L., Atomization of Liquids, In Hermans Chapt. VII, Interscience Publishers Inc., N. Y., 1953.
7. Strutt, J. W., (Baron Rayleigh), The Theory of Sound, p. 361, Dover Publ., N. Y., N. Y., 1945.
8. Mayer, E., Theory of Liquid Atomization in High Velocity Gas Streams, ARS Jour. p. 1783 to 1785, Dec., 1961.
9. Nukiyama, S., Y. Tanasarwa as quoted in A. A. Putnam, et al, Injection and Combustion of Liquid Fuels, Battelle Memorial Institute, WADC Technical Report 56-344, May 1957.
10. Pearson, K., Tables of the Incomplete Gamma-Function, Cambridge University Press, 1957.
11. Dickerson, R. A., and M. D. Schuman, Rate of Aerodynamic Atomization of Droplets, Spacecraft, Vol. 2, No. 1, pp. 99 and 100, Jan., Feb. 1965.
12. Lambiris, S., and L. P. Combs, Steady State Combustion Measurements in a LOX-RP-1 Rocket Chamber and Related Spray Burning Analysis, Detonation and Two-Phase Flow, Academic Press, New York, Vol. 6 p. 283, 1962.
13. Wolfe, H. E., and W. H. Andersen, Kinetics, Mechanism and Resultant Droplet Sizes of the Aerodynamic Breakup of Liquids, Report 0395-04-18SP, Aerojet-General Corp., April 1964.
14. Fyall, A. A., R. B. King, and R. N. C. Strain, Rain Erosion Part III-A Gravimetric Assessment of the Erosion Resistance of the Various Materials, Report No. Chem. 513, Royal Aircraft Establishment, England, September 1957.

APPENDIX 2 A

DROP FORMATION BY "SQUIRT GUN" ATOMIZATION

Observations on pendant drop atomization in a turbine-like stationary cascade have been made at the CERL of Great Britain. A description of a pendant drop atomization process based on this work has been published by Hays.

That the atomization process is indeed complex is illustrated in figure 2A-1 which is taken directly from Hay's report. As shown in this figure, liquid collects as a large drop on the trailing edge of a vane, the pendant drop then oscillates with increasing amplitude until disrupted. After disruption, several drops are given up from the tip. Upon release of the drops, the pendant drop shrinks, atomization ceases, and the buildup process begins again.

Hays comments upon the CERL cascade results are as follows: "The quantitative results obtained may have been influenced by the specific blade design to the extent that they are not representative of what occurs in a well designed turbine." Figure 2A-2, taken directly from Hays' report, is a sketch of the blade profile tested at CERL.

There are several prominent breaks in the profile of the suction surface which can cause flow separation and low velocity regions that would not be present in well designed and constructed turbines. However, the breaks are on the suction surface where boundary layers will be quite thick in any case, and not on the pressure surface with its relatively thin boundary layer. Because of the normal difference in boundary layer thickness, it would be expected that the air forces causing pendant drop atomization would be more influenced by changes in the pressure side than in suction side forces. The results may be reasonably applicable in terms of the actual atomization process in turbines with the exception of the effects of fluid distribution.

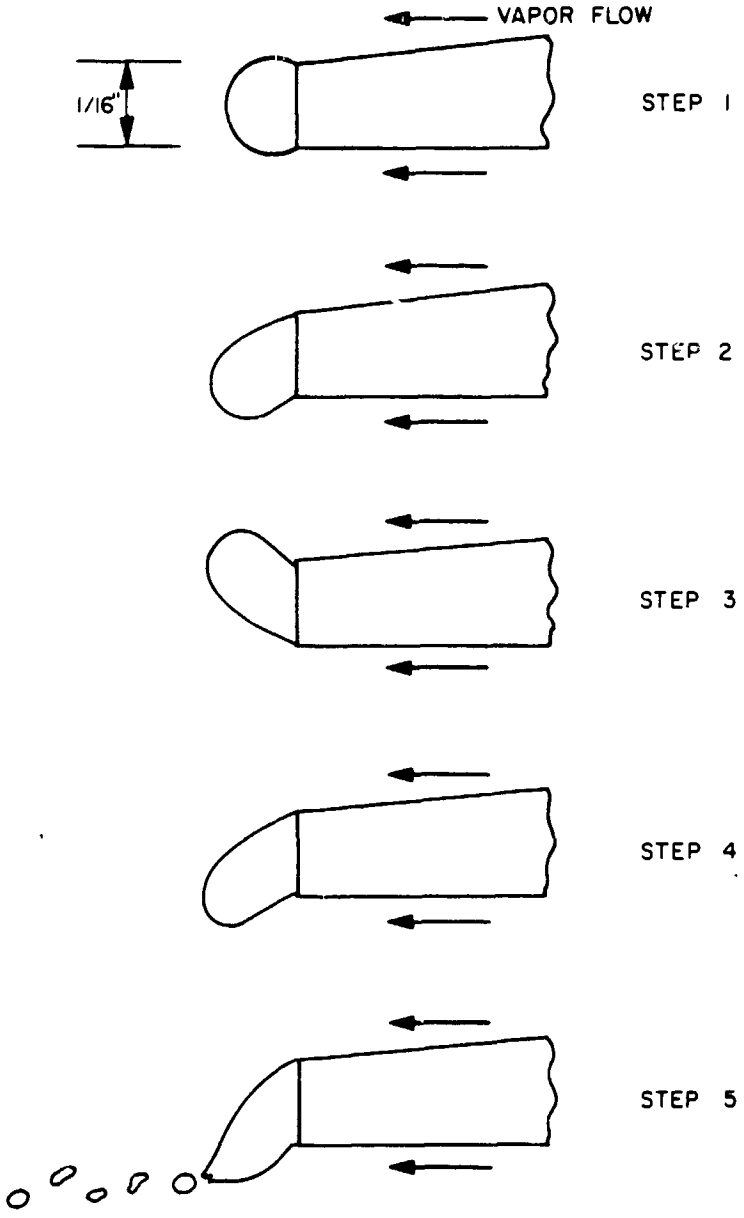

NOTES

1 PERIOD OF OSCILLATIONS ≈2-3 MILLISECONDS
2 ~5-10 DROPLETS SHED FOR EACH CYCLE
3 ~5-10 OSCILLATIONS PER CYCLE
4 VAPOR VELOCITY 700-1000 FPS
5 DROPLET SIZE 360-1700 MICRONS
6 NON-WETTING OF SOLID SURFACES BY DROPLETS

Figure 2A-1. Observed Stages in Droplet Shedding Process from Trailing Edge of Nozzle Blade

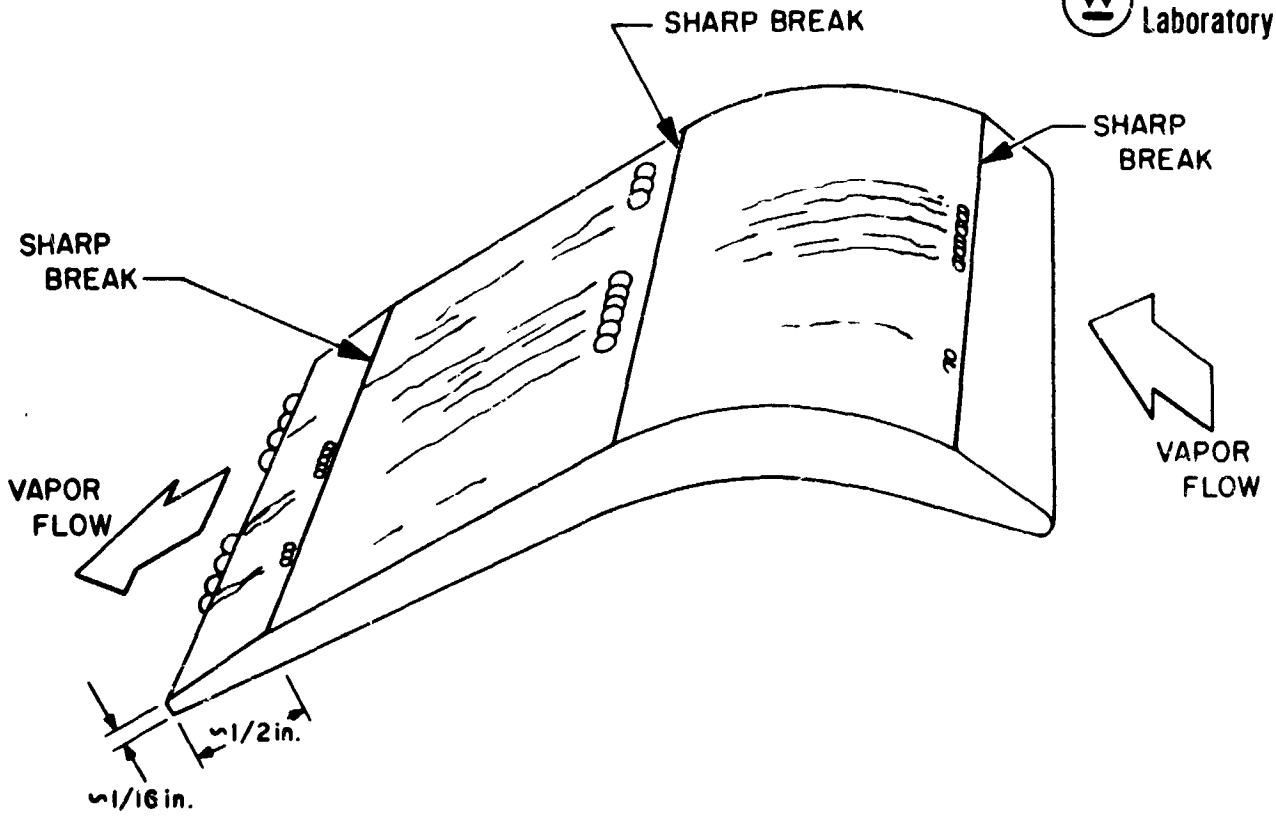

Figure2A-2. Schematic of CERL Nozzle Blade Tested in Steam Tunnel Showing Areas of Droplet Attachment and Features of Design

A possible explanation of the atomization process from the swinging pendant drop is that as the drop grows in size under influx of liquid, its amplitude of vibration also increases. Eventually, the tip of the drop protrudes far enough into the boundary layer so that the air velocities impinging on and passing over it within the time of swing available are sufficient to strip the drop. This stripping action is similar to the stripping of a large drop of liquid suddenly exposed to a high velocity gas stream.

Considered in detail, this concept encounters difficulties. First, there is the swinging of the drop in a pendulum mode. This action implies a vibration at the natural frequency of the pendant drop occasioned by a negative lift coefficient with angle of attack (or selective tuning to turbulent pulses in the gas flow). Assuming a negative lift coefficient, gives a net force on the drop in the plane of swing in the wrong direction for stripping to occur from the air forces in the boundary layer into which the drop is protruding (but in the right direction to cause an oscillation).

An expression for the natural frequency of such a pendulum drop is derived in Appendix 1C. Numerical evaluation of this expression gives a period of vibration twice that reported by Hays (figure 2A-1). However, considering the approximations involved in the derivation, this numerical difference can be considered as supporting evidence for an assumption of natural frequency oscillation.

A second difficulty with the tip stripping concept is the verbally reported observation by Hays that the drop remains motionless during ejection of the droplets at the tip at some angle of attack with respect to the bulk gas flow direction. This implies that the forces on the drop are largely directed along the axis of the drop during the ejection process. If stripping were the mechanism of removal, it would seem that a force of magnitude and direction to strip the drop should have a component of sufficient magnitude to blow the ejecting pendant back into the shadow of the trailing edge. In the absence of such an air force, the drop stops swinging because tip rupture removes the surface tension forces which return the drop towards its null position.

A start on a stripping model of atomization is included as Appendix 2B. This work was discontinued in favor of what might be called a "squirt gun" model.

"Squirt Gun" Pendant Atomization Model

Nomenclature

Symbol	Definition
c	Pendant drop transverse flow zone length
C_f	Stator wall friction drag coefficient
d	Drop size
$\bar{d}$	An average drop size
d_t	Diameter of tip rupture
D	Rotor diameter
g	Gravitational constant
h	Axial flow zone length
ℓ	Pendant drop length
$\dot{m}$	1/2 Mass flow rate into pendant drop per unit width
ΔP	Pressure differential over pendant drop tip
t	Time
U_s	Bulk steam velocity
$\bar{u}_f$	Average velocity of liquid entering a pendant drop

Symbol	Definition
V_s	Velocity of liquid at (or just underneath) the surface of pendant drop
W	Stator trailing edge thickness
w	Pendant drop axial flow zone width
ρ_L	Density of liquid
ρ_s	Density of vapor (bulk)
σ_L	Liquid surface tension
τ_s	Stator wall friction drag per unit area
μ_L	Liquid viscosity
ω	Rotor angular velocity

In the "squirt gun" model, as the pendant drop grows in length, the air force on the drop also increases because of the increase in surface area. This increased air force on the drop is reflected not only in an increased total force tending to tear the complete pendant from its attachment to the stator trailing edge, but is also reflected in increased internal pressure on the pendant drop tip.

It is assumed that this surface pressure to tip pressure translation occurs through circulations set up within the drop by the air (in effect) dragging the surface of the liquid along with it. Such circulations can be set up in soap bubble films by flowing air across them and without disrupting the bubble. It is not known whether this is also true for a small pendant drop of water but it seems likely that such circulations could come about through rippling of the surface. The process is depicted schematically in the following figure.

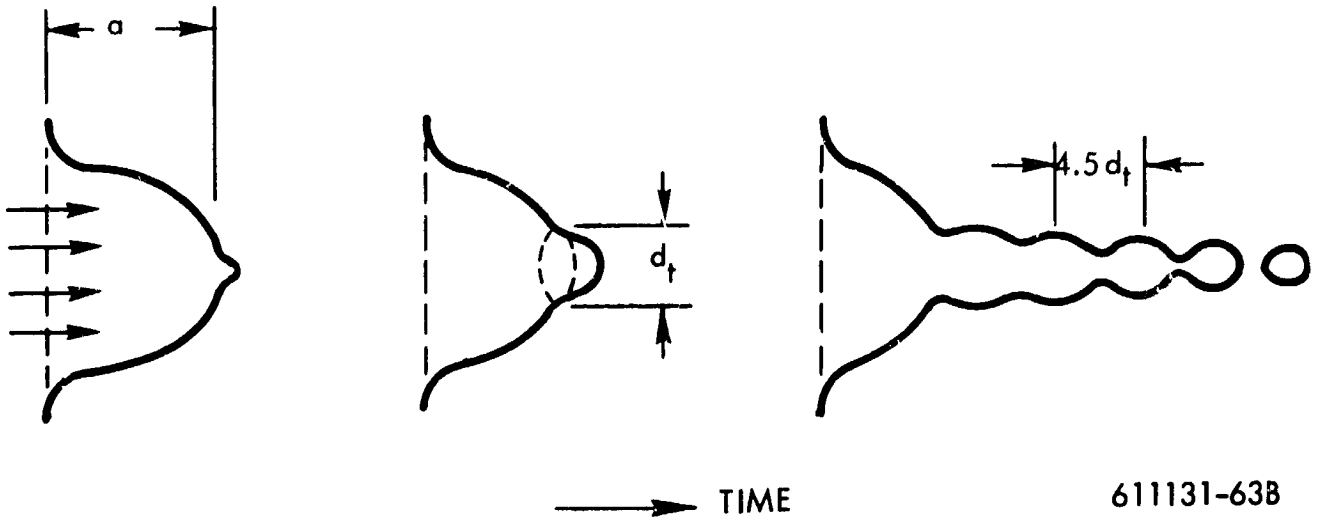

As the drop grows in length under the influx of liquid, the pressures on the tip of the drop increase until a local protrusion develops. This protrusion enlarges with time until the pressure force on the projected area of the protrusion exceeds the local surface tension forces around its rim. When this critical condition is reached, the surface ruptures and a stream of liquid squirts out. This initially cylindrical stream of liquid develops varicosities which pinch off into a parade of drops.

Equating the pressure (ΔP) forces and surface tension (σ_L) forces gives an expression for (d_t) in terms of these forces:

$$d_t = \frac{4\sigma_L}{\Delta P} \quad . \tag{1}$$

According to Rayleigh, as quoted in Green[6], the most probable pitch of the varicosities is 4.5 times the cylindrical diameter (d_t). Using this relation, the diameter (d) of an average drop can be written in terms of the pressure and surface tension as:

$$d = 7.45 \frac{\sigma_L}{\Delta P} \tag{2}$$

This "squirt gun" model is applicable, in general terms, to atomization from a whirling cup or disk atomizer when the feed rate is low enough so that drops originate at discretely spaced points about the rim of the disk or cup. The difference between the two atomization processes being in the origin of the forces causing tip pressure. For the whirling disk this origin is the centrifugal force on the liquid (inlet momentum is negligible in comparison) from rotation. In the trailing edge pendant the forces originate from the inlet momentum and the air friction forces on sides of the pendant drop.

As noted previously, there are three modes of atomization reported for whirling disc atomizers, depending upon flow rate. The first stage occurs at low rates of flow (for discs) and the drops depart the disc singly. A second stage occurs at somewhat higher rates of flow. In the second stage, the fluid departs the disc as visible ligament which then breaks into drops.

From the description of Hays it would appear that the CERL tests on stator vane atomization correspond to Stage 1 1/2. The chief difference in the end results between Stages 1 and 2 atomization in whirling discs is a greater dispersion of drop sizes from the average in Stage 2 than Stage 1.

Am empirical expression given by Green for Stage 1 atomization in disc atomizers is:

$$d = 3.8 \sqrt{\frac{\sigma_L}{\rho_L D\omega^2}} \quad . \tag{3}$$

The pressure on the tip of a drop of liquid as it whirls around attached to the rim of a disc is given by:

$$\Delta P = \frac{\ell}{2} \left(\rho_L D\omega^2\right) \tag{4}$$

Where ℓ is the length of the pendant drop in the direction of the centrifugal force.

Substituting this expression in equation 3 gives:

$$d = 2.7 \sqrt{\frac{\sigma_L \ell}{\Delta P}} \qquad (5)$$

Equation 5 can be used to empirically relate the "squirt gun" model to reality by eliminating d between equations 2 and 5 and solving for ℓ. This gives:

$$\ell = 7.6 \frac{\sigma_L}{\Delta P} \qquad (6)$$

Comparing equation 6 with equation 2 reveals that:

$$\ell = 1.02d \quad .$$

That is the average size of drops ejected from a pendant drop are directly proportional to the length of the pendant.

Application "Squirt Gun" Atomization Model to Trailing Edge Pendant Drop

A means of applying the "squirt gun" model to a stator trailing edge pendant drop is discussed. A system of eight equations results even though substantial simplifying assumptions are used:

Consider a pendant drop, such as described by Hays[4], attached to a thick trailing edge such as found in large Central Station Steam Turbines. It is assumed that the pendant drop contains circulating flows caused by drag forces from the steam vapor flowing past. Such a situation is depicted in the following figure.

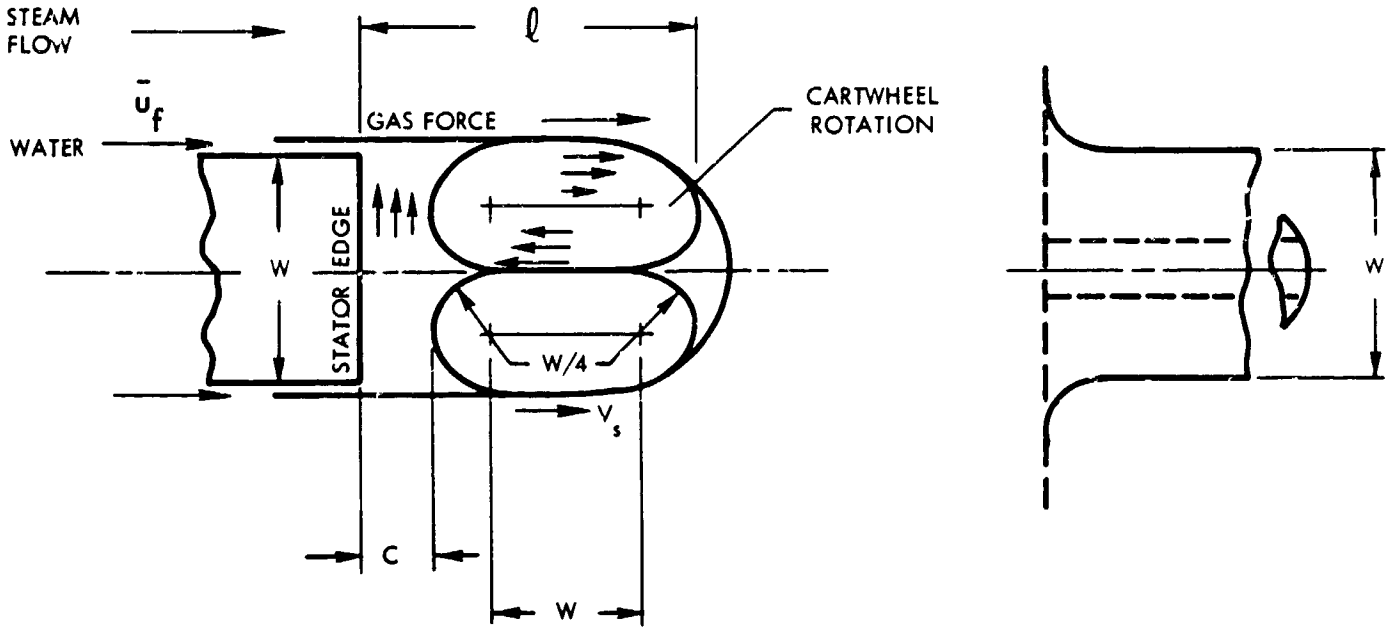

As this drop grows from an influx of water from surface of the stator, the pressure on the tip of the drop is increasing because the surface area of the drop exposed to drag forces is increasing. When this drop reaches some critical value of tip pressure differential, a stream of liquid shoots out and breaks into drops. The pendant shrinks during this process, flow from the drop tip ceases, and the cycle starts over again.

Geometric assumptions about the drop are: (1) that the width of the cylindrical cross-section of the drop is equal to the trailing edge thickness, (2) the circulations are symmetric about the center line of the stator trailing edge and have a half-width of 1/4 the trailing edge thickness, (3) the flow zones within the drop, from tip to base, consist of a rotating flow zone of dimension (W/4), an axial flow zone of dimension (h) a rotating flow zone of dimension (W/4), and a spacing zone (c) with a net transverse flow per side. The total length dimension (ℓ) of the pendant being equal to the sum of the axial lengths of the respective zones.

Fluid dynamic assumptions about the drop are: (1) that the internal flow is laminar, has linear velocity gradients and has a maximum velocity (V_s) at the surface of the drop,

(2) that the rotating flow zones contain a cartwheel type rotation and (3) the gas force is all attributable to frictional drag on the surface of the drop of the same value as if the drop was a solid stationary surface. Of this latter assumption it can be said that it ignores the increase in drag forces that probably result from the drop oscillating into the boundary layers but it also ignores the reduction in drag force from the movement of the liquid. These two effects, at least in part, should be compensating.

An additional assumption made in this application is that consideration of the forces and fluid movements over a central slice of the drop (two dimensional analysis) is adequate. A justification for this is that the break-through hole in the drop tip will be of relatively small dimension compared to the total cylindrical diameter of the pendant.

Considering only half the drop, since it is assumed symmetrical about the trailing edge centerline, the primary equations are:

Overall Momentum

$$\tau_s \ell - \mu_L V_s \left(\frac{4h}{W}\right) - \mu_L V_s \left(\frac{W}{2c}\right) = \frac{2}{3} \dot{m} t \frac{dV_s}{dt} + \frac{4}{3} \dot{m} \left(\frac{V_s}{2} - \bar{u}_f\right) \qquad (7)$$

Tip pressure from cartwheel rotation:

$$\Delta P = 1/2 \rho_L V_s^2 \quad . \qquad (8)$$

Gas friction force per unit drop surface:

$$\tau_s = \frac{C_f}{2} \rho_s U_s^2 \quad . \qquad (9)$$

Energy equation (overall):

$$\tau_s \ell V_s - \mu_L V_s^2 \left(\frac{4h}{W}\right) - \mu_L V_s^2 \left(\frac{W}{2c}\right) = \dot{m} t V_s \frac{dV_s}{dt} + \dot{m} \left(\left(\frac{V_s}{2}\right)^2 - \bar{u}_f^2\right) \qquad (10)$$

Continuity:

$$\dot{m}t = M \approx \rho_L \frac{\pi}{4} W^2 \ell \tag{11}$$

Geometry:

$$\ell = c + \frac{W}{2} + h \tag{12}$$

"Squirt Gun" atomization model relations

$$\ell = 7.6 \frac{\sigma_L}{\Delta P} \tag{13}$$

$$\ell = 1.02\, d \tag{14}$$

When these equations were solved for the geometric variables c and h , it was discovered that h could never take on a real positive value. The geometry of the pendant drop was therefore changed to eliminate axial length h or:

$$\ell = c + \frac{W}{2} \tag{15}$$

Using the new geometric relation (equation 15), a solution for drop diameter d was sought. The relationship (equation 16) was developed.

$$\frac{(d)\rho_L}{\sigma_L} = \frac{14.9}{\left(\left(\frac{\dot{m}(4d-W)}{2W\mu_L + \dot{m}(4d-W)}\right)\left(\left(\frac{\tau_S d}{2\dot{m}} - 2\bar{u}_f\right) \pm \sqrt{\left(\frac{\tau_S d}{2\dot{m}} - 2\bar{u}_f\right)^2 - 2\bar{u}_f\left(\frac{2W\mu_L + \dot{m}(4d-W)}{\dot{m}(4d-W)}\right)}\right)\right)^2} \tag{16}$$

APPENDIX 2 B

DROP FORMATION BY "TIP STRIPPING"

As discussed in Appendix 2A, a possible mechanism of atomization from a pendant drop attached to the trailing edge of a turbine stator is by "tip stripping". This appendix presents a partial analysis of such a mechanism.

Assume the pendulum drop to be swinging at a frequency close to its natural frequency. [This could be as a result of a selective tuning to certain noise components of the turbulent boundary layer or because the lift coefficient has a negative slope with angle of attack. This latter condition could arise from the non-steady nature of the flow about the drop.] An approximate expression for the period of vibration of the drop (as derived in Appendix 2c) is:

$$\tau_n = 2\pi \sqrt{\frac{\rho_L a^3}{10\sigma + 15/4\ \vec{g}\rho_L a^2}} \qquad (1)$$

where

a = one-half the thickness of the trailing edge.

$\vec{g}$ = component of gravity oriented normal to the face of the trailing edge

ρ_1 = density of the liquid of the drop

σ = surface tension of the drop

τ_n = natural period of vibration of the drop

As the drop swing increases in amplitude, the tip will eventually protrude into the boundary far enough and will remain there long enough, either during a single cycle or a succession of cycles, to encounter a summation of forces sufficient to disrupt the tip and strip off liquid. This liquid will then collapse into drops of smaller size than the original pendulum drop. This, of course, assumes that the boundary layers are thin enough relative to the size of the pendulum drop so that the stripping mechanism can occur before the entire drop is torn off.

As is well known, the disruption of a drop even when exposed suddenly to a high relative velocity is not instantaneous, but takes a finite time to occur. This time can be divided into two periods: the time from initiation of the process until stripping starts, and the time from the start of stripping until disruption is complete. An expression for the time to start of disruption of water drops based on experimental information presented in Wolfe-Andersen[13] is:

$$t_1 = 1.1 \left(\frac{d_p}{U}\right) \sqrt{\frac{\rho_L}{\rho_v}} \qquad (2)$$

where

t_1 = time to start the stripping of a drop

d_p = diameter of the drop being stripped

U = relative velocity between the drop and vapor into which the drop has been suddenly introduced

ρ_v = vapor density

ρ_L = liquid density

Under the conditions of d_p, U, etc., represented by equation 2, the mass mean diameter of the secondary drops which will be stripped from the primary drops, during $t > t_1$, is given by Wolfe and Andersen as:

$$d_{mn} = \left[\frac{136 g^{3/2} \mu_L \sigma^{3/2} d_p^{1/2}}{\rho_v^2 \rho_L^{1/2} U^4}\right]^{1/3} \qquad (3)$$

where

d_{mn} = mass mean diameter of the stripped droplets

μ_L = viscosity of the liquid

(The other symbols have been defined previously.)

Making the additional assumptions that:

$$d_p \sim 2a \tag{4}$$

$$t_1 \sim K \tau_n \tag{5}$$

$$10\sigma >> 15/4 \vec{g} \rho_L a^2$$

Equations 1 and 2 can be solved for a velocity (U) and the appropriate substitutions made in equation 3:

$$d_{mn} = 5.0 K^{4/3} a \left[\frac{\mu_L}{\sqrt{a \rho_L \sigma}}\right]^{1/3} \tag{6}$$

This expression involves only the trailing edge thickness of the stator and the liquid properties and is independent of the vapor flow conditions. This is based on the assumptions made in the derivation that the bulk velocity of the vapor substantially exceeds an average velocity (U) necessary to strip the drop. It is interesting to note that the vapor density cancelled out. There is, of course, the unknown K in equation 6, but there is no particular reason to prefer one value over another. Probably the minimum value of K is a function of the gas forces in the form of a Weber Number and,to a lesser extent,of blade Reynolds Number and geometry. The reasoning is that the amplitude of the disrupting mechanism as well as the amplitude of the drop could build up over a number of cycles if the available gas forces are low due to flow periodicity or low values of bulk parameters. That is, the disruptions resulting in stripping do not necessarily have to be active only within the period near the maximum gas velocity exposure during a single cycle if both damping and gas forces are low.

If K = 1, (the effective time of disruption equals one periodic swing of the drop) and:

a = 1/32 in = 2.6 (10^{-3}) ft

μ_L = 14.7 (10^{-6}) lb - sec/ft^2

ρ_L = 1.94 lb - sec^2/ft^4

σ = 48 (10^{-4}) lb/ft

then:

d_{mn} = 18.7 (10^{-4}) ft = 571 (10^{-6}) meters

If K = 2: d_{mn} = 1430 (10^{-6}) meters and if K = 3, the drop should detach as a whole.

APPENDIX 2C

NATURAL FREQUENCY OF A PENDULUM DROP (OF WATER)

Assume that a drop of hemispherical shape attached to a solid surface is oscillating in a manner similar to a pendulum in the plane of the paper as shown in figure 2C-1. Also assume: (1) that the displacements are small enough so that a simple harmonic motion results, (2) Rayleigh's approximation (the displacement increases linearly with radius) holds, (3) the surface tension forces (at any location $y \leq a$) have the net component acting parallel to the rotated centerline, (4) no gravity forces, (5) coordinates of points on the droplet surface may be related by the equation of a circle (distorted conditions included) and (6) no damping.

By the second and third assumptions, there exists a restoring force which is proportional to the displacement of the drop in the plane of oscillation and an approximate equation for the maximum potential energy at the extremal of swing:

$$(P.E.)_{max} = \frac{2\pi\sigma}{a^3} x_o^2 \int_{y=o}^{y=a} y^2\, dy = \frac{2}{3}\pi\sigma x_o^2 \qquad (1)$$

where σ is the surface tension of the liquid.

The approximate maximum kinetic energy is:

$$(KE)_{max} = \frac{\rho_L}{2} \int_{y=o}^{y=a} \pi(a^2 - y^2) \left(\frac{y}{a}\right)^2 (x_o^2\, \omega^2)\, dy$$

$$= \frac{\rho_L \pi}{15} x_o^2\, \omega^2\, a^3 \qquad (2)$$

where

ρ_L = density of the liquid

ω = is the circular frequency of the simple harmonic motion.

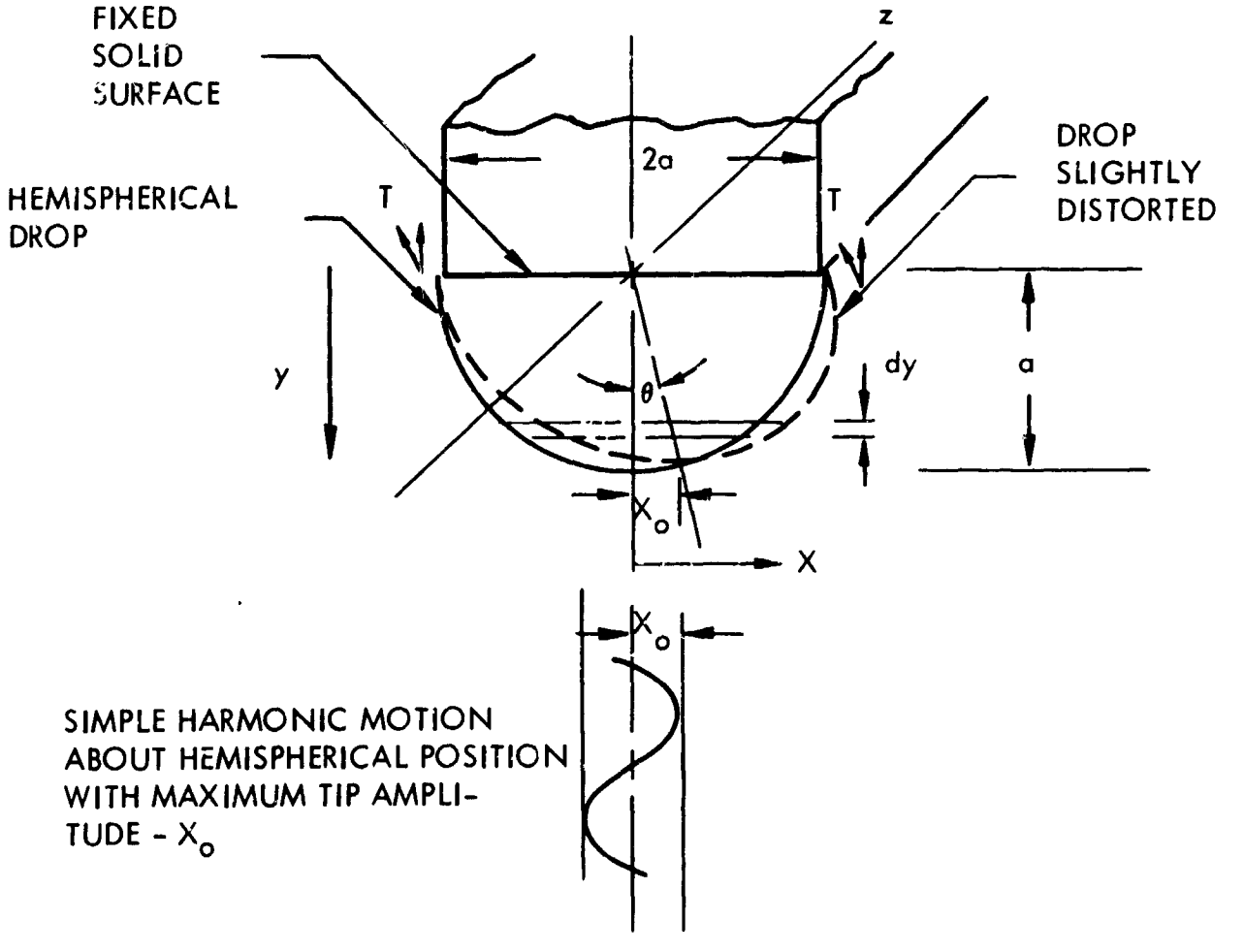

Figure 2C-1. Pendulum Drop

Equating the maximum kinetic and potential energies and solving for the circular frequency (ω) gives:

$$\omega = \sqrt{\frac{10\sigma}{\rho_L a^3}} \tag{3}$$

By definition, the period of vibration (τ) is:

$$\tau = \frac{2\pi}{\omega} = 2\pi \sqrt{\frac{\rho_L a^3}{10\sigma}} \tag{4}$$

Equation 5 gives the natural period of vibration of the pendulum drop in the absence of gravity. In the presence of gravity this natural period will be different depending upon the orientation of the drop with respect to gravity, since restoring forces over and above those of surface tension may be available.

Assume a gravitational field of 1.0 g directed downwards and perpendicular to the fixed solid surface of figure 2C-1 (other conditions remaining the same as for the zero gravity case). With gravity acting there is an additional restoring force per unit of drop mass equal to g θ and a corresponding increase in the maximum potential energy of the swinging drop.

This increase in maximum potential energy $(PE)_{g\ max}$ is:

$$(PE)_{g\ max} = \frac{g \rho_L \pi x_o^2}{4} a^2 \tag{5}$$

The total maximum potential energy then is:

$$(PE)_{max\ tot.} = \pi x_o^2 \left\{ \frac{2.8}{3} \sigma + \frac{9 \rho_L a^2}{4} \right\} \tag{6}$$

Equating this to the maximum kinetic energy (eq. 2) gives:

$$\omega = \sqrt{\frac{10\sigma + 15/4\, g\, \rho_L a^2}{\rho_L a^3}} \tag{7}$$

$$\tau = 2\pi \sqrt{\frac{\rho_L a^3}{10\sigma + 15/4\, g\, \rho_L a^2}} \tag{8}$$

if $\sigma = 0$,

then:

$$\tau \simeq \pi \sqrt{\frac{a}{g}} \tag{9}$$

In an example given by Hays[4] water drops attached to the trailing edge of a blade in a steam cascade rig were observed to swing pendulously with a period of 2 to 3 milliseconds. The orientation of the face of the trailing edge with respect to gravity is shown pictorially as intermediate between perpendicular and parallel to gravity. The trailing edge thickness is given as approximately 1/16 inch. Assuming that:

$2a$ = 1/16 in. = trailing edge thickness, $a = 2.6\ (10^{-3})$ ft

$\rho_L = 1.94$ lb - sec^2/ft^4

$\sigma = 48\ (10^{-4})$ lb/ft

$g = 32.2$ ft/sec^2

Then, if gravity acts normal to the face of the trailing edge, the period of vibration (τ) calculated using equation 8 is 5.4 milliseconds.

The numerical evaluation indicated that the gravitational term is of small importance even with this large size drop. The difference between the observed periods of vibration and the calculated natural period of vibration may be because of the approximations introduced in deriving an expression for natural frequency or because the drop is being driven at higher than natural frequency by a periodic aerodynamic forcing function of high frequency. The latter case seems unlikely.

APPENDIX 3

COLLECTION OF MOISTURE ON THE CONCAVE SIDE OF THE BLADE

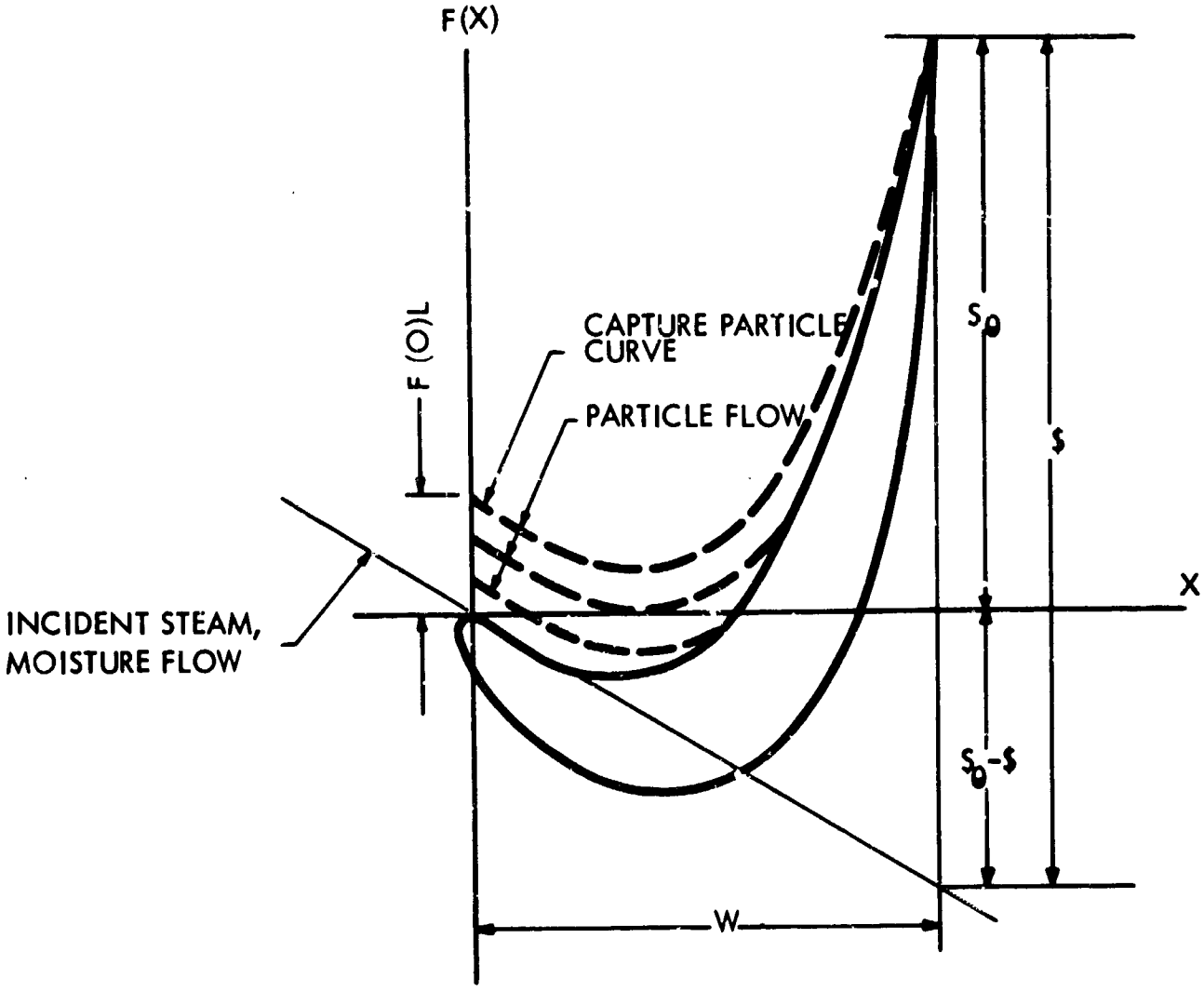

The concave surface of the blade is approximated by the third degree polynomial

$$F(x) = A_1 X + A_3 X^3 \quad (1)$$

The coefficients are specified by the inlet angle and the exit point as:

$$F'(o) = A_1 = (S_\theta - \$)/W \quad (2)$$

$$F(W) = S_\theta - \$ + A_3 W^3 = S_\theta;\ A_3 = \$/W^3 \quad (3)$$

Assume that the path of the steam is the same as the blade surface shape; then, the path and direction of the steam flow is:

$$F(X)_s = A_1 X + A_3 X^3, \tag{4}$$

$$F'(X)_s = A_1 + 3 A_3 X^2 \tag{5}$$

Where constants A_1 and A_3 are as defined by equations 2 and 3, and the subscript s is for the vapor.

The path of the moisture particles is related to that of the vapor by the conventional trajectory equations:

$$\dot{V}_t = \frac{C_D R_e}{24} \frac{C_{D,\ slip\ flow}}{C_D} \frac{9 \mu_s}{2 \rho_L r^2} (U_t - V_t) \text{ - tangential} \tag{6}$$

$$\dot{V}_a = \frac{C_D R_e}{24} \frac{C_{D,\ slip\ flow}}{C_D} \frac{9 \mu_s}{2 \rho_L r^2} (U_a - V_a) \text{ - axial}$$

Where U and V are the absolute vapor and particle velocity.

Assume that the vapor and particle axial velocity are equal and constant:

$$U_a = V_a = \text{const.}$$

By this assumption the particle acceleration is described in equation 6, and noting that.

$$U_t = V_a F'(X)_s \tag{7}$$

$$V_t = V_a F'(X)_L \tag{8}$$

$$\dot{V}_t = V_a^2 F''(X)_L \tag{9}$$

where subscripts s and L are for vapor and moisture particles. By substituting in equation 6:

$$W F''(X)_L = (1/K_c)\ (F'(X)_s - F'(X)_L) \tag{10}$$

where K_c, the inertia parameter, is as follows:

$$K_c = \frac{24}{C_D R_e} \frac{C_D}{C_{D,\ slip\ flow}} \frac{2 \rho_L r^2 V_a}{9 \mu_s W} \tag{11}$$

Substituting in equation 5 yields:

$$W F''(X)_L + (1/K_c)\ F'(X)_L = (1/K_c)\ (A_1 + 3 A_3 X^2) \tag{12}$$

This is the final differential equation of motion for the moisture particles.

Integrating equation 12 gives the following general solution:

$$F(x)_L = C_1 + C_2 e^{-X/(W K_c)} + A_3 X^3 - 3 A_3 W K_c X^2 + (A_1 + 6 A_3 W^2 K_c^2) X$$

$$- W K_c\ (A_1 + 6 A_3 W^2 K_c^2) \tag{13}$$

Constants C_1 and C_2 are determined by the following boundary conditions:

1) the direction of flow of the vapor and moisture particles are the same at the blade inlet position; thus, by equation 5, $F'(o)_L = F'(o)_s = A_1$

2) the end point position of the capture particle curve, is coincident with the blade surface point at the trailing edge, thus by equation 3, $F(W)_L = F(W) = S_\theta$.

Solving for C_1 and C_2 and substituting in equation 13 gives the following equation for the capture particle curve:

$$F(x)_L = 6 A_3 W^3 K_c^3 (1 - e^{-1/K_c}) + A_3 (X^3 - W^3) - 3 A_3 K_c W (X^2 - W^2)$$
$$+ (A_1 + 6 A_3 K_c^2 W^2) (X - W) + S_\theta \qquad (14)$$

The inlet width of the capture band is specified by the value of equation 14 for the inlet of blade as:

$$F(o)_L = 6 A_3 K_c^3 W^3 (1 - e^{-1/K_c}) - A_3 W^3 + 3 A_3 K_c W^3$$
$$- (A_1 + 6 A_3 K_c^2 W^2) W + S_\theta \qquad (15)$$

Substituting for A_1 and A_3 (equations 2 and 3) in equations 14 and 15 gives the final equations for capture particle curve and for the referred inlet width of the band.

$$F(x)_L / \mathcal{S} = 6 K_c^3 (e^{(-1/K_c)} (X/W) - e^{-1/K_c}) + (X/W)^3 - 3 K_c (X/W)^2$$
$$+ ((S_\theta/\mathcal{S}) + 6 K_c^2 - 1) (X/W) + 3 K_c - 6 K_c^2 \qquad (14a)$$

$$F(o)_L / \mathcal{S} = 6 K_c^3 (1 - e^{-1/K_c}) - 6 K_c^2 + 3 K_c \qquad (15a)$$

$$F(o)_L / \mathcal{S} \approx 3 K_c : K_c < .03 \approx 3 K_c - 6 K_c^2 : K_c < .10 \qquad (15b)$$

where the inertia parameter K_c is:

$$K_c = \frac{24}{C_D R_e} \frac{C_D}{C_{D'\text{ slip flow}}} \frac{2 \rho_L \tau^2 V_a}{9 \mu_s W}$$

Note that the referred inlet width of the band is, in effect, the referred collection efficiency.

The above equations consider the blade surface shape as by a third degree polynomial. A similar development assuming the surface shape as by a second degree polynomial gives the following equation for the inlet referred width of the capture band:

$$F(o)_L/\mathcal{S} = 2K_c^2 (e^{-1/K_c} - 1) + 2K_c \qquad (16)$$

$$F(o)_L/\mathcal{S} \approx 2K_c : K_c < .05 \qquad (16a)$$

where K_c is as before.

Equations 15a and 16 are plotted and shown in figure 3A-1.

The calculation of figure C-11 (Part C, Volume II) collection of drops on the concave side of the ninth stator blade, is illustrated by the following calculation of a curve point:

Moisture drop size: $.4\mu$ radius $= 1.311 \times 10^{-6}$ f radius

Fluid properties: $\rho_L = 1.935\ \rho\text{-s}^2/\text{f}^4$, $\mu_s = 2.4 \times 10^{-7}$ p-s/f^2, $V_a = 456$ f/s

Blade geometry: $W = .715$ f, $\mathcal{S} = .566$ f, $S = .485$ f

Inertia parameter:

$$K_c = \frac{24}{C_D R_e} \frac{C_D}{C_{D,\ \text{slip flow}}} \frac{2\rho_L \tau^2 V_a}{9\mu_s W} = .00445$$

where:

$$\frac{24}{C_D R_e} = 1, \text{ assuming Stokes' law drag}$$

$$\frac{C_D}{C_{D,\ \text{slip flow}}} = 1/.44 = 2.275, \text{ (figure C-6, Part C, Volume II)}$$

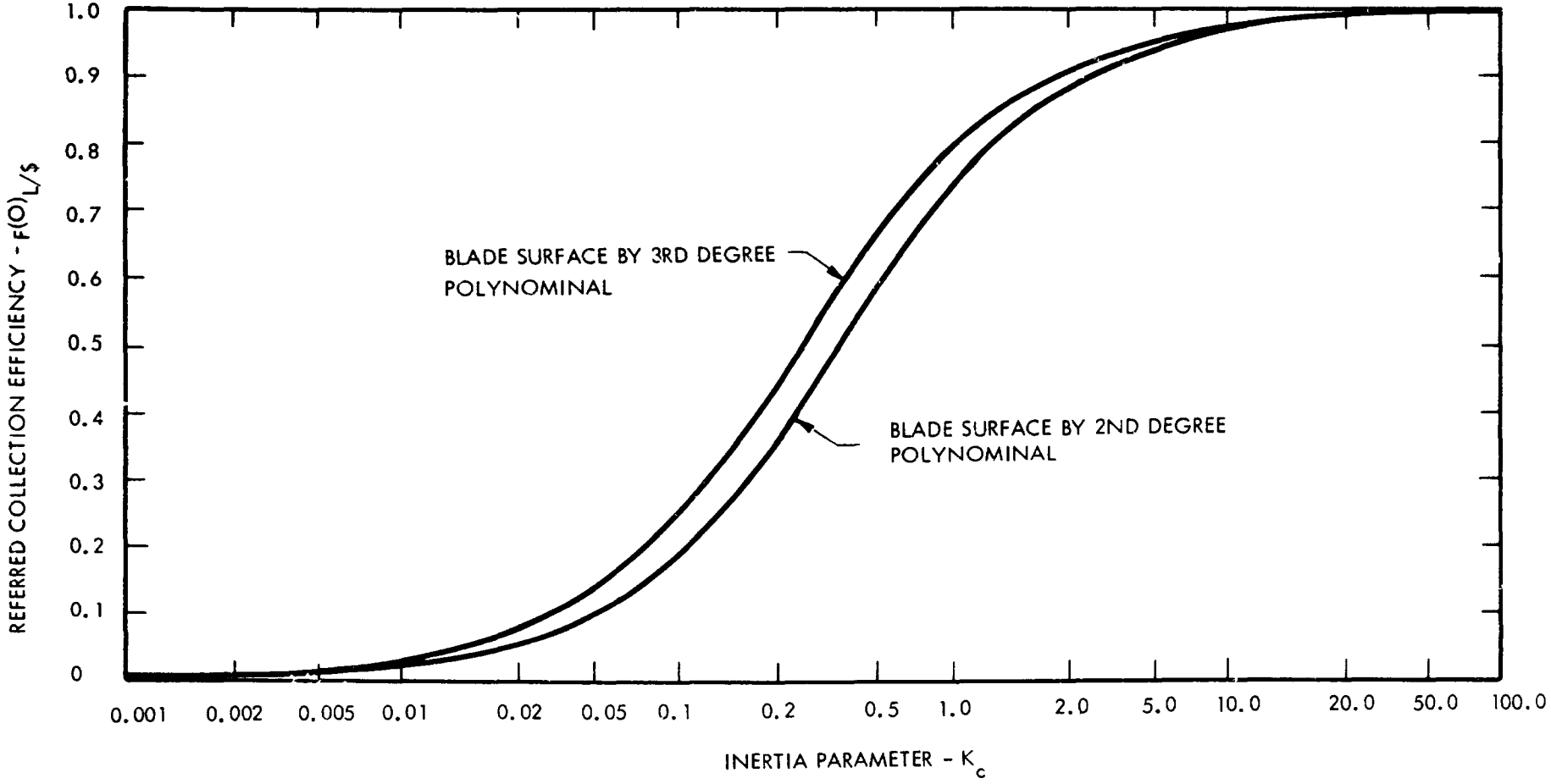

Figure 3A-1. Referred Collection Efficiency on the Concave Side of the Blade

The blade surface shape in this instance is closely approximated by the average between a 2 and 3 degree polynomial. Hence, the referred efficiency is specified by the average curve value, figure 3A-1, or by the average of equations 15b and 16a:

$$F(o)_L/\beta \qquad 5\,K_c = .0111 \ .$$

The inlet width of the capture curve (figure C-11, Part C, Volume II)

$$\zeta = (F(o)_L/\beta)\ \beta = .00629\ f$$

The portion of drops collected with respect to the total number approaching the blade is the ratio of the band width to the blade pitch.

Portion = $\zeta / S = .013.$

Referring to figure C-11, (μ, portion) = (.4, .013) is a point on the curve.

APPENDIX 4

COMPUTER PROGRAMS USED IN CALCULATION OF MOISTURE CONDENSATION AND DROPLET TRAJECTORIES

J. D. Miiton

INTRODUCTION

In the past three years much interest has been generated in the solution of differential equations by digital simulation techniques. Digital simulation makes available to the user of high speed digital computers the ease and flexibility previously associated only with analog computers. Essentially, a digital simulation code eliminates the laborious "bookkeeping" task of tracking all phases of the calculation and properly updating all variables. Most digital simulation codes (of which there are over 30) solve differential equations merely by reading in a block diagram or the actual equations themselves in a properly coded format, or "tell" the computer to integrate a variable with respect to a single independent variable. The master program then automatically sets the independent variable step size, the order in which the calculations are performed, integration, etc. Desired changes in the equations being solved or model being simulated are easily accomplished if such a digital simulation code is employed. This is especially important in a research program where flexibility is a necessity, since by the usual digital computer programing methods, a relatively minor change can take several days.

Thus, the digital simulation method was chosen to simulate the various processes for which no digital code existed. Five of the most "popular" digital simulation codes investigated were: MIDAS, MIMIC, DSL/90, SLASH, and ANALOG-ALGOL. The latter code was chosen because the authors (at Westinghouse Research and Development Center) were available for consultations when the inevitable problems arose during the solution. The quick (on the order of 10 minutes) turn around of the Burroughs B-5500 computer was also an important factor in the selection of ANALOG-ALGOL.

CONDENSATION AND DROP TRAJECTORY CODE

Rather than reproduce a listing of the condensation and droplet trajectory codes, it was believed that an abbreviated block diagram would be more informative, since the ALGOL language (and especially ANALOG-ALGOL) is not in general use. Refer to Sections C and D for the detailed nature of the mathematical equations being solved. The nomenclature used in each code is repeated for convenience in interpreting the flow diagrams.

The block diagram for the condensation code is given as figure 4-1 and the nomenclature in subsection 4.4. The block diagram for the drop trajectory code is given as figure 4-2 and the nomenclature in subsection 4.5.

RECOMMENDATIONS

In the condensation program the droplets were arbitrarily divided into nine groups because of ease in programming. The existing program could be modified without difficulty to make a general procedure (or subroutine) so that any number of droplet groups could be considered with only computer run time a factor. Although nine groups are believed to be adequate for our purposes, a capability of including more groups would be very useful.

The droplet trajectory code could be extended to include stripping and disruption of drops into smaller droplets. Combined with equations relating material damage and subsequent removal and turbine geometry, the computer could make direct calculations of turbine erosion and thereby relieve the manual "interfacing" problems.

The digital plots in both the condensation and droplet trajectory codes permitted a rapid view of results without waiting for hand plotted results.

Theoretically, it is possible to combine the condensation, collection of droplets, movement of the moisture over blade surfaces, wake effects, primary atomization of droplets from stators, droplet trajectories and secondary atomization, droplet impingement and material removal into a single gigantic code which would give the amount of turbine blade material eroded at any given position. Practically speaking, however, such a combination would involve many man months of labor and thousands of dollars of computer time. Some codes are in FORTRAN, others in ALGOL, and others in ANALOG-ALGOL. It is therefore

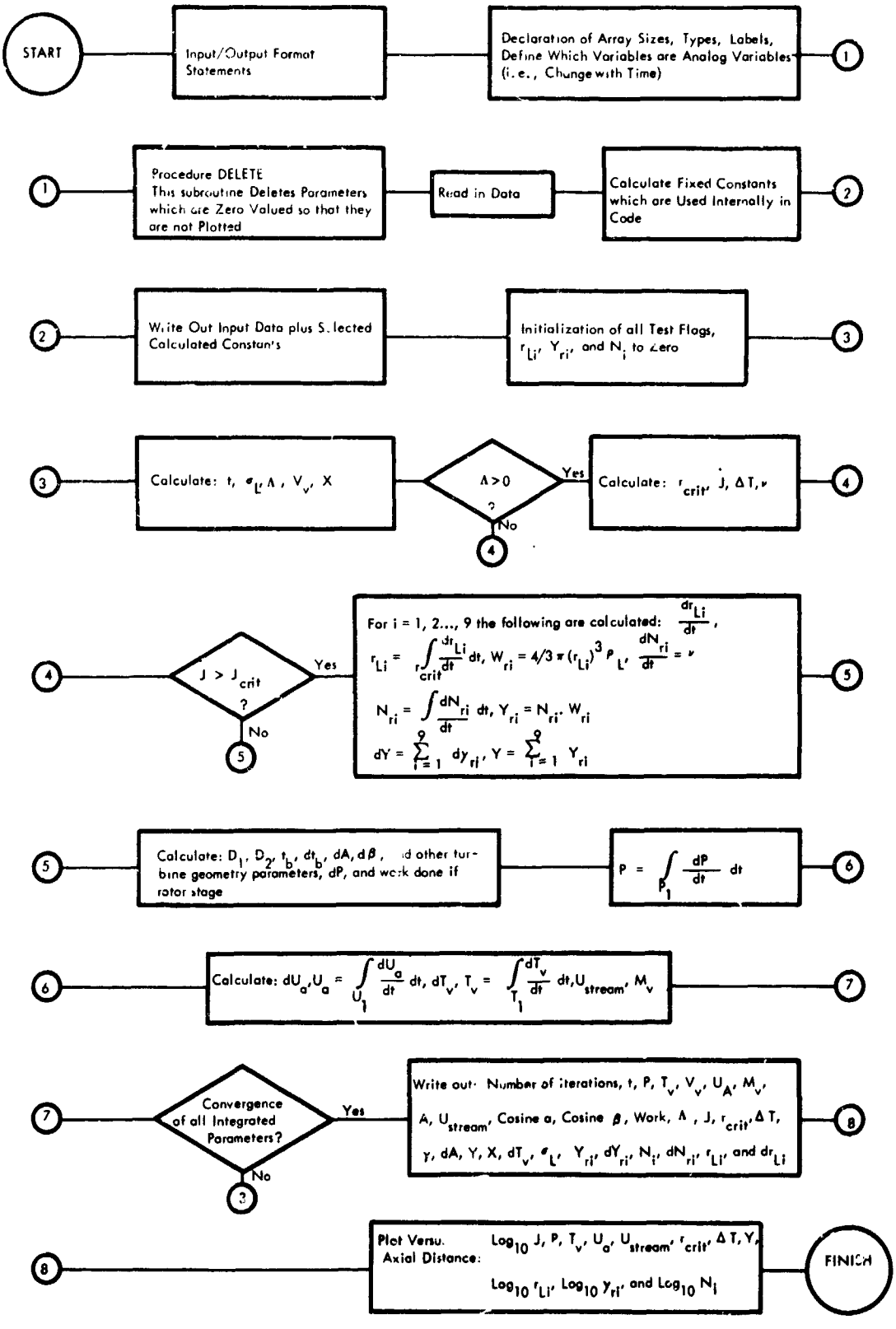

Figure 4-1. Abbreviated Flow Diagram of Condensation Code (Much of the complex logic has been deleted to improve readibility)

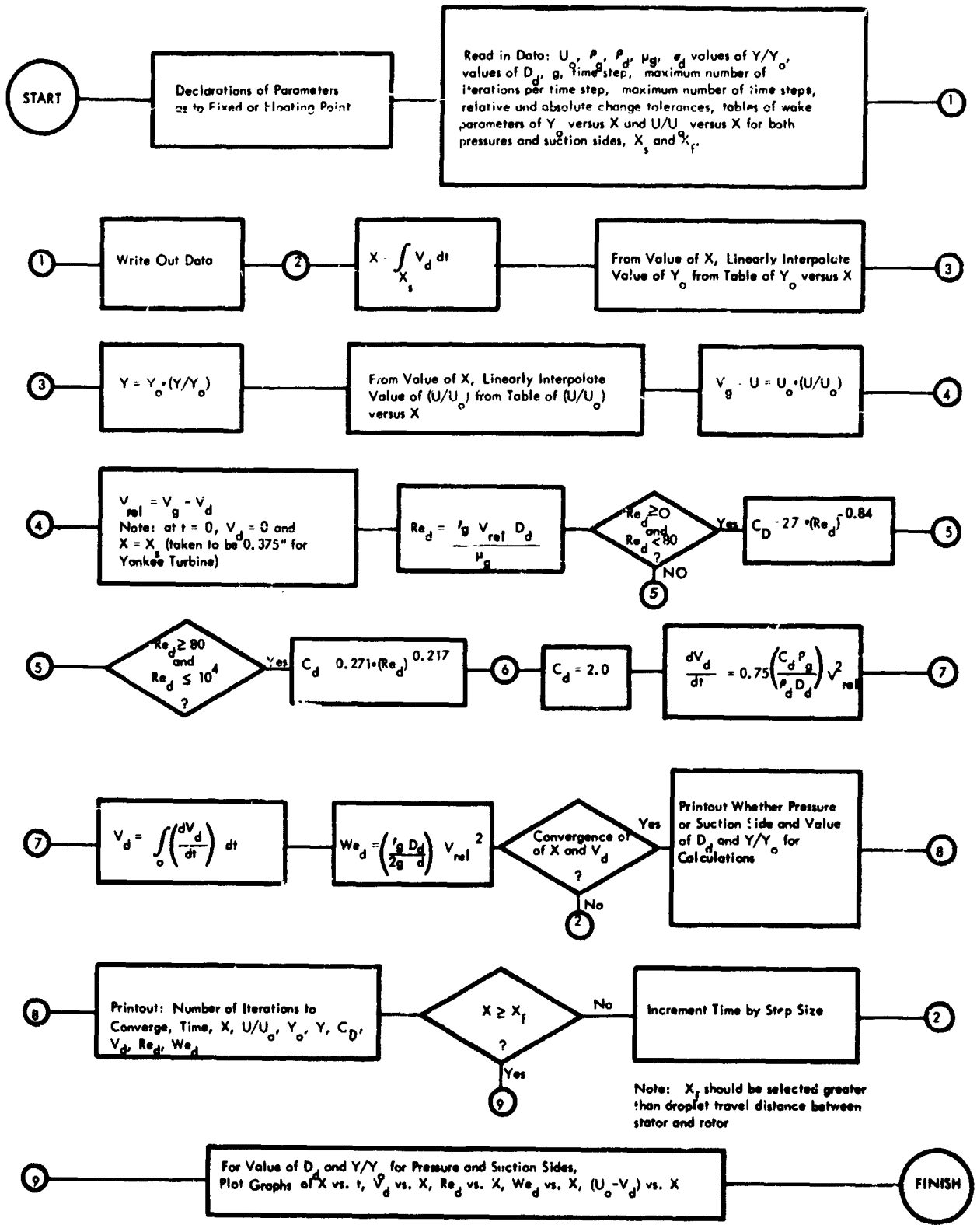

Figure 4-2. Simplified Flow Diagram of Droplet Trajectory Code

believed that effective "communication" between the hand calculations and the various computer programs is still best achieved by manual interfacing. Substantial amounts of engineering "insight" are involved which are difficult (if not impossible) to efficiently program into a computer.

NOMENCLATURE

Symbol	Definition	Units
A	Cross sectional area normal to flow	ft^2
A_a	Cross sectional area normal to turbine axis	ft^2
c	Jet velocity relative to blade	ft/sec
C_{p_v}	Specific heat of vapor at constant pressure	Btu/lb°R
C_{p_L}	Specific heat of condensate at constant pressure	Btu/lb°R
D_1, D_{1i}, D_{1o}	Inner diameter of turbine blade passage, inner diameter at blade row inlet, at blade row exit	ft
D_2, D_{2i}, D_{2o}	Outer diameter of turbine blade passage, outer diameter at blade row inlet, at blade row exit	ft
g	Gravitational constant	32.2 ft/sec^2
h_{fg}	Latent heat of vaporization	Btu/lb
h_L	Specific enthalpy of condensate	Btu/lb
h_v	Specific enthalpy of vapor	Btu/lb
i	Subscript denoting group of drops	-
J_{crit}	Critical nucleation rate	nuclei/sec ft^3
$\dot{J}$	Nucleation rate	nuclei/sec ft^3
k_v	Thermal conductivity of vapor	Btu/sec ft°R
L	Axial length of blade row	ft
M_v	Mach number of vapor	-

Symbol	Definition	Units
N_i	Number of drops per pound in group i	lb^{-1}
P	Static pressure	lb/ft^2
P_s	Saturation pressure at actual vapor temperature	lb/ft^2
R	Specific gas constant	$ft\text{-}lb/lb^{\circ}R$
r	Drop radius	ft
r_{li}	Radius of condensate drop of group i	ft
r_{crit}	Critical droplet radius	ft
t	Time	sec
t_b	Blade thickness in peripheral direction	ft
t_{bo}	Minimum blade thickness	ft
t_{bm}	Maximum blade thickness	ft
t_{bs}	Blade spacing in peripheral direction	ft
T_L	Condensate temperature	$^{\circ}R$
T_{LC}	Critical point temperature	$^{\circ}R$
T_v	Vapor temperature	$^{\circ}R$
T_s	Saturation temperature at the actual vapor pressure	$^{\circ}R$
ΔT	Supercooling	$^{\circ}R$
U_a	Axial velocity component	ft/sec
U_{stream}	Absolute stream velocity	ft/sec
v_m	Specific volume of mixture	ft^3/lb
v_v	Specific volume of vapor	ft^3/lb
w_{ri}	Weight of drops of group i	lb

Symbol	Definition	Units
x	Vapor quality	-
y	Total moisture fraction	-
y_{ri}	Moisture fraction of condensate belonging to group i	-
z	Axial coordinate, along turbine axis	ft
β	Blade angle	radians
β_i	Blade angle at inlet to row	radians
β_o	Blade angle at exit from row	radians
Λ	Logrithmic supersaturation	-
ν	Rate of droplet formation per pound	$sec^{-1}\ lb^{-1}$
υ_v	Kinematic viscosity	ft^2/sec
ρ_L	Density of condensate	lb/ft^3
σ_1	Surface tension of condensate	lb/ft

NOMENCLATURE

Symbol	Definition	Units
C_D	Drag coefficient	-
D_d	Diameter of droplet	inch
g	Gravitational acceleration constant	in/sec^2
Re_d	Droplet Reynolds number	-
t	Time	sec
U	Gas velocity of wake at the point $(X, Y) = V_g$	in/sec
U_o	Gas velocity of free stream boundary at the point (X, Y_o)	in/sec

Symbol	Definition	Units
U/U_o	Ratio of gas velocity in wake to free stream gas velocity	—
We_d	Droplet Weber number	—
V_d	Velocity of droplet	in./sec
V_g	Velocity of gas (steam)	in./sec
V_{rel}	Relative velocity	in./sec
X	Length downstream of the trailing edge of the stator	in.
X_s	Position at which droplets are assumed to be accelerated	in.
X_f	Largest value of X for which calculations are made	in.
Y	Direction perpendicular to X	in.
Y_o	Width of wake at X	in.
Y/Y_o	Position of droplet in wake at X	—
μ_g	Gas viscosity	lb/in. sec
ρ_d	Density of droplet	$lb/in.^3$
ρ_g	Density of gas	$lb/in.^3$
σ_d	Droplet surface tension	lb/in.